



Vaal University of Technology

**Thin film deposition of metal sulfide and metal oxide
layers with and without polymer intercalation by using
chemical bath deposition technique**

By

Mothepane Happy Chiloane BTech (Chemistry)

Dissertation submitted in fulfillment of the requirements for the Degree of **Magister Technologiae** in the Department of Chemistry, Faculty of Applied and Computer Sciences, Vaal University of Technology.

Supervisor: Prof. M. J. Moloto [BSc&BSc(Hons) (UNIN), MSc (UWC), Ph.D. (UZ)]

Co – Supervisor: Prof. N. Moloto [BSc&BSc(Hons) & MSc (UZ), Ph.D. (Wits)]

Date: 2017

DECLARATION

This research has not been previously accepted for any degree and is not being currently considered for any other degree at any other university. I declare that this dissertation contains my own work except where specifically acknowledged.

Mothepane Happy Chiloane

Signed.....

Date.....

ACKNOWLEDGEMENTS

The undertaking of this project and completion was very intense as this study would not be without the contribution of the almighty for continued strength and patience. It is not possible to single out all those who offered support and encouragement during what at times seemed to be a 'never ending journey'. However, there are individuals without whom this project would not have been completed, and to them go my special thanks and acknowledgment to their contributions.

Firstly, I am indebted to my supervisor Prof MJ Moloto who helped me shape my scientific outlook through his valuable guidance, suggestions and continuous encouragement, during the research work and the preparation of this manuscript. His patience at explaining different concepts and words of constant encouragement to explore deeper issues and to maintain a renaissance attitude towards education kept me and my faith in the belief that education serves the educated on its own. I have learned quite a lot from his extensive knowledge in nanotechnology and many brilliant and creative ideas.

Secondly, I would like to acknowledge National Research Foundation (NRF) for financial support of the project. My biggest gratitude goes to Vaal University of Technology research directorate for their assistance, support, interest and valuable hints. To all members of staff at the Department of Chemistry (Vanderbijlpark campus) and the NCAP group, I thank you for the advice and time offered with presentations. To Mokae Bambo thank you for the assistance with XRD characterization, Sanele Nyembe for assistance with SEM characterization and Bongani Mlasi for assistance with AFM characterization at Advanced Material Division (AMD). To Mintek, thank you for helping me with measurements and for your unwavering help by borrowing me the necessary materials and apparatus during the synthesis and preparation of the samples.

Special thanks to my family, my husband Robert Mabowa, our beautiful daughter Tshegofatso and our son Moloko for their support and understanding of sacrificing our

family time in doing this work. I also dedicate this work to my parents for continuous encouragement and support towards my studies. Finally, I would like to thank the beginning teachers, mentor Dr. Philemon Matabola whom has continued to mentor and me through all this work and Mintek for their assistance with this project. Their excitement and willingness to provide feedback made the completion of this research an enjoyable experience.

ABSTRACT

A well adherent single layer thin film of zinc oxide (ZnO), zinc sulfide (ZnS), cadmium oxide (CdO) and cadmium sulfide (CdS) has been deposited on silica glass substrates from basic baths containing zinc acetate, cadmium acetate, ammonium hydroxide, triethanolamine, thiourea, and sodium hydroxide as precursors by chemical bath deposition (CBD), followed by multilayer deposition of metal oxide/metal sulfide and metal sulfide/metal oxide then intercalated by polyvinyl alcohol (PVA). CBD was used for the deposition of the metal sulfide/oxide thin films under acidic and basic conditions for single layer thin film by varying temperature and pH. SEM micrograph of the as-deposited ZnS, ZnO, CdO, and CdS thin film, show the film to be uniform, dense, homogeneous at lower temperatures and composed of large irregular shaped grains that are scattered at higher temperatures. These large grains are comprised of smaller spherical grains. Star shapes were observed for ZnO and ZnS thin films while spherical shapes were observed for CdO and CdS thin films.

The effect of temperature on the optical properties was studied by varying the deposited films at different temperatures of 60°C, 70°C, and 90°C. The increase in temperature on the single layer depositions caused the decrease in %T which was in support with the large SEM results which in higher absorbance. Films of different thickness of (114.4 nm, 107.7 nm, 100.4 nm, and 99.67 nm) respectively were obtained for single layer deposition. The XRD study of the ZnS, ZnO, CdO, and CdS monolayer films deposited does not reveal any well-defined peak, indicating a highly disordered material. The XRD of CdO thin films showed one broad peak around 2θ value 26.37° corresponding to (111) plane. The structural studies had similar behavior of CdS, ZnO, and ZnS was similar with CdO with one broad peak at $2\theta \sim 26^\circ$.

To enhance the property of MO, MS thin film was formed on the interfaces of MO thin film as a passivation and a substrate layer at 60°C with a pH value of 11 for 60 minutes deposition time and vice versa for enhancing the property of MS. The structural, morphological and optical properties of CBD deposited thin films have been studied by varying the processing parameters and the MO/MS multilayer ratio of the starting

precursors to provide a better understanding of the growth conditions by studying the MO/MS and MS/MO multilayer thin film materials with further intercalation of polyvinyl alcohol (PVA). Multilayer thin films show different physical properties other than the conventional monolayer thin films. The films were deposited as the matrix of MO/MS and MS/MO of respectively at temperatures of 60°C at alkaline medium for 60 minutes deposition time. SEM micrograph of CdO/CdS was observed to be spherical shapes which show the film to be uniform, dense, and homogeneous. Large spherical particles that appear to be increasing in size and non-homogeneous were observed in the deposition of CdS/CdO. The deposited ZnO/ZnS thin films show large conglomerate of snowflake structures and that of ZnS/ZnO thin film were polycrystalline in structure. The optical properties and band-gap energy were studied by depositing the films at 60°C for 60 minutes.

Transparent multilayer thin films were successfully deposited on the silica glass substrate. The %T was relative ~89% in the visible the region, and some oscillations due to thin film interference effects. The optical %T of the multilayer deposition showed slight changes from the monolayer. The multilayer film thickness was increased for deposition of CdO/CdS, CdS/CdO, ZnO/ZnS and ZnS/ZnO series (145.47, 131.0, 128.8, 148.38 nm) illustrating that an increase in layer increases the thickness of the material deposited. The increase in thickness showed that CBD deposition technique does not wash away the pre-deposited layer of the thin film material and hence the structure should be enhanced. XRD measurements are performed to investigate the change in the crystal structure of the film, as the number of layers deposited was increased, and the composition of the growth solution is varied the deposited CdO/CdS and CdS/CdO thin film has a monocrystalline and hexagonal structure which is ($\theta = 8.2^\circ$ and 11.878°) with one large broad peak at $\sim \theta = 27^\circ$ which was due to the amorphous glass substrate that was detected. The presence of diffraction peaks of ZnO/ZnS indicates that the film is polycrystalline with cubic structure is detected at $2\theta = 26.79^\circ$. It is revealed that the films have peaks corresponding to (111), (220) and (311). There was only one peak that occurred in XRD pattern at 2θ of 12.488° at (002) for deposition of ZnS/ZnO thin film was polycrystalline.

To enhance the structure and study the effect of thickness intercalation of MO and MS with polyvinyl alcohol (PVA) was deposited to create the layers of MO/PVA/MS. Intercalated MO and MS thin films were successfully deposited on the glass substrate by chemical bath deposition (CBD) using PVA as the intercalation polymer by varying the effect the polymer on the inorganic layers. The intercalation by polymers followed multiple layer deposition of the metal chalcogenide in which MO becomes the first layer and the polymer as the second layer followed by the MS as the third layer respectively at temperatures of 60°C at alkaline medium for 60 minutes deposition time. The thin film composition materials of the intercalated growth are composed of CdO/PVA/CdS, CdS/PVA/CdO, ZnO/PVA/ZnS and ZnS/PVA/ZnO. The intercalated SEM imaging was more smooth, homogeneous and spherical shape.

The optical properties of the intercalated thin films are transparent at %T of ~88 % showing a more transparent material. The film thickness of the intercalated MO/PVA/MS and MS/PVA/MO was decreased to (52.67, 37.15, 102.45 and 116.6 nm) respectively, illustrating that the PVA has a huge impact on the thickness as well as the structure of the deposited material by use of CBD technique. The XRD patterns showed the formation of the polycrystalline and monocrystalline structure of CdS/PVA/CdO and ZnO/PVA/ZnS multilayer thin film. The pattern of ZnS/PVA/ZnO and CdO/PVA/CdS was amorphous in structure. The intercalated PVA reduced the crystallinity of the deposited material.

STRUCTURE OF DISSERTATION

This dissertation contains five chapters. The early chapter (1-3) provides introductory information: CBD basics, literature review, and experimental techniques. The later chapters provide experimental results and discussion of results followed by conclusion and recommendations in the final chapter.

Chapter 2 consists of an introduction of thin film technology which is followed by a literature review of CBD chalcogenide materials.

Chapter 3 provides the condition that was used to deposit the thin films. This is followed by a summary of the experimental techniques used in this project which includes an introduction to the theory behind the main technique and the experimental conditions used in this project.

Chapter 4 focuses on single layer deposition of metal oxide and metal sulfide of CdO, CdS, ZnO, and ZnS thin film by chemical bath deposition (CBD) by varying their morphology and optical properties for commissioning of multilayer stack by characterization with SEM-EDX, XRD, AFM, and UV-Vis. From the observations made on the SEM and UV-Vis, an increase in temperature increases the particle size and thus decreases the %T. The structure of the deposited single layer has a large broad peak.

Chapter 4 also focuses on the effect of multilayer deposition without PVA intercalation by chemical bath deposition of CdO/CdS, CdS/CdO, ZnO/ZnS, and ZnS/ZnO thin film by varying their structure, morphology and optical properties by characterization with SEM-EDX, AFM, XRD, and UV-Vis. It was observed that the thickness of the material increased as the deposition layer increase and the surface roughness decreased. The structure was showed intensified peaks as an improvement in the crystallinity of the multilayer deposition.

Chapter 4 also focus on the effect of multilayer deposition with PVA intercalation by chemical bath deposition of CdO/PVA/CdS, CdS/PVA/CdO, ZnO/PVA/ZnS, and ZnS/PVA/ZNO thin film by varying their structure, morphology and optical properties by

characterization with SEM-EDX, AFM, XRD and UV-Vis. The thickness of the deposited material decreased with the insertion of PVA and the surface roughness decreased.

The final chapter 5 presents a conclusion that can be made from the results that have been presented in the preceding chapters. Suggestions relating to possible future work complete the dissertation.

TABLE OF CONTENTS

DECLARATION	I
ACKNOWLEDGEMENTS	II
ABSTRACT	IV
STRUCTURE OF DISSERTATION	VII
TABLE OF CONTENTS	IX
LIST OF FIGURES	XII
LIST OF TABLES	XIV
LIST OF ABBREVIATIONS	XV
CHAPTER 1	1
1.1 INTRODUCTION.....	1
1.2 PROBLEM STATEMENT.....	5
1.3 AIMS AND OBJECTIVES.....	7
CHAPTER 2	9
2.1 LITERATURE REVIEW	9
2.2 THIN FILM.....	11
2.3 APPLICATIONS OF THIN FILM.....	16
2.3.1 <i>Optical Coatings</i>	17
2.3.2 <i>Optoelectronic</i>	17
2.4 PRINCIPLES OF CHEMICAL BATH DEPOSITION (CBD)	18
2.4.1 <i>Basic Mechanism of Chemical Bath Deposition</i>	19
2.4.2 <i>Selection of Deposition Process</i>	21
2.5 CHEMISTRY OF BATH DEPOSITION OF ZN AND CD OXIDE AND SULFIDES.....	24
2.6 SEMICONDUCTOR MATERIALS	25
2.6.1 <i>Zinc Oxide (ZnO)</i>	26
2.6.2 <i>Cadmium Oxide (CdO)</i>	28
2.6.3 <i>Cadmium Sulfide (CdS)</i>	30
2.6.4 <i>Zinc Sulfide (ZnS)</i>	32
2.7 INTERCALATION OF INORGANIC-ORGANIC	34
2.8 POLYVINYL ALCOHOL (PVA)	35
CHAPTER 3: METHODOLOGY	37
3.1 INSTRUMENTATION	37
3.1.1 <i>UV-Vis Spectroscopy</i>	37
3.1.2 <i>Scanning Electron Microscopy (SEM) and Energy Dispersive X-Ray Spectroscopy (EDS)</i>	38
3.1.3 <i>Atomic Force Microscopy (AFM)</i>	38
3.1.4 <i>X-Ray Diffraction (XRD)</i>	39
3.2 CHEMICAL REAGENTS.....	40

3.3	EXPERIMENTAL PROCEDURE	40
3.3.1	<i>CdO thin film deposition</i>	40
3.3.2	<i>PVA/CdS thin film deposition</i>	40
3.3.3	<i>ZnO thin film deposition</i>	41
3.3.4	<i>PVA/ZnS thin film deposition</i>	41
RESULTS AND DISCUSSIONS		42
CHAPTER 4.....		43
SINGLE LAYER DEPOSITION OF METAL SULFIDE AND OXIDE THIN FILM		43
4.1	DEPOSITION OF METAL SULFIDE/OXIDE SINGLE LAYER	43
4.1.1	<i>Transmittance of single layer thin film</i>	43
4.2	SURFACE MATERIALS USING SCANNING ELECTRON MICROSCOPY (SEM)	50
4.2.1	<i>Surface analysis of CdO thin film at various temperatures</i>	51
4.2.2	<i>Surface analysis of CdS thin film at various temperatures</i>	53
4.2.3	<i>Surface analysis of ZnO thin film at various temperatures</i>	54
4.2.4	<i>Surface analysis of ZnS thin film at various temperatures</i>	56
4.3	STRUCTURAL ANALYSIS USING ATOMIC FORCE MICROSCOPY (AFM)	59
4.3.1	<i>Structural analysis of CdO thin film</i>	59
4.3.2	<i>Structural analysis of CdS thin film</i>	60
4.3.3	<i>Structural analysis of ZnO thin film</i>	61
4.3.4	<i>Structural analysis of ZnS thin film</i>	62
4.4	CRYSTALLINITY OF A COMPOUND USING X-RAY DIFFRACTION (XRD)	63
4.4.1	<i>Crystal structure of CdO thin film</i>	63
4.4.2	<i>Crystal structure of CdS thin film</i>	64
4.4.3	<i>Crystal structure of ZnO thin film</i>	66
4.4.4	<i>Crystal structure of ZnS thin film</i>	67
MULTILAYERS WITHOUT POLYMER INTERCALATION.....		69
4.5	OPTICAL CHARACTERIZATION OF MULTILAYER DEPOSITION WITHOUT POLYMER INTERCALATION	69
4.5.1	<i>%T of multilayer CdO/CdS thin film</i>	69
4.5.2	<i>%T of multilayer CdS/CdO thin film</i>	70
4.5.3	<i>%T of multilayer ZnO/ZnS thin film</i>	70
4.5.4	<i>%T of multilayer ZnS/ZnO thin film</i>	71
4.6	SURFACE MATERIALS USING SCANNING ELECTRON MICROSCOPY (SEM)	71
4.6.1	<i>Surface of multilayer CdO/CdS thin film</i>	72
4.6.2	<i>Surface of multilayer CdS/CdO thin film</i>	74
4.6.3	<i>Surface of multilayer ZnO/ZnS thin film</i>	75
4.6.4	<i>Surface of multilayer ZnS/ZnO thin film</i>	77
4.7	STRUCTURAL ANALYSIS USING ATOMIC FORCE MICROSCOPY (AFM)	78
4.7.1	<i>Structural analysis of multilayer CdO/CdS thin film</i>	78
4.7.2	<i>Structural analysis of multilayer CdS/CdO thin film</i>	80
4.7.3	<i>Structural analysis of multilayer ZnO/ZnS thin film</i>	81
4.7.4	<i>Structural analysis of multilayer ZnS/ZnO thin film</i>	83
4.8	CRYSTALLINITY OF A COMPOUND USING X-RAY DIFFRACTION (XRD)	85

4.8.1	<i>Crystal structure of multilayer CdO/CdS thin film</i>	85
4.8.2	<i>Crystal structure of multilayer CdS/CdO thin film</i>	86
4.8.3	<i>Crystal structure of multilayer ZnO/ZnS thin film</i>	88
4.8.4	<i>Crystal structure of multilayer ZnS/ZnO thin film</i>	89
MULTILAYERS WITH POLYMER INTERCALATION		91
4.9	OPTICAL CHARACTERIZATION OF MULTILAYER DEPOSITION WITHOUT POLYMER INTERCALATION	91
4.9.1	<i>%T of intercalated CdO/PVA/CdS thin film</i>	91
4.9.2	<i>%T of intercalated CdS/PVA/CdO thin film</i>	91
4.9.3	<i>%T of intercalated ZnO/PVA/ZnS thin film</i>	92
4.9.4	<i>%T of intercalated ZnS/PVA/ZnO thin film</i>	92
4.10	SURFACE MATERIALS USING SCANNING ELECTRON MICROSCOPY (SEM)	93
4.10.1	<i>Surface of intercalated CdO/PVA/CdS thin film</i>	93
4.10.2	<i>Surface of intercalated CdS/PVA/CdO thin film</i>	94
4.10.3	<i>Surface of intercalated ZnO/PVA/ZnS thin film</i>	96
4.10.4	<i>Surface of intercalated ZnS/PVA/ZnO thin film</i>	97
4.11	STRUCTURAL ANALYSIS USING ATOMIC FORCE MICROSCOPY (AFM)	98
4.11.1	<i>Structural analysis of intercalated CdO/PVA/CdS thin film</i>	99
4.11.2	<i>Structural analysis of intercalated CdS/PVA/CdO thin film</i>	100
4.11.3	<i>Structural analysis of intercalated ZnO/PVA/ZnS thin film</i>	101
4.11.4	<i>Structural analysis of intercalated ZnS/PVA/ZnO thin film</i>	102
4.12	CRYSTALLINITY OF A COMPOUND USING X-RAY DIFFRACTION (XRD)	105
4.12.1	<i>Crystal structure of intercalated CdO/PVA/CdS thin film</i>	105
4.12.2	<i>Crystal structure of intercalated CdS/PVA/CdO thin film</i>	106
4.12.3	<i>Crystal structure of intercalated ZnO/PVA/ZnS thin film</i>	108
4.12.4	<i>Crystal structure of intercalated ZnS/PVA/ZnO thin film</i>	108
CHAPTER 5: CONCLUSIONS AND RECOMMENDATIONS		110
5.1	CONCLUSIONS	110
5.2	RECOMMENDATIONS	113
REFERENCES		114

LIST OF FIGURES

FIGURE 1: DEPOSITED THIN FILM ON A GLASS SUBSTRATE (THIN FILM OF CdS DEPOSITED BY CBD).....	12
FIGURE 2: SET UP OF THE CHEMICAL BATH DEPOSITION TECHNIQUE (CBD)	22
FIGURE 3: EXAMPLES OF DEPOSITED FILM OF METAL CHALCOGENIDE [ZHANG, ET AL., 2016]	23
FIGURE 4: ZNO HEXAGONAL WURTZITE STRUCTURE [EL-SHAER, ET AL., 2007].....	28
FIGURE 5: THE REAL SPACE CRYSTAL STRUCTURE OF CdO (B) THE FCC BZ OF CdO AND THE SURFACE BZ FOR THE (001) SURFACE. THE BULK AND SURFACE HIGH SYMMETRY POINTS ARE LABELED [MRIDHA, DUTTA, & BASAK, 2009] AND [KIM, KWACK, KIM, YOON, BAHANG, & PARK, 2003]	29
FIGURE 6: CdS HEXAGONAL WURTZITE STRUCTURE [WIBERG & HOLLEMAN, 2001]	31
FIGURE 7: CdS GROWTH ON THE SUBSTRATE [SMITH, 2002]	32
FIGURE 8: THE SPHALERITE OR ZINC BLENDE AND THE WURTZITE CRYSTAL STRUCTURE OF ZNS [GILBERT, ET AL., 2002]	33
FIGURE 9: SCHEMATIC DESCRIPTION OF INTERCALATION BETWEEN POLYMER AND LAYERED INORGANIC MATERIAL FOR THE FORMATION OF PINCs [KICKELBICK, 2003]	35
FIGURE 10: PVA EXCELLENT FOR MULTILAYER [GAUME, WONG-WAH-CHUNG, RIVATON, THÉRIAS, & GARDETTE, 2011]	36
FIGURE 11: PLOTS OF TRANSMITTANCE VERSUS WAVELENGTH SHOWING TRANSMITTANCE DEPENDENCE OF PH 11 AT TEMPERATURE VARIATION, (A) CdS, (B) CdO, (C) ZNO, (D) ZNS.....	44
FIGURE 12: PLOTS OF TRANSMITTANCE VERSUS WAVELENGTH SHOWING TRANSMITTANCE DEPENDENCE OF PH VARIATION AT 60°C, (A) CdS, (B) CdO, (C) ZNO, AND (D) ZNS	48
FIGURE 13: SEM IMAGES OF CdO THIN FILM AT MAGNIFICATIONS OF 5µM (A) 60°C, (B) 70°C, (C) AND 90°C.....	52
FIGURE 14: SEM IMAGES OF CdS THIN FILM AT MAGNIFICATIONS OF 5µM (A) 60°C, (B) 70°C, AND (C) 90°C	54
FIGURE 15: SEM IMAGES OF ZNO THIN FILM AT MAGNIFICATIONS OF 5µM (A) 60°C, (B) 70°C, AND (C) 90°C	56
FIGURE 16: SEM IMAGES OF ZNS THIN FILM AT MAGNIFICATIONS OF 5µM (A) 60°C, (B) 70°C, AND (C) 90°C.....	58
FIGURE 17: (A) AFM MICROGRAPHS ROUGHNESS OF CdO THIN FILM AT 60°C; (B) AFM 3D MICROGRAPHS OF CdO THIN FILM.....	59
FIGURE 18: (A) AFM MICROGRAPHS ROUGHNESS OF CdS THIN FILM AT 60°C; (B) AFM 3D MICROGRAPHS OF CdS THIN FILM	60
FIGURE 19: (A) AFM MICROGRAPHS ROUGHNESS OF ZNO THIN FILM AT 60°C; (B) AFM 3D MICROGRAPHS OF ZNO THIN FILM	61
FIGURE 20: (A) AFM MICROGRAPHS ROUGHNESS OF ZNS THIN FILM AT 60°C; (B) AFM 3D MICROGRAPHS OF ZNS THIN FILM	62
FIGURE 22: XRD PATTERNS OF CdO THIN FILM	64
FIGURE 23: XRD PATTERNS OF CdS THIN FILM.....	65
FIGURE 24: XRD PATTERNS OF ZNO THIN FILM.....	66

FIGURE 25: XRD PATTERNS OF ZNS THIN FILM	67
FIGURE 26: %T OF MULTILAYER CdO/CdS, CdS/CdO, ZNO/ZNS, AND ZNS/ZNO THIN FILM	70
FIGURE 27: SEM IMAGE OF MULTILAYER CdO/CdS THIN FILM	73
FIGURE 28: SEM IMAGE OF MULTILAYER CdS/CdO THIN FILM	74
FIGURE 29: SEM IMAGE OF MULTILAYER ZNO/ZNS THIN FILM	76
FIGURE 30: SEM IMAGE OF MULTILAYER ZNS/ZNO THIN FILM	77
FIGURE 31: (A) AFM MICROGRAPHS ROUGHNESS OF MULTILAYER CdO/CdS THIN FILM; (B) AFM 3D MICROGRAPHS OF MULTILAYER CdO/CdS THIN FILM	79
FIGURE 32: (A) AFM MICROGRAPHS ROUGHNESS OF MULTILAYER CdS/CdO THIN FILM; (B) AFM 3D MICROGRAPHS OF MULTILAYER CdS/CdO THIN FILM	80
FIGURE 33: (A) AFM MICROGRAPHS ROUGHNESS OF MULTILAYER ZNO/ZNS THIN FILM; (B) AFM 3D MICROGRAPHS OF MULTILAYER ZNO/ZNS THIN FILM	82
FIGURE 34: (A) AFM MICROGRAPHS ROUGHNESS OF MULTILAYER ZNS/ZNO THIN FILM; (B) AFM 3D MICROGRAPHS OF MULTILAYER ZNS/ZNO THIN FILM	83
FIGURE 35: XRD PATTERNS OF MULTILAYER CdO/CdS THIN FILM	86
FIGURE 36: XRD PATTERNS OF MULTILAYER CdS/CdO THIN FILM	87
FIGURE 37: XRD PATTERNS OF MULTILAYER ZNO/ZNS THIN FILM	88
FIGURE 38: XRD PATTERNS OF MULTILAYER ZNS/ZNO THIN FILM	89
FIGURE 39: %T OF INTERCALATED CdO/PVA/CdS, CdS/PVA/CdO, ZNO/PVA/ZNS, AND ZNS/PVA/ZNO THIN FILM	91
FIGURE 40: SEM IMAGE OF INTERCALATED CdO/PVA/CdS THIN FILM	94
FIGURE 41: SEM IMAGE OF INTERCALATED CdS/PVA/CdO THIN FILM	95
FIGURE 42: SEM IMAGE OF INTERCALATED ZNO/ZNS/PVA THIN FILM	96
FIGURE 43: SEM IMAGE OF INTERCALATED ZNO/PVA/ZNS THIN FILM	98
FIGURE 44: (A) AFM MICROGRAPHS ROUGHNESS OF INTERCALATED CdO/PVA/CdS THIN FILM; (B) AFM 3D MICROGRAPHS OF INTERCALATED CdO/PVA/CdS THIN FILM	99
FIGURE 45: (A) AFM MICROGRAPHS ROUGHNESS OF INTERCALATED CdS/PVA/CdO THIN FILM; (B) AFM 3D MICROGRAPHS OF INTERCALATED CdS/PVA/CdO THIN FILM	101
FIGURE 46: (A) AFM MICROGRAPHS ROUGHNESS OF INTERCALATED ZNO/PVA/ZNS THIN FILM; (B) AFM 3D MICROGRAPHS OF INTERCALATED ZNO/PVA/ZNS THIN FILM	102
FIGURE 47: (A) AFM MICROGRAPHS ROUGHNESS OF INTERCALATED ZNS/PVA/ZNO THIN FILM; (B) AFM 3D MICROGRAPHS OF INTERCALATED ZNS/PVA/ZNO THIN FILM	103
FIGURE 48: XRD PATTERNS OF INTERCALATED CdO/PVA/CdS THIN FILM	106
FIGURE 49: XRD PATTERNS OF INTERCALATED CdS/PVA/CdO THIN FILM	107
FIGURE 50: XRD PATTERNS OF INTERCALATED ZNO/PVA/ZNS THIN FILM	108
FIGURE 51: XRD PATTERNS OF INTERCALATED ZNS/PVA/ZNO THIN FILM	109

LIST OF TABLES

TABLE 1: RMS (R _q) AND RA OF THE MATERIAL DEPOSITION OF CdO, CdS, ZNO AND ZNS THIN FILM.....	63
TABLE 2: RMS (R _q) AND RA OF THE MATERIAL DEPOSITION OF CdO/CdS, CdS/CdO, ZNO/ZNS AND ZNS/ZNO MULTILAYER THIN FILM	84
TABLE 3: RMS AND RA OF THE MATERIAL DEPOSITION OF INTERCALATED CdO/PVA/CdS, CdS/PVA/CdO, ZNO/PVA/ZNS AND ZNS/PVA/ZNO MULTILAYER THIN FILM	104

LIST OF ABBREVIATIONS

Aluminum-doped zinc oxide (AZO)
Arithmetic average (Ra)
Atomic Force Microscopy (AFM)
Brillouin zone (BZ)
Building integrated photovoltaics (BIPV)
Chemical bath deposition (CBD)
Chemical Deposition (CD)
Chemical Solution Deposition (CSD)
Chemical Vapour Deposition (CVD)
Copper Indium Diselenide or Disulphide (CIS)
Conduction band minimum (CBM)
Dominant atomic (DA)
Self-interaction-corrected pseudopotentials (SIC-PP)
Dye-sensitized solar cells (DSSCs)
Electrodeposition (ED)
Energy dispersive X-ray spectroscopy (EDS)
Face-centered cubic (FCC)
Fluorine-doped tin oxide (FTO)
Copper indium gallium selenide (GIGS)
Liquid petroleum gas (LPG)
Local density approximation (LDA)
Metal oxide (MO)
Metal sulfide (MS)
Metal-organic chemical vapor deposition (MOCVD)
Microelectromechanical systems (MEMS)
Organic solar cells (OSCs)
Photo electrochemical cells (PEC)
Photovoltaic (PV)
Polyethylene glycol (PEG)

Polymers and layered inorganic materials for the formation of (PINCs)

Polyvinyl alcohol (PVA)

Root mean square average (RMS)

Scanning electron microscope (SEM)

Scanning probe microscope (SPM)

Scanning tunneling microscopy (STM)

Thermogravimetric (TG)

Tin-doped indium oxide (ITO)

Transitional metal chalcogenides (TMC)

Transparent conductive oxide (TCO)

Triethanolamine (TEA)

Ultraviolet-visible spectroscopy (UV-VIS)

Valence band maximum (VBM)

X-Ray Diffraction (XRD)

Yttrium stabilized zirconia (YSZ)

CHAPTER 1

1.1 Introduction

Deposition of the thin film is of immense interest in leading research laboratories. Previously there was a need for various costly equipment and they could be synthesized at a higher cost for advanced applications. The introduction of chemical routes enabled even rural educational institutes to establish simple techniques and deal with most advanced materials at low cost. This project strived to deposit monolayer thin film of metal sulfide (MS) and metal oxide (MO) films followed by multilayer deposition of MS/MO and MO/MS, lastly intercalation of the multilayer thin film with PVA. The general aim of the work presented in this dissertation was to deposit coatings of MS and MO multilayer thin film by chemical bath deposition (CBD) on a glass substrate.

This work was mainly focused on the deposition of CdO, CdS, ZnO, and ZnS multilayer thin films with intercalation of the polymer by varying the effect of the polymer on the deposited surface film. It was expected that the thickness of the deposited material should increase with an increase in the layer on the multilayer stack. Further to study the effect of layer insertion on the surface material as well as intercalated with a polymer. Transitional metal chalcogenides (TMC) of sulfides, oxides, selenides, and telluride remain vital in technological materials due to their vast application. The potential application of TMC of sulfides, oxides, selenides, and telluride are increasingly being recognized and the literature review showed that current and potential applications include solar control coatings, catalysts, microelectronic devices, sensors, optical filters and laser sources as studied by Yamaguchi, Savadogo, and Teteris [Yamaguchi, Yamamoto, Takaka, Demizi, & Yoshida, 1996], [Savago, 1998], [Sang, Shafarman, & Birkmire, 2002] and [Teteris, 2003].

Chalcogenide compounds of lead and copper have been the main focus for a significant number of investigations for these types of application. Cadmium oxide (CdO), cadmium sulfide (CdS), zinc oxide (ZnO), zinc sulfide (ZdS) and polyvinyl alcohol (PVA) were reviewed further in this report as the MO and MS multilayer deposition with and without a polymer intercalation by use of CBD technique due to their vast application that covers areas such as, solar control coatings, electronic and low-temperature gas applications. The

research study was to elaborate the matrix behavior of the MS and MO by varying the effect of the later matrix of multilayer thin film as well as the effect that the intercalation of a PVA on the stack. The field of material science and engineering community had the ability to create unique materials by using thin film technology with an extraordinary combination of chemical, physical and mechanical, properties that have continued to change modern society into pilot approach (i.e. smartphones). There is an increase in the new technological growth as far as thin film technology due to high demand in the market and continuous upgrade in society. Modern technology to date requires thin films for different applications [West, 2003]. Thin film technology is one of the basic of astounding developments in solid state electronics. The usefulness of the optical properties of metal films and scientific curiosity about the behavior of two-dimensional solids has been responsible for the immense interest in the study of science and technology of the thin films.

Thin film studies have directly or indirectly advanced in many new areas of research in solid state physics and chemistry which are based on the phenomena of uniquely characteristic of the thickness, geometry, and structure of the film [West, 2003]. In recent times, the study of semiconductors in the bulk has been replaced with that of thin films. Thin film technique is one of the most fully-fledged technologies that greatly contribute to developing the study of semiconductors by giving a clear indication of their chemical and physical properties. Thin films have mechanical, electrical, magnetic and optical properties which may differ from those of the bulk material and are used commonly in the form of a deposit on a suitable substrate. Presently, rapidly changing needs for thin film materials and devices are creating new opportunities for the development of new processes, materials, and technologies [Venables, 2003].

Considerations of a very thin film on some substrate, have a situation in which the two surfaces are so close to each other that they can have a decisive influence on the internal physical properties and processes of the substrate, which differ, therefore, in a profound way from those of a bulk material. In deposition of multilayer of MO and MS polymer intercalation thin film, the dimension of the material is reduced to an order of several

atomic layers which creates an intermediate system between macro systems and molecular systems, thus this provides a method of investigation of the microphysical nature of various processes that multilayers of MO and MS matrix with and without the polymer intercalation on the substrate. Thin films are especially appropriate for applications in microelectronics and integrated optics. However, the physical properties of the films like electrical resistivity do not substantially differ from the properties of the bulk material. For a thin film, the limit of thickness is considered between tenths of nanometer and several micrometers.

There are a variety of methods that have conventionally been used to prepare high quality of TMC. Each technique, however, has its own limitations, for example, solid state reaction requires the use of high temperatures to ensure the transition of solid reactants into the molten state. Spray pyrolysis, chemical vapor deposition (CVD) and vacuum evaporations are few techniques that also require high temperatures to enable the successful formation of the required chalcogenide. The heat is applied either directly by heating the reactants or indirectly through heating the substrate. Chemical solution methods such as hydrothermal, solvothermal, and chemical bath deposition (CBD) which is studied in this research generally requires low temperatures for successful generation of quality films [Chopra, Kainthla, Pandya, & Thakoor, 1982] making it a compatible and safe technique for laboratory scale tests. CBD as one of the chemical solutions used in this study requires low temperatures for good quality of growth of thin film on the substrate. These advantages make CBD technique a suitable method for deposition the MS and MO multilayer by controlling the temperature and pH to improve their properties as well as enhancing the properties by introducing a polymer onto to embedded multilayer stack.

In CBD, the chalcogenide film formed when the substrate is immersed into a dilute, generally alkaline solution containing metal ions and an appropriate source of chalcogenide ions. Complexation of the metal ions enables the rate of the reaction to be controlled. The chalcogenide anion is usually generated by the decomposition or hydrolysis of an organic or inorganic precursor.

CBD is widely used in the laboratory and industry for the creation of thin films and nanostructures for semiconductors and photovoltaic, its actual molecular workings have remained something of a mystery. This has somewhat limited its utility because precise tailoring of CBD products is not possible without a clear understanding and thus control of CBD mechanics. Despite the advances that have been made using CBD, the full development of the technology has been hampered by poor understanding of the relationship between process chemistry and film structure, factors that are dependent on the properties of the bath and deposition precursor. The process is sensitive to precursor concentrations and to the substrate used [Shandalov & Golan, 2003]. This becomes more of a challenge when more than one layer is deposited onto the substrate. These results to some of the problem associated with CBD which was studied in details in this study as the optimal deposition parameters are generally different for each compound deposited.

Although it is has been difficult to obtain simultaneously a high transmittance coefficient and good conductivity, these properties of CdO thin films have been reported by [Ortega, Sanatana, & Acevedo, 1999]. Regardless of CBD being more cost-effective, it has been reported by [Call, Jabern, Seshan, & Whyte, 1980] that MO deposited by CBD partially deposit on the substrate as well having cracks. To overcome the problem an understanding of the relationship of the process chemistry and understanding the ratios into details was carried out by employing polymer matrix to the embedded MO/MS multilayer thin film. The integration on inorganic into a polymer matrix allows both properties to be enhanced and thus advanced new functions can be generated. Therefore intercalation of the metals and polymer such as polyvinyl alcohol (PVA) was introduced in this study where the polymer controls the viscosity and binds metal ions of MO and MS, resulting in a homogeneous distribution of metal precursors in the solution and the formation of uniform metal–organic films.

The polymer, on the other hand, is flexible, lightweight materials and can be produced at a low cost. Polymers are known to allow easy processing and can be shaped to thin films by various techniques. Polymers are already widely used in the optoelectronics industries. Both the deposition products and the deposition solutions are studied in order to clarify the

deposition mechanism, with special emphasis on the question how the polymer control the process. The function of the PVA in this study was to verify that can CBD technique be used to deposit a polymer and does PVA enhance the multilayer deposition of MO and MS structure. The matrix of the MO and MS was studied in details as to which order must the matrix be deposited on the substrate before and after intercalation can take place.

The control of stoichiometry is not always possible for organic/inorganic owing to differences in chemical reactivity among the metals, which is a great challenge to have to encounter. This study was compared if the latter feature that makes it possible to grow simple and complex crack-free epitaxial MO of CdO and ZnO as well MS of ZnS and CdS multilayer with the presence of PVA intercalation. Although there have been numerous papers published reporting the preparation of chalcogenide thin films using CBD [Kaur, Pandya, & Chopra, 1980] point out that the criticism that the process of CBD has remained recipe oriented with a little understanding of the kinetics of the process. With a few exceptions, this is also true regarding a mechanistic understanding of the process. There is, therefore, a need for careful investigations of the CBD process and identification of the conditions that favor high-quality coherent deposits of multilayer CdO/CdS and ZnO/ZnS with PVA intercalation carried out in this study.

1.2 Problem statement

It has been determined that the mechanism in terms of chemical reaction and technique in which a film grows can be determined by the quality and the properties of the resulting film. MS thin films deposited by CBD generally exhibit poor adhesion and MO exhibit cracking therefore, intercalation with a polymer was studied in the MO/MS multilayer as part of solving the problem associated with thin film deposition. When using CBD technique precipitate formation in the bulk solution is an inherent problem. This normally results in unnecessary precipitation and loss of material during film deposition on a glass substrate. The chemical deposition technique involves the use of dilute solutions of compounds involved in the reaction [Chopra K. K., 1982].

This offers minimum toxicity and occupational hazards since the vapor phase of the reactants are avoided. It is well known that toxicity hazards associated with lead, cadmium,

mercury, selenium etc., are severe when inhaled. Further, the unreacted ions can be precipitated in the bath as sulfides or selenides and the solid can be separated and stored for use or recycled to produce starting material. The formation of multilayer films by interdiffusion and recrystallization in multilayer films can be considered as an environmentally sound process since very few effluents are produced. Overall, the large-area capability and the ease of scaling up with complete control of material handling in solid or liquid phase offers perspective toward the industrial production of coatings and devices by the chemical bath deposition technique.

Although CBD has a number of advantages over other more intensive methods thin film deposition, has a limitation. It has been claimed by [Bayer, Boyle, Heinrich, O'Brien, Otway, & Robbe, 2000] and [Boyle, Bayer, Heinrich, Robbe, & O'Brien, 2000] that in the case of CBD of CdS, only approximately 2% of the initial cadmium concentration is used in film formation, resulting in high levels of cadmium waste. This along with the volatility of ammonia (commonly used in the bath solutions) on a large scale of CBD operations, lead to a significant environmental hazard if not addressed were studied by Kostoglou, Bayer, and Bayer [Kostoglou, Andritsos, & Karabelas, 2003], [Bayer, Boyle, Heinrich, O'Brien, Otway, & Robbe, 2000], and [(Boyle, Bayer, Heinrich, Robbe, & O'Brien, 2000)]. Homogeneous precipitation and deposition of the chalcogenide material on the walls of the reactor vessels are also limitations of the method. These reagents effect of depleting of chemical bath (CB) of vital which, in turn, leads to a reduction in both film thickness and film quality [Bayer, Boyle, Heinrich, O'Brien, Otway, & Robbe, 2000] and [Herrero, Gutierrez, Dona, Martinez, Chaparro, & Bayon, 2000]. The presence of contaminants, introduced during the deposition process can also result in a reduction in film quality and performance [Kostoglou, Andritsos, & Karabelas, 2003].

In order to make the CBD process more economical, not only the financially aspects but also the state of art in terms of maximum yield, various methods have been employed such as CVD and MOCVD. These methods serve to minimize the extent of particulate growth within the solutions. To archive this aim, techniques such as the careful spacing of the substrate in the bath solution [Nair, Garcia, Gomez-Daza, & Nair, 2001], and [Readigos,

Garcia, Gomez-Daza, Campos, Nair, & Nair, 2000] and the minimisation of the initial concentrations of reagents [Oladeji, et al., 2000] and [Oladeji & Chow, 1997] have been reported in the literature. In an attempt to minimize the environmental impact of cadmium residues from CBD bath, a method was developed whereby excess cadmium could be recovered and the reagents recycled [Bayer, Boyle, Heinrich, O'Brien, Otway, & Robbe, 2000] and [Boyle, Bayer, Heinrich, Robbe, & O'Brien, 2000]. It was also noted that by keeping the bath solution at a lower temperature and heating only the substrate, both homogeneous precipitation and deposition onto the walls of the reaction chamber could be minimized.

Observations made by Nair and Nair was that for constant bath composition, an increase in bath temperature reduced the induction period, but produced films with poor adhesion to a glass substrate [Nair & Nair, 1989]. Issues with multilayer designs are surface roughness that increases with total film thickness (increased scattering losses) and precise film thickness control necessary for photonic band gap structure.

1.3 Aims and objectives

It has been proposed that the mechanism by which a film grows can determine both the quality and the properties of the resulting film. The aim of this study was to investigate the deposition of metal sulfide (MS) and metal oxides (MO) by intercalating with a polymer using the CBD technique. In order to achieve the aim of this study, the following objectives were adopted:

- ✓ To investigate the effect of MO-MS or MS-MO multilayer matrix with and without polymer intercalation
- ✓ To determine optical properties of the deposited thin films using Uv-Vis spectroscopy
- ✓ To characterize the deposited thin films surface morphology by SEM and EDX
- ✓ To characterize the deposited thin films structural analysis by AFM
- ✓ To evaluate the crystal structure of the thin films by XRD

The XRD techniques was utilized for crystal structure, average grain size and elemental analysis of the thin film. The surface morphology texture & surface roughness was studied by SEM and AFM, and optical properties of the thin film was studied by optical absorption measurements. The main goal of this magister research activity was the study of chemical bath deposition of multilayer thin film of MO and MS of ZnO, CdO, CdS and ZnS thin films on glass substrates. In particular, the most important synthesis parameters (such as temperature and time and solution pH value) were examined in-depth for single layer thin films prior commissioning multilayer thin film. The deposited layers were characterized from a structural, morphological and optical.

CHAPTER 2

2.1 Literature review

Semiconductor thin film technology has attracted much attention, because of its unique size dependent properties and applications in the optoelectronics devices, solar cells, sensors and laser materials. Thin film deposition processes have developed very rapidly over the past 25 years, particularly in the context of semiconductor devices [Ohring, 1992] and [Venables, 2003]. Sulfide thin films such as zinc sulfide (ZnS) have generated a lot of interest among scientists because of its extensive use in the fabrication of solid state devices. There is a diverse range of applications of thin films of this semiconductor and this is reflected in a large amount of literature available on its properties reported by various authors using different deposition techniques. In 2008, Ilenikena [Ilenikhena, 2008] successfully produced semiconductor thin films of copper sulfide (CuS) and zinc sulfide (ZnS) on glass microscope slides at 320 K and pH values of 7, 9, 10, 11 and 12 using improved chemical bath deposition method. The results show that pH increases with the optical and solid-state properties (such as transmittance, thickness, absorbance and so on) of the films. The deposition of ZnS thin film was varied at different temperature of 60, 70 and 90°C at different pH ranging from 1.6 to 11. This research produced the thin film at pH of 11 at temperatures of 60°C for 120 minutes by use of chemical bath deposition technique following by multilayer deposition of ZnS/ZnO the intercalation with PVA to form a thin film of ZnS/PVA/ZnO.

The results obtained by [Nadeem, Ahmed, & Wasiq, 2005] and [Ndukwe, 1996] on the optical absorbance of ZnS thin films for wavelengths in the infrared (up to 1000 nm) and visible spectrum showed that ZnS is practically non-absorbing in these regions. Similar behavior was previously observed by [Hammer, 1943] in the visible region. ZnS films deposited on the glass substrate at room temperature have shown an enhanced absorption in the area of $\lambda = 330$ nm [Nadeem, Ahmed, & Wasiq, 2005] expected to have a fine-grained structure. The absorption peak shifts towards longer wavelength with increasing thickness. [Ndukwe, 1996], observed that some ZnS films have high absorbance (~0.56) in the near infrared and low absorbance (~0.01 – 0.1) in the

ultraviolet and visible region. This research also produced ZnS thin film with absorption high absorption (~ 0.54) at higher temperatures of 70 and 90°C and lower pH values which recommended the deposition of ZnS at relatively lower temperatures of 60°C at a high pH. ZnS films prepared by [Nadeem, Ahmed, & Wasiq, 2005] using resistive heating technique had a high transmittance (60–99 %) in the visible and near-infrared region; the reported transmittance of ZnS was 83-90 %. ZnS thin films coated on (Germanium) Ge [Yamaguchi, Yamamoto, Takaka, Demizi, & Yoshida, 1996] using ionized cluster beam (ICB) method were found to have a transmittance of 96 %. So they are used as an antireflection coating for the optical transmission window. [Yamaguchi, Yamamoto, Takaka, Demizi, & Yoshida, 1996], deposited the (Cd, Zn)S thin films on a glass substrate using chemical bath deposition (CBD) technique for photovoltaic devices.

Thin films with zero concentration of Cd demonstrated more than 70 % transmittance at Wavelengths longer than 600 nm. ZnS films grown by [Ndukwe, 1996] had a high transmittance (~ 64 –98 %) in the visible and near infrared regions. He also observed that some of the films had low transmittance (~ 30 –37 %) in near infrared region and high transmittance (~ 78 –98 %) in the visible and ultraviolet region. The transmittance of ZnS films grown on polyester foils [Lindroos, Kannianen, & Leskela, 1997] using successive ionic layer adsorption and reaction method was more than 60 % above 400 nm.

Many researchers have deposited CdS thin films from an aqueous, alkaline and non-aqueous medium. Several techniques have been used to fabricate CdS thin films, such as electrodeposition, chemical bath deposition (CBD), screen printing (SP) and physical vapor deposition (PVD). Today, there has been a need for efficient, low temperature and low-cost deposition methods of material preparations for thin films as technological industrial applications. Chemical bath deposition (CBD) is a soft solution process that is capable of producing the high-quality thin film at relatively low temperature. Historically, the first application of CBD was reported [Reynolds, 1884] for the fabrication of lead sulfide (PbS) photoconductive detectors in 1884. The reaction proceeded in a basic solution and a strongly adherent layer was formed on the interior surfaces of the reaction vessel. The general review for CBD was published by [Chopra K. K., 1982] and

[Lokhande, 1991] for deposition of metal chalcogenides which also deposited 0.0 % Cd. The review by [Nair P. , *et al.*, 1998] reported on their extensive work in the field on solar energy related issues. A large number of studies have been carried out to reach the goal in order to produce CdS thin films with good optoelectronic properties suitable for photovoltaic applications. [Ates, Yildirim, Kundakci, & Yildirim, 2007], have deposited CdS thin films by solution growth method using CdCl₂, Na₂S in the alkaline medium on a glass substrate, this work has deposited CdS using cadmium acetate, ammonium hydroxide and thiourea by CBD technique. The optical properties have been investigated as a function of temperature. [Khomane, 2011], reported the deposition CdS thin films using polysulfide as a sulfide source at room temperature. It has been observed that films are polycrystalline in nature with cubic and hexagonal phase.

[Kawar, 2011], have synthesized CdS thin films using CdSO₄, thiourea and ammonia solution and have reported its photovoltaic applications. It has been observed that band gap decreases with a decrease in particle size. [Nanda, Sarangi, & Sabu, 1998], prepared CdS of different crystalline size over metal/glass substrates by a precipitation technique using precursors as CdSO₄, thiourea, and NH₄OH. The different crystalline sizes were obtained by controlling the reaction time period/thickness, temperature, and pH of the solution. Nanocrystalline CdS showing quantum size effect were prepared at 300 K having solution pH=11.7. SEM study shows CdS films were homogeneous and without cracks and covered substrate. [Dongre, Nongriya, & Ramrakhiani, 2009], synthesized flower like CdS nanostructured films and they studied their application in photoelectrochemical solar cells, this work synthesized spherical like CdS nanostructured films. The films of CdS on this report have been grown on glass substrates by a CBD technique using precursors as Cd(CH₃COO)₂.2H₂O, thiourea and NH₄OH were spherical in shape.

2.2 Thin film

A thin film is a layer of material ranging from fractions of a nanometer (monolayer) to several micrometers in thickness. The thin film is also regarded as a very thin layer of a

substance on a supporting material; especially: a coating (as of a semiconductor) that is deposited in a layer one atom or one molecule thick. Electronic semiconductor devices and optical coatings are the main applications benefiting from thin film construction. A familiar application of thin films is the household mirror which typically has a thin metal coating on the back of a sheet of glass to form a reflective interface. The process of silvering was once commonly used to produce mirrors.

A very thin film coating (less than a nanometer) is used to produce two-way mirrors. The performance of optical coatings (e.g. antireflective, or AR {anti-reflection} coatings) are typically enhanced when the thin film coating consists of multiple layers having varying thicknesses and refractive indices. Similarly, a periodic structure of alternating thin films of different materials may collectively form a so-called superlattice which exploits the phenomenon of quantum confinement by restricting electronic phenomena to two-dimensions.



Figure 1: Deposited thin film on a glass substrate (thin film of CdS deposited by CBD)

Preparative Parameters: Usually inexpensive precursors such as metal nitrate, chloride, acetate are typically used for forming solutions to use in CBD technique; this research a medium of acetate was used. Figure 1 illustrates the deposition of CdS thin film deposited by CBD technique. The following preparative parameters are important in order to obtain desired final product thin or thick film.

Substrate surface temperature: The pyrolytic decomposition behavior of precursor salt solution is decided by substrate surface temperature. Decomposition of salt plays an important role in film formation. It is always preferred to understand decomposition behavior by performing thermogravimetric (TG) analysis of salt; before selecting desired substrate surface temperature. When a droplet hits the surface of the substrate multiple processes occur at the same time, evaporation of the solvent, spreading of the droplet, and salt decomposition. Various schemes have been proposed. Most of the investigators suggest that only a kind of CVD process gives high-quality films by spray pyrolysis.

Solution flow rate: The solution flow rate has to be optimum, although it affects film morphology negligible. It should not exceed the optimum value otherwise rapid cooling of the substrate may lead to cracking of substrate in the case of the glass substrate. The optimum value depends on the type of atomizer, deposition temperature, nozzle to substrate distance, etc. Typically, several mL/min flow rate is desirable [Desai, Pathan, & Joo, 2005].

Nature of salt: Ordinarily available inexpensive precursor salts is a great advantage in CBD. The additional requirements of salt are viz. it should be aqueous soluble or alcoholic solvents with low decomposition temperature. Usually, chlorides, nitrates, acetates or metal-organic salts have been used. Amongst them, chlorides provide high solubility in water and ethyl alcohol, but chemical corrosion of the in the CBD set up and to some extent surroundings. Another important aspect for the reduction of costs in the area of raw materials used for the synthesis of thin films is the implementation of the use of reagents that are inexpensive and generate higher yields. A clear example of this is the substitution of KOH, the commonly used alkali, by NaOH, which is a more advantageous reagent. The most relevant subjects that were considered for this comparison are the hygroscopicity and absorption of carbon dioxide (CO₂) from the environment, the purity and the price of the commercial presentations. In the cases of water and CO₂ absorption, it is well-known that KOH is more hygroscopic than NaOH in fact, KOH is a desiccant of greater intensity than NaOH [Armarego & Chai, 2009] and it is a better absorber of CO₂ compared with the absorbing capacity shown by NaOH

[Singhal, 2012]. Also, there are some reports that showed that KOH aqueous solutions are better CO₂ absorbers than NaOH aqueous solutions was reported by Ledig, Blum, and Strotmann [Lepig, 1924], [Blum, Stutzman, & Dodds, 1952] and [Strotmann, Reuschenbach, Schwarz, & Pagga, 2004]. For reagent solution preparation and storage purposes, these aspects are a disadvantage of KOH, since to prevent rapid loss of purity due to the absorption of water and the formation of carbonate (CO₃⁻² as a consequence of absorption of CO₂ [Blum, Stutzman, & Dodds, 1952], its handling requires more care compared with NaOH.

Solvent: The physical properties of the solution such as boiling point, the solubility of salts, spreading behavior of droplets on the substrate are bound to change due to solvent. It is reported that it is necessary to use a solvent with a high boiling point in order to deposit a dense film [Ruiz, Vesteghem, Giampaolo, Di, & Lira, 1997]. By employing methanol and ethanol solution mixture of magnetite and hematite phases have been reported [Desai, Pathan, & Joo, 2005]. This has been attributed to be mainly due to under the identical conditions of deposition, the heat of combustion of solvent influences crystalline structure and morphology also.

Additives in precursor solutions: There are scarce reports regarding the role of additives in the precursor solutions [Perednis, 2003]. The lower surface roughness has been obtained by adding polyethylene glycol (PEG) as an additive in the case of yttrium-stabilized zirconia (YSZ) thin film deposition. The polymer improves the spreading behavior of the deposition on the substrate. The results demonstrate a significant role of additives on the microstructure of the films [Perednis, 2003].

Deposition time: Deposition time does not have a remarkable effect on the film morphology. The More the deposition time, the more film formed remaining on the hot substrate surface which may be one of the reasons for the change in the morphology. One would think that the synthesis of CdS thin films at room temperature, or simply at low temperatures, is an advantage in the applying of a given chemical formulation in the deposition process. However, several authors have reported explicitly or implicitly that the lower the reaction temperature the lower the thin film growth rate [Kaur, Pandya, &

Chopra, 1980], [Mondal, Chanudhuri, & Pramanik, 1983], [Nair, Nair, & Campos, 1988], and [Sebastian & Nair, 1992]. Thus, without delving into the cases in which homogeneous precipitation is favoured, which limits the maximum d —a limit which was directly reported by [Kaur, Pandya, & Chopra, 1980] and [Mondal, Chanudhuri, & Pramanik, 1983] or simply evident in the results reported [Gutiérrez-Lazos, *et al.*, 2008], [Liu, *et al.*, 2010], and [Ouachtari, Ramili, El Bachir, Bouaoud, Erguig, & Elies, 2011] by some authors the use of low temperatures lengthens the time required to achieve a thin film with determined d compared to the time required at higher temperatures.

The time between two consecutive inter-layers: This parameter provides sufficient time for accumulation of the particles at a high temperature that is formed due to decomposition; otherwise undesirable crack formation on film surface due to thickness is obvious [Desai, Pathan, & Joo, 2005]). Sufficient time between two successive sprays enables substrate surface to attain temperature enough for decomposition of precursor particle.

The substrate to nozzle separation: Each nozzle has a spraying cone formed in PSPD set up. The larger the distance of the atomizer to the substrate, the smaller the deposition rate and the larger the area of coating covered. Ordinarily, 20-30 cm distance between substrate and nozzle are typical.

Deposition rate: Deposition rate measurement in terms of film thickness is rather difficult. Thickness measurement by profilometer requires sharp steps between a film and a substrate - which is very difficult to achieve in the spray pyrolysis process but this is achievable by use of CBD. SEM analysis which is used in this research is the most reliable of all the techniques mentioned but is time-consuming. A quick but approximate estimate of deposition rate in terms of film thickness is possible by gravimetric weight difference method [Desai, Pathan, & Joo, 2005] but this technique is not used in this research.

2.3 Applications of thin film

Although the study of thin film phenomena dates back well over a century, it is really only over the last four decades that they have been used to a significant extent in practical situations. The requirement of micro-miniaturization made the use of thin and thick films virtually imperative. The development of computer technology led to a requirement for very high-density storage techniques and it is this which has stimulated most of the research on the magnetic properties of thin films. Many thin film devices have been developed which have found themselves looking for an application or, perhaps more importantly market. In general, these devices have resulted from research into the physical properties of thin films.

Secondly, as well as generating ideas for new devices, fundamental research has led to a dramatic improvement in understanding of thin films and surfaces. This, in turn, has resulted in a greater ability to fabricate devices with predictable, controllable and reproducible properties. The cleanliness and nature of the substrate, the deposition conditions, post-deposition heat treatment, and passivation are vital process variables in thin film fabrication. Therefore, prior to this improvement in our understanding of thin films, it has not really been possible to apply them to real devices. Thirdly, much of the finance for early thin film research originated from space and defence programmes to which the device cost is less important than its lightweight and other advantages, the major applications of thin film technology are not now exclusively in these areas but rather often lie in the domestic sector in which low cost is essential [West, 2003] and [Chopra K. , 1969].

Thin film materials have already been used in semiconductor devices, wireless communications, telecommunications, integrated circuits, rectifiers, transistors, solar cells, light-emitting diodes, photoconductors, light crystal displays, magneto-optic memories, audio and video systems, compact discs, electro-optic coatings, memories, multilayer capacitors, flat-panel displays, smart windows, computer chips, magneto-optic discs, lithography, microelectromechanical systems (MEMS), and multifunctional emerging coatings, as well as other emerging cutting technologies.

2.3.1 Optical Coatings

An optical coating is one or more thin layers of material deposited on an optical component such as a lens or mirror, which alters the way in which the optic reflects and transmits light. One type of optical coating is an antireflection coating, which reduces unwanted reflections from surfaces, and is commonly used on spectacle and photographic lenses. Another type is the high reflector coating which can be used to produce mirrors which reflect greater than 99.99 % of the light which falls on them. More complex optical coatings exhibit high reflection over some range of wavelengths, and anti-reflection over another range, allowing the production of dichroic thin-film optical filters.

2.3.2 Optoelectronic

An optoelectronic thin-film chip, comprising at least one radiation-emitting region in an active zone of a thin-film layer and a lens disposed downstream of the radiation emitting region, said lens being formed by at least one partial region of the thin-film layer, the lateral extent of the lens being greater than the lateral extent of the radiation emitting region. The thin-film layer is provided for example by a layer sequence which is deposited epitaxially on a growth substrate and from which the growth substrate is at least partly removed. That is to say that the thickness of the substrate is reduced. In other words, the substrate is thinned. It is furthermore possible for the entire growth substrate to be removed from the thin-film layer.

The thin-film layer has at least one active zone suitable for generating electromagnetic radiation. The active zone may be provided for example by a layer or layer sequence which has a pn junction, a double heterostructure, a single quantum well structure or a multiple quantum well structure. Particularly preferably, the active zone has at least one radiation-emitting region. In this case, the radiation-emitting region is formed for example by a partial region of the active zone. Electromagnetic radiation is generated in said partial region of the active zone during operation of the optoelectronic thin-film chip.

2.4 Principles of Chemical Bath Deposition (CBD)

Thin films can be deposited by a number of physical and chemical techniques as classified in figure 2. amongst the methods mentioned above, the chemical methods are economical and easier than that of the physical methods. Physical methods are expensive but give relatively more reliable and more reproducible results. Most of the chemical methods are cost effective, but their full potential for obtaining device quality films has not been fully explored [Chopra K. , 1969]. However there is no ideal method to prepare thin films, to satisfy all possible requirements. The electrodeposition technique (ED) is the most popular technique today because a large number of conducting and semiconducting thin films that can be prepared by this technique. Amongst the chemical methods of thin film depositions, CBD is probably the simplest method available for this purpose and it is also known as chemical solution deposition (CSD) or chemical deposition (CD). CBD is not a new technique as early as in 1835 Liebig reported the first deposition of silver, the silver mirror deposition using a chemical solution technique [Liang & Gordon, 2007].

The deposition technique was first described in 1869. The only requirements of these methods were a vessel to contain the solution (usually an aqueous solution of common chemicals) and the substrate on which deposition is to be carried out. In addition to this various complication such as some mechanism for stirring and a thermos stated bath to maintain a specific and constant temperature are options that may be useful. The first general review on this topic was published by [Chopra K. K., 1982]. Next review was published by [Lokhande, 1991]. Then a comprehensive and general review was published by [Lincol, Forment, Cachet, Alkite, & Kolb, 1998].

Chemical deposition is the deposition of films on a solid substrate from a reaction occurring in a solution using the prototypical MS (metal sulphide) as an example, M salt in solution can be converted to MS by adding sulphide ions (i.e. H_2S), MS immediately precipitates unless the solution is very dilute a few millimolar or less in which case MS often forms as a colloidal solution. Another pathway for MS formation, one that does not require free sulfide ions, is decomposition of an MS-this complex. In MS, the trick is to

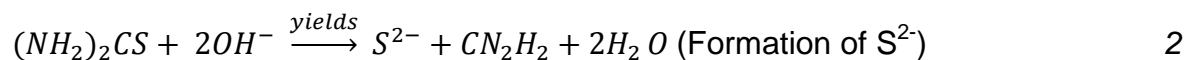
control the rate of these reactions so that they occur slowly enough to allow the MS either to form gradually on the substrate itself (at the early stages of deposition) or to the growing film, rather than aggregate into larger particles in solution and precipitate out.

This rate control can be accomplished by generating the sulfide slowly in the deposition solution. The rate of generation of sulfide, and therefore reaction, can be controlled through a number of parameters, in particular, the concentration of sulfide forming precursor, solution temperature, and pH. Although CBD can be carried out both acidic and alkaline solutions, most of the CBD reactions have been carried out in alkaline solutions.

2.4.1 Basic Mechanism of Chemical Bath Deposition

In spite of the fact that CBD has been in use for a long time and that the reactions involved appear to be quite simple, the mechanism of the CBD process is often uncertain. There are several different mechanisms of CBD. These can be divided into four fundamentally different types. Deposition of cadmium sulfide (CdS) is taken as an example.

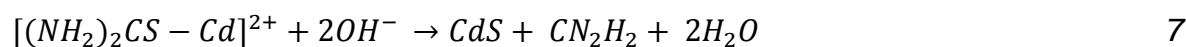
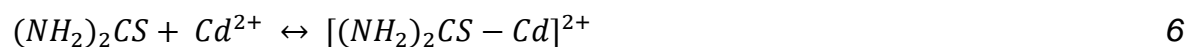
1) The simple ion by ion mechanism



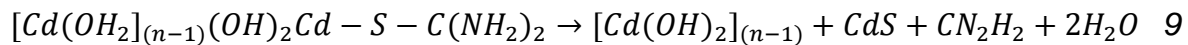
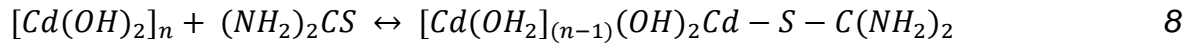
2) The simple cluster (hydroxide) mechanism



3) The complex decomposition ion - by - ion mechanism



4) The complex decomposition cluster mechanism



The last reaction continues until the conversion of all the $Cd(OH)_2$ to CdS . The first two mechanisms involved free sulfide ions (or other anions). While the last two are based on breaking of a carbon-chalcogen bond and do not involve the formation of free chalcogenide [Hodes & Dekker, 2003]. Chemical reaction either takes place on the surface of the dipped substrate or in the solution itself, where a mixing of components on the surface to be coated is required. Most of the coatings are formed in a two-step fashion:

- i. "Sensitizing" the surface for the nucleation reaction of the adhering coating layer.
- ii. Deposition of the coating by selected reactions.

The most widely used deposition methods are listed below

- *Homogeneous chemical reduction* of a metal ion solution by a reducing agent regardless the substrates.
- *Electroless plating* for the deposition of the metallic coating by controlled chemical reduction that is catalyzed by the metal or alloy being deposited.
- *Conversion coatings* forming a sacrificial layer containing a compound of the metal substrate.
- *Displacement deposition or galvanic deposition* makes use of the electronegativity differences of metals.
- *Arrested precipitation technique* means a metal ion is arrested by an organic complexing agent which is then made available by slow dissociation of the organometallic complex at specific pH value.

Among the various chemical deposition systems, CBD has attracted a great deal of attention because of its overriding advantages over the other conventional thin film deposition methods. The CBD method for the preparation of thin films has recently been shown to be an attractive technique because of its simplicity, convenience, low cost and low temperature, and it has been successfully used for depositing ternary metal chalcogenide thin films [Sharma, Patil, Bhavsar, Patil, & Dori, 1999]. Understanding of

the chemistry and physics of the various process involved in deposition processes has now made it possible to obtain undoped/doped, multicomponent semiconductor thin films of usual or unusual and metastable structure.

2.4.2 Selection of Deposition Process

No single technique is ideally suited for preparation of large area thin films with all the desired properties. Hence choice and selection of deposition process play a vital role in the formation of good quality thin films, and while selecting a particular technique it should be tested satisfactorily for the following aspects:

- Cost effectiveness
- It should be able to deposit desired material
- Film microstructure and deposition rate should be controlled
- Stoichiometry should be maintained as that of the starting materials
- Operation at reduced temperature
- Adhesive at reduced temperature
- Abundance of deposit materials
- Scaling up of the process
- Masking of the substrates
- Control of film substrate interface and defects created in the film

Among the various techniques discussed above, arrested precipitation technique as well as electrodeposition technique used for the synthesis of binary transition metal dichalcogenides and hybrid process of these two is employed in the synthesis of ternary mixed transition metal dichalcogenide in the present investigation. As mentioned in chapter one, CBD method is most commonly used because it is a very simple, cost-effective and economically reproducible technique that can be applied in large area deposition at low temperature. CBD is used to deposit thin films of a wide-range of materials [Nair P. , *et al.*, 1998] and [Savago, 1998].

The deposition mechanism is largely the same for all such materials. A soluble salt of the required metal is dissolved in an aqueous solution, to release cations. The non-metallic

element is provided by a suitable source compound, which decomposes in the presence of hydroxide ions, releasing the anions. The anions and cations then react to form the compound [Johnson, Corletto, Reddy, Forbes, & Miles, 2002].



Figure 2: Set up of the chemical bath deposition technique (CBD)

Figure 2 demonstrate the CBD setup technique used in this research. The source materials used in this work were cadmium acetate $[Cd(AcO)_2]$, thiourea (H_2NCSNH_2) , ammonium hydroxide 25 % (NH_4OH) , polyvinyl alcohol (PVA), Zinc acetate $[Zn(AcO)_2]$. This technique is based on the controlled release of metal ion (M^{2+}) and sulfide (S^{2-}) or oxide (O^{2-}) ions in an aqueous bath in which the substrates are immersed. In this process, the release of metal ion (M^{2+}) is controlled by using a suitable complexing agent. The deposition begins with nucleation phase followed by growth phase in which the thickness of the film increases with duration up to the terminal phase where film depletion into constituent ions occurs after a certain time [Dongre, Nongriya, & Ramrakhiani, 2009]. Typical CBD processes for sulfides employ an alkaline medium containing the chalcogenide source, the metal ion, and added base.

A chelating agent is used to limit the hydrolysis of the metal ion and impart some stability to the bath, which would otherwise undergo rapid hydrolysis and precipitation. The technique under these conditions relies on the slow release of ions into an alkaline solution in which the free metal ion is buffered at a low concentration for example as shown in figure 3 the metal chalcogenide. There are a few reports of the CBD of the binary ZnS [Chopra K. K., 1982] and [Padam, Rao, & Maholtra, 1988], the most convincing studies demonstrate that the production of good quality thin films is very difficult by conventional chemical bath systems [Al-Sabayleh, 2008], due to the stability of hydroxyl species. Unlike, cadmium and lead chalcogenides in which the formation of hydroxide species in solution is an important factor for the formation of high-quality films as illustrated below, ZnS is not favored with the hydroxide formation.

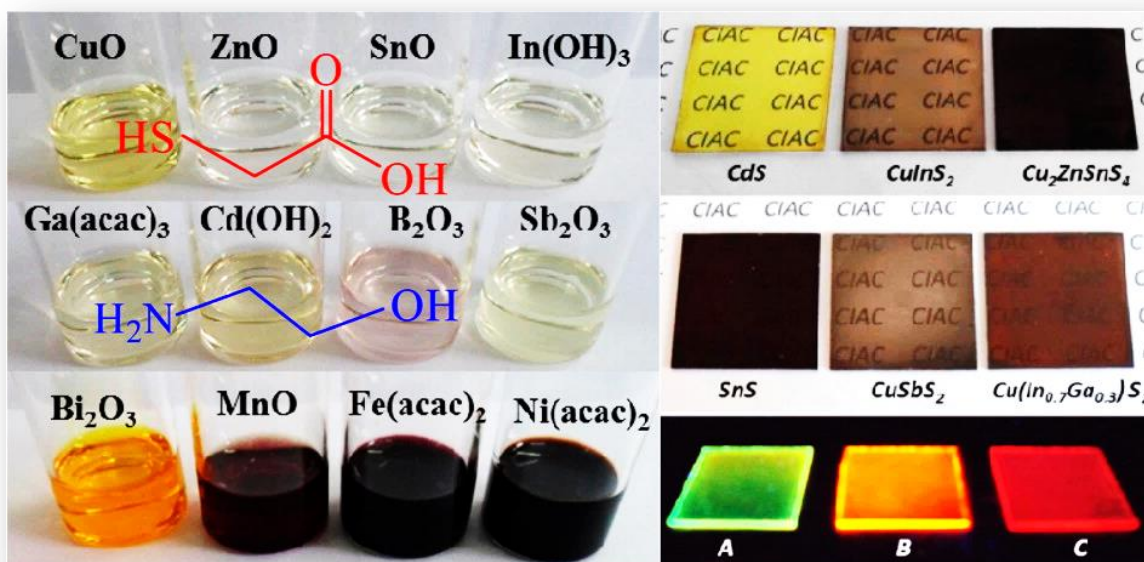


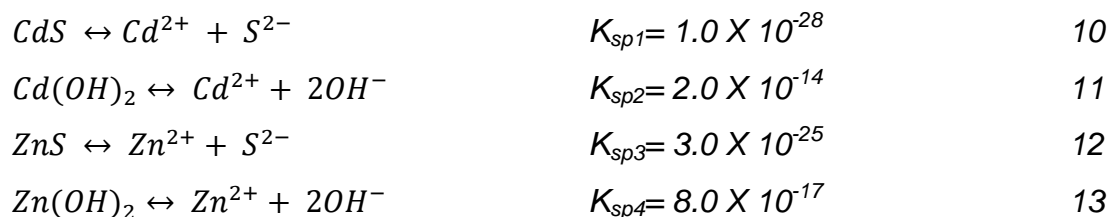
Figure 3: Examples of deposited film of metal chalcogenide [Zhang, *et al.*, 2016]

The problem statement further expand at the relatively small difference in the solubility products of ZnS and ZnOH that leads to possible competition between the formation of sulfide and hydroxide in alkaline solutions, with the presence of significant quantities of oxides or hydroxides observed in CBD zinc sulfide films [O'Brien & McAleese, 1998], thus in this study ZnO is studied. For this reason, hydroxide formation needs to be

minimized in order to form quality CBD-ZnS thin films [Edelson, 2007]. This has led to the development of a more favorable medium for the formation of ZnS thin films. Development was made by [Lincot, Froment, & Cachet, 1999] about the deposition of ZnS from acidic solutions in which urea hydrolysis is used to control the pH and produced among the best ZnS films reported to date.

2.5 Chemistry of bath deposition of Zn and Cd oxide and sulfides

Chemistry of Zn and Cd are similar in many aspects, so it might be expected that deposition of their chalcogenides is also similar. However, there is a significant difference in their chalcogenide formation tendency. This difference is caused by the large solubility product difference for various compound formations.

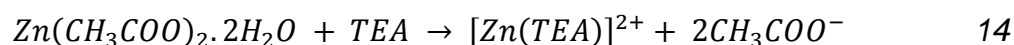


The tendency of zinc ions to form hydroxides is almost two orders of magnitude higher as compared to that of cadmium ions as can be calculated by solubility products of $Zn(OH)_2$ and $Cd(OH)_2$. Whereas sulfide formation tendency is lower for zinc ion. Therefore, for ZnS deposition, it is important to have lower pH values as compared to CdS deposition. However, if too low pH value is maintained, the very slow rates of hydrolysis of thiourea limit the reaction rates. In an alkaline solution CdS, deposition is preferred over ZnS. For $Zn_xCd_{1-x}S$ deposition, the free Cd^{2+} concentration must be much lower than the free Zn^{2+} concentration in the solution in order to deposit ZnS according to simple solubility product considerations.

The strength of complexation (with NH_4OH) is almost comparable, therefore it is possible to adjust the complexant concentration such that there is no $Cd(OH)_2$ present in the solution. In that case, CdS deposition occurs by ion-to-ion mechanism, while ZnS deposition occurs by cluster mechanism. ZnS with wide band gap energy (3.8 eV) is an attractive heterojunction partner because it is transparent to almost the complete solar

spectrum. ZnS as heterojunction partner has shown better blue photon response resulting in higher short circuit current ZnS as heterojunction partner has also shown a high conduction band offset (spike) with CIGS absorber layer [Contreras, Nakada, Hongo, Pudova, & Sites, 2003], [Nakada & Mizutani, 2002] and [Call, Jabern, Seshan, & Whyte, 1980]. The ZnO thin films have been deposited using CBD by many researchers [Nakada & Mizutani, 2002]. The effect of dopants such as Sn, Li, Al, and Br on structural, optical and electrical properties of ZnO thin films has been studied. The ZnO thin films are used for different applications such as PEC solar cell, dye-sensitized solar cell, gas sensors and thin films transistors [Cheng, Chen, & Lee, 2006] and [Zhang & Kerr, 2008], also synthesized ZnO thin films with different morphologies.

The CBD method offers a new opportunity for manipulating the morphologies of ZnO thin films by controlling the size and growth orientation of ZnO crystal, which has important applications in optoelectronic devices. ZnO has been of interest in the optical and electronic industries, because of its electrical, optical and acoustic characteristics. Thin films of ZnO have been prepared from the alkaline medium using zinc salt and ammonia solution and subsequently heating the films at elevated temperature [Zhang & Kerr, 2008].



Cadmium oxide has been of interest in the optical and electronic industries. Its band gap is about 2.4 eV and low conductivities make it useful in optoelectronic devices. A chemical method of deposition of CdO has been developed by [Wu, Bai, Li, Lu, & Shi, 2006] using granular KCN in the bath.

2.6 Semiconductor materials

The research reported in this dissertation involves the synthesis and characterization of various semiconductor materials that are promising candidates for applications in

photovoltaic devices. This section briefly discusses the crystal structures as well as the electrical and physical properties of these materials.

2.6.1 Zinc Oxide (ZnO)

Zinc oxide (ZnO) is no stranger to scientific study. ZnO is an n-type semiconductor material with a direct and wide band gap of 3.37 eV, [Ozgur, *et al.*, 2005] which makes it transparent to the visible light and functional in the UV and blue ranges. The exciton binding energy of this material is about 60 meV at room temperature, 2.4 times of the room temperature thermal energy (25 meV), which gives rise to an intense near-band-edge exciton emission in ZnO at room temperature and beyond [Chu, Olmedo, Yang, Kong, & Liu, 2008] and [Bayram, Teherani, Rogers, & Razeghi, 2008]. Over the last several decades, significant efforts have focused on both syntheses and applications of this material due to its outstanding performance in the functional devices such as light emitting diodes [Harako, Yokoyama, Ide, Zhao, & Komoro, 2008] and [Bao, Zimmler, Capasso, Wang, & Ren, 2006], laser diodes [Konenkamp, Word, & Godinez, 2005], UV detectors [Leong, Yu, & Lau, 2006] and [Chu, Olmedo, Yang, Kong, & Liu, 2008], piezoelectric diodes [Leong, Yu, & Lau, 2006], [Huang, *et al.*, 2001], and [Tang, *et al.*, 1998], field effect transistors [Martinson, Elam, Hupp, & Pellin, 2007], gas sensors [Ahn, *et al.*, 2008], [Martinson, Elam, Hupp, & Pellin, 2007] and [Nonomura, Komatsu, Yoshida, Minoura, & Schlettwein, 2007], and solar cells [Yuhas & Yang, 2009], [Jeong, Mittiga, Salza, Masci, & Passerini, 2008], [Izaki, Mizuno, Shinagawa, Inaba, & Tasaka, 2006] and [Minami, Miyata, Ihara, Minamino, & Tsukada, 2006].

ZnO is a group II–VI binary oxide, the iconicity of which is between that of covalent and ionic compounds. ZnO has three crystal structures: primitive hexagonal wurtzite, face-centered cubic zinc blende, and face-centered cubic rock-salt structures. In the first two cases, each cation is coordinated with four anions at the corners of the tetrahedron, whereas in the rock salt structure each cation is surrounded by six anions. Under ambient conditions, ZnO is thermodynamically stable only in the wurtzite structure; therefore it has a tendency to be formed in this phase. The zinc blende structure has been observed on the ZnS substrate with the same structure [Mridha, Dutta, & Basak,

2009] and [Ajimsha, Jayaraj, & Kukreja, 2008]. Further, it has been observed surprisingly to exist in the arms of ZnO wurtzite tetrapods [Einsele, Rostan, Schubert, & Rau, 2007] and [Wenas & Riyadi, 2006]. The rocksalt structure has been observed only under higher pressures [Hsueh, *et al.*, 2007]) and [Kaminska, *et al.*, 2004]. The present work does not only address the ZnO structure but also address the structure of the multilayer deposition in such that does the shape remain the same in a multi-stack and does the intercalation with the polymer enhance the shape.

The polarity in wurtzite ZnO is responsible for piezoelectricity spontaneous polarization and affect the crystal growth habits as well as defect generation. The space group of wurtzite ZnO is $P6_3mc$, with lattice parameters were:

$$a = b = 3.25 \text{ \AA},$$

$$c = 5.21 \text{ \AA},$$

$\alpha = \beta = 120^\circ$ and $\gamma = 90^\circ$. As shown in the Figure below, the Zn^{2+} cations (ionic radii = 0.6 Å) in a unit cell are presented as smaller green triangle, occupying the (0, 0, 0,) and (2/3, 1/3, 1/2) positions; whereas O^{2-} anions (ionic radii = 1.38 Å), represented as red balls, take the positions of (0, 0, 3/8) and (2/3, 1/3, 7/8). The polarity is due to the lack of inversion center in the crystal. The basal plane (0001) is different from the top plane (0001), one having oxygen and the other having zinc. Thus, the polarity forms along the c-axis, pointing positively to the (0001) plane. The side planes {1010} have an equal number of Zn and O, on the other hand, are nonpolar [El-Shaer, et al., 2007].

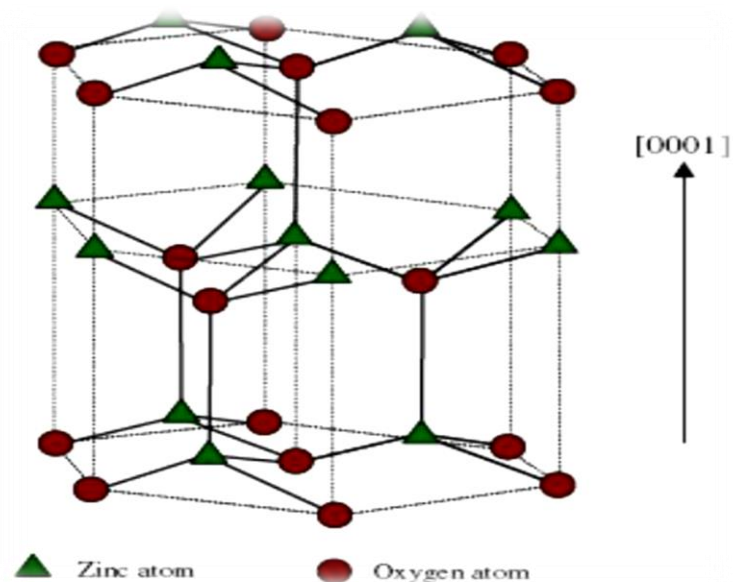


Figure 4: ZnO hexagonal wurtzite structure [El-Shaer, *et al.*, 2007]

Many groups have calculated the electronic band structure of ZnO [Liu, Vertegel, Bohannan, Sorenson, & Switzer, 2001]. Figure 4 show the resulting band structure along the hexagonal Brillouin zone. The conduction band minima and valence band maxima occur at the point, indicating that ZnO is a direct bandgap semiconductor material. From bottom to top, the groups of bands are Zn 3d levels (10 bands, -9 eV), O 2p levels (6 bands, -5 to 0 eV), and Zn 3s levels (2 bands, top).

The possibility for band gap engineering is important for industrial applications of ZnO. By doping or alloying with another material of a different band gap, the band gap of ZnO can be finely tuned for example, $Zn_xMg_{1-x}O$ may have a band gap range of 3.37 to 4.0 eV [Kim, Kwack, Kim, Yoon, Bahang, & Park, 2003], and for $Zn_xCd_{1-x}O$ the range is from 2.9 to 3.37 eV [Andeen, Loeffler, Padture, & Lange, 2003] and [Green & Wenham, 1994].

2.6.2 Cadmium Oxide (CdO)

Cadmium oxide (CdO) was the first TCO to be discovered in 1902 by F. Streintz [Streintz, 1902] was reported by [Jeong, Mittiga, Salza, Masci, & Passerini, 2008], and the first to be produced as a thin film in 1907 by K. Bädeker [Bädeker, 1907] was published by [Izaki, Mizuno, Shinagawa, Inaba, & Tasaka, 2006]. This was some forty (40) years before the now commonplace TCOs of latter SnO_2 and In_2O_3 were developed [Harako, Yokoyama, Ide, Zhao, & Komoro, 2008]. A recent review article by Minami [Minami, Miyata, Ihara, Minamino, & Tsukada, 2006], suggested an interest in CdO has rapidly increased since the year 2005, with the growth of higher quality films and nanomaterials opening up new fundamental studies and application possibilities. CdO can be produced by a wide variety of growth processes including MOVPE [Mridha, Dutta, & Basak, 2009] and [Ajimsha, Jayaraj, & Kukreja, 2008], MBE [Einsele, Rostan, Schubert, & Rau, 2007], [Wenas & Riyadi, 2006], PLD [Kaminska, *et al.*, 2004], sol-gel [El-Shaer, *et al.*, 2007] and sputtering.

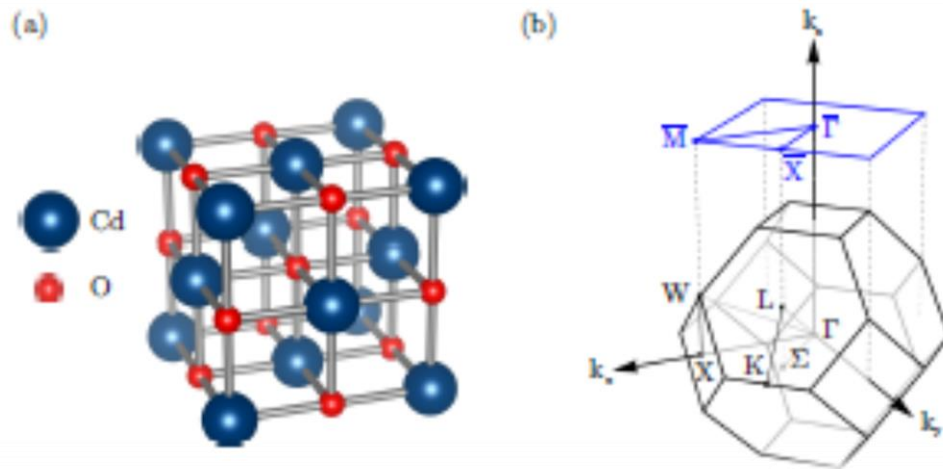


Figure 5: The real space crystal structure of CdO (b) The FCC BZ of CdO and the surface BZ for the (001) surface. The bulk and surface high symmetry points are labeled [Mridha, Dutta, & Basak, 2009] and [Kim, Kwack, Kim, Yoon, Bahang, & Park, 2003]

CdO crystallizes in the rock-salt structure ($Fm\bar{3}m$) consisting of a face centred cubic (FCC) lattice with a two-atom basis, Cd at (0, 0, 0) and O at (1/2, 1/2, 1/2), with a lattice parameter of 4.695 Å [Mridha, Dutta, & Basak, 2009] and [Kim, Kwack, Kim, Yoon, Bahang, & Park, 2003] as shown in the figure 5 above (a). The Brillouin zone (BZ) for CdO is, therefore, the FCC BZ as shown in figure 5 (b), where the (001) surface projection is also shown. The fundamental band gap of CdO is ~ 0.9 eV (~ 1400 nm) [Andeen, Loeffler, Padture, & Lange, 2003] and [Green & Wenham, 1994] and while this is much too low for optical transparency (400 to 700 nm), this gap is indirect and therefore significant optical absorption is suppressed until the direct band gap of ~ 2.2 eV (~ 560 nm) [Green & Wenham, 1994]. While this band gap is still insufficient for full optical transparency, CdO can be heavily doped, with the resulting Moss-Burstein shift leading to optical band gaps > 3.1 eV (~ 400 nm). This makes CdO fully optically transparent, along with extremely high carrier concentrations ($> 10^{21}$ cm $^{-3}$) [Ajimsha, Jayaraj, & Kukreja, 2008] and [Liu, Vertegel, Bohannan, Sorenson, & Switzer, 2001], which results in high conductivity.

2.6.3 Cadmium Sulfide (CdS)

Thin films of CdS have been grown onto suitably clean glass substrates by chemical bath deposition (CBD) technique. CBD is an "electro-less" technique that is attractive as a simple, low-cost deposition method and also promising for large area film deposition. CBD is also a useful method for obtaining CdS thin films as a buffer layer in a window of the thin film solar cell, because, it is inherently a low-temperature process which does not damage the surface of the deposited thin film as an absorber during deposition and can be applied to rough one. Although the CdS polycrystalline films grown by CBD methods have a poor crystalline quality, as compared with CdS films grown by other techniques. CdS is a direct gap semiconductor with the smallest energy gap in the center of the Brillouin Zone. The Band Gap of CdS is 2.42 eV [Britt, 1993].

The top most valence band is split due to crystal field and spin-orbit coupling into three spin-degenerate states. Exciton states formed with holes in these valence band states are denoted A, B, and C exciton, respectively. CdS are the inorganic compound with the formula CdS. CdS is a yellow solid [Wiberg & Holleman, 2001], reported that CdS occurs in nature with two different crystal structures as the rare minerals greenockite and hawleyite, but is more prevalent as an impurity substituent in the similarly structured zinc ores sphalerite and wurtzite, which are the major economic sources of cadmium as showed in figure 6 below. As a compound that is easy to isolate and purify, it is the principal source of cadmium for all commercial applications [Wiberg & Holleman, 2001]. CdS is a vivid yellow color led to its adoption as a pigment for the yellow paint "cadmium yellow" in the 18th century [Wiberg & Holleman, 2001].

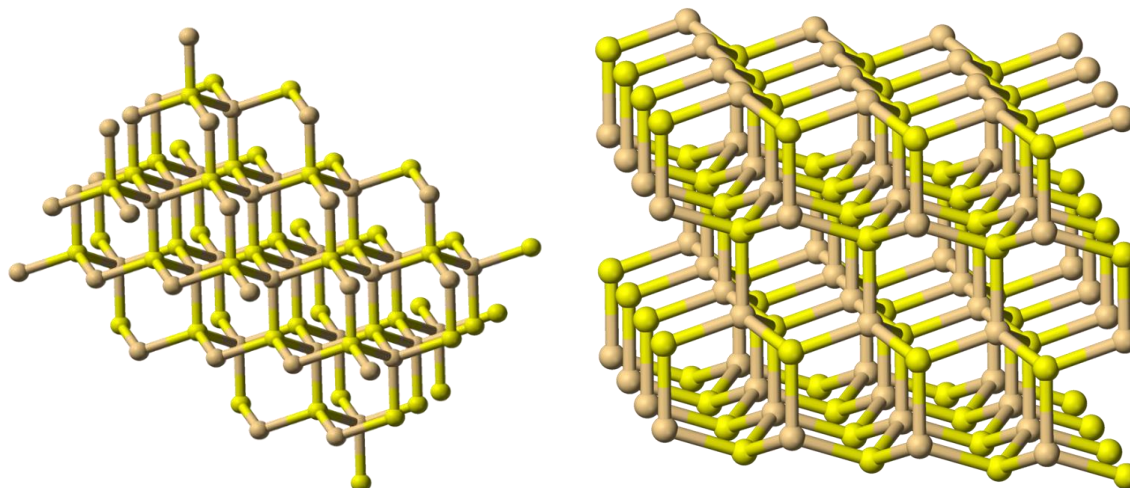


Figure 6: CdS hexagonal wurtzite structure [Wiberg & Holleman, 2001]

Cadmium sulfide can be prepared by the precipitation from soluble cadmium (II) salts with sulfide ion. This reaction has been used for gravimetric analysis and qualitative inorganic analysis. The preparative route and the subsequent treatment of the product affect the polymorphic form that is produced (i.e., cubic vs hexagonal). It has been asserted that chemical precipitation methods result in the cubic zincblende form [Ibbotson, 2007]. Pigment production usually involves the precipitation of CdS, the washing of the solid precipitate to remove soluble cadmium salts followed by calcination (roasting) to convert it to the hexagonal form followed by milling to produce a powder [Klocek, 1991].

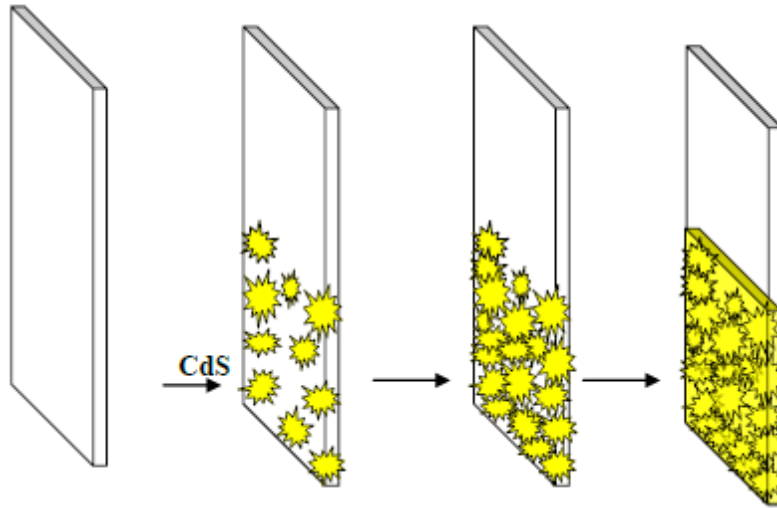


Figure 7: CdS growth on the substrate [Smith, 2002]

When cadmium sulfide selenides are required the CdSe is co-precipitated with CdS and cadmium sulfoselenide is created during the calcination step [Smith, 2002]. CdS have, like zinc sulfide, two crystal forms. The more stable hexagonal wurtzite structure found in the mineral Greenockite (Greenockite is a rare cadmium bearing metal sulfide (MS) mineral consisting of CdS in crystalline form) and the cubic zinc blende structure found in the mineral Hawleyite (Hawleyite is a rare sulfide mineral in the sphalerite group, dimorphous and easily confused with greenockite). In both of these forms, the cadmium and sulfur atoms are four coordinate. Synthetic cadmium pigments based on cadmium sulfide are valued for their good thermal stability, light and weather fastness, chemical resistance and high opacity [Smith, 2002] as shown in figure 7. CdS are used as a pigment in plastics further reports by [Smith, 2002].

2.6.4 Zinc Sulfide (ZnS)

ZnS is an important II-VI group semiconductor with a large direct band gap of 3.5–3.7 eV in the UV range [Vipin, Sharma, Gaur, & Sharma, 2008]. ZnS is a white to yellow-colored powder or crystal with a molecular mass of $97.474 \text{ g mol}^{-1}$ and a density of 4.090 g cm^{-3} . It is typically encountered in the more stable cubic form, known also as zinc blende or sphalerite. The hexagonal form is also known both as a synthetic material and as the mineral wurtzite. Both sphalerite and wurtzite as shown in figure 8 are intrinsic, wide-

band gap semiconductors. ZnS has a melting point (phase transition) of 1020° C. The cubic form is stable at room temperature, while the less dense hexagonal form (wurtzite) is stable above 1020°C at atmospheric pressure [Gilbert, *et al.*, 2002]. The figure below shows each crystal structure.

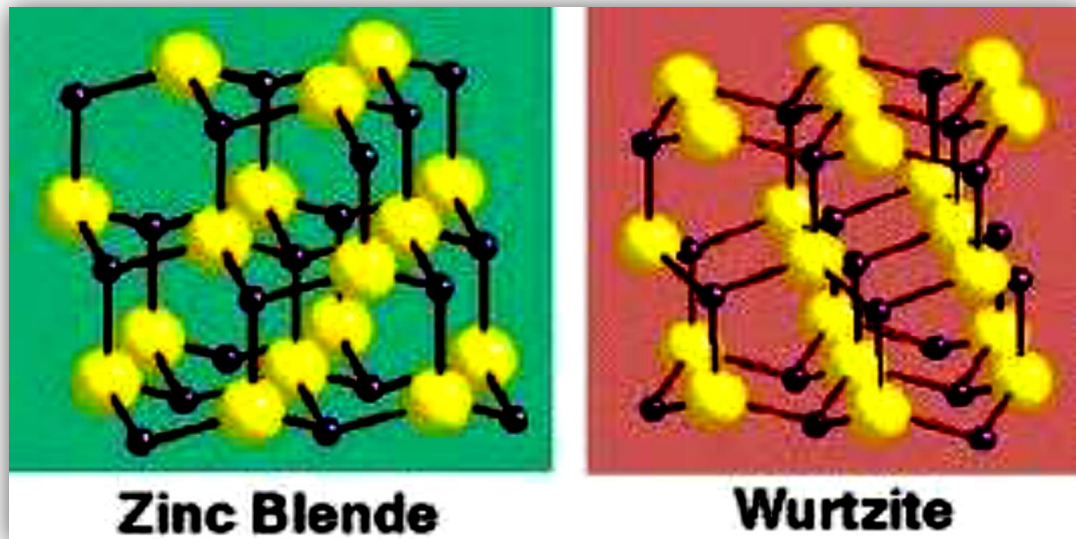


Figure 8: The sphalerite or zinc blende and the wurtzite crystal structure of ZnS [Gilbert, *et al.*, 2002]

The sphalerite structure can be derived from cubic close packed ions, while the wurtzite structure is derived from a hexagonal close packing scheme. This situation is not that simple, however, because the difference in energy of the two structures is small. Report by Arterton [Arterton, Brightwell, Mason, Ray, & Viney, 1992], states that electroluminescent material must contain both sphalerite and wurtzite phases. The wurtzite type structure predominates when the bonding is primarily ionic whereas the more covalent systems favor the sphalerite form. The nature of the end product is usually dependent on heat treatment temperature, cooling profile, and cooling atmosphere. One phase can be more suitable than the other in certain applications. The cubic phase of ZnS is not grown as easily as the hexagonal phase, thus making the hexagonal phase more appealing for electroluminescence device applications reported by [Bellotti, Brennen, Wang, & Ruden, 1988].

ZnS was used by Ernest Rutherford and others in the early years of nuclear physics as a scintillation detector, because it emits light on excitation by X-rays or electron beam, making it useful for X-ray screens and cathode ray tubes. It also exhibits phosphorescence due to impurities on illumination with blue or ultraviolet light [Greenwood & Earnshaw, 1984]. Thin films have been found valuable in various devices. The application of ZnS thin films which cover a wide area of interest are: antireflection coating for the solar cell [Boyle, Bayer, Heinrich, Robbe, & O'Brien, 2000], Environmental friendly buffer layer as compared to CdS layer in CIS-based thin film solar cell [Katsumi, 1995], photosynthetic coating [Ndukwe, 1996] and blue light emitting laser diodes [Hasse, Qui, DePuydt, & Cheng, 1991].

In thin film solar cells based on $\text{CuGaIn}(\text{S}, \text{Se})_2$ absorbers, a CdS (cadmium sulfide) buffer layer is generally required in order to obtain high conversion efficiency. However, there are toxic hazards with respect to the production and use of the CdS layer. Therefore research in developing cadmium (Cd) free buffer layers has been encouraged. This has led to the investigation of ZnS as a buffer layer in ZnO / ZnS / CuInS_2 devices [Ortega & Borges, 1992]. ZnS has a wider energy band gap than CdS, which results in the transmittance of more high-energy photons to the junction, and to the enhancement of the blue response of the photovoltaic cells.

2.7 Intercalation of Inorganic-Organic

In chemistry, intercalation is the reversible inclusion or insertion of a molecule (or ion) into compounds with layered structures. Examples are found in graphite and transition metal chalcogenides [Müller-Warmuth & Schöllhorn, 2012]. Intercalated structures are formed when a single or more extended polymer chain is intercalated between the clay layers. A scheme describing the possible interactions of polymers with layered inorganic structures is presented in below. The results are a well-ordered multilayer structure of alternating polymeric and inorganic layers.

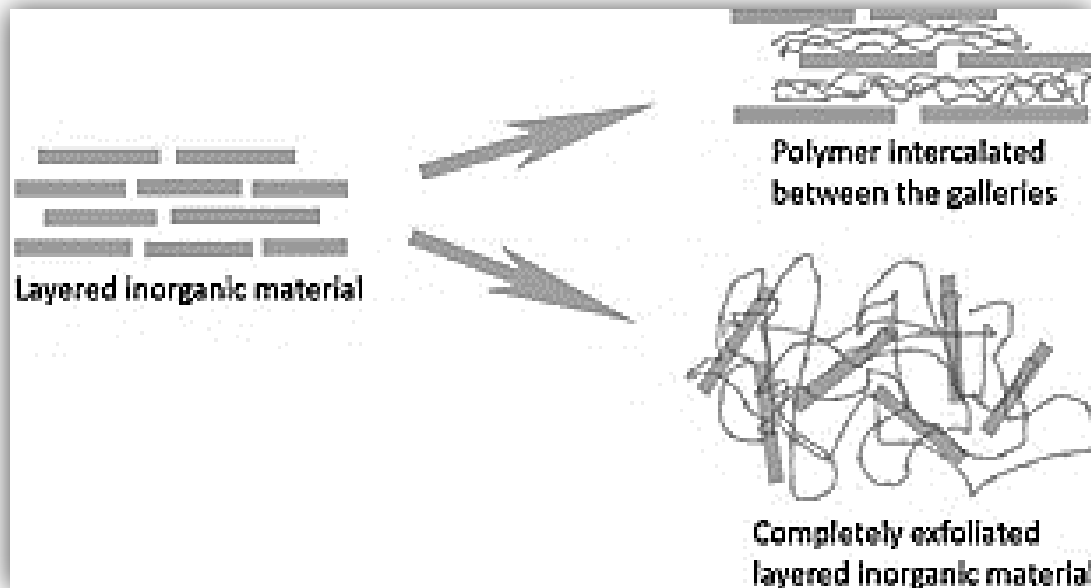


Figure 9: Schematic description of intercalation between polymer and layered inorganic material for the formation of PINCs [Kickelbick, 2003]

Intercalation of polymer chains into the galleries of an organo-clay can occur spontaneously on heating a mixture of polymer and silicate clay powder above the polymer glass transition or melt temperature as demonstrated in figure 9 . Once sufficient polymer mobility is achieved, chains diffuse into the host silicate clay galleries, thereby producing an expanded polymer-silicate structure. From the theoretical model, the outcome of hybrid formation via polymer melt intercalation was found to depend on energetic factors that may be determined from the surface energies of the polymer.

2.8 Polyvinyl alcohol (PVA)

The selected choice of polymer used in this research is PVA. PVA is an excellent oxygen barrier polymer for solar cell encapsulation as photochemical studies of PVA under solar light was conducted [Gaume, Wong-wah-chung, Rivaton, Thérias, & Gardette, 2011] at the University of Clermont. It showed that the photo-oxidative degradation of PVA is restricted to the first 5 microns at the surface of the exposed films. The researchers also identified the low molecular weight products such as carboxylic acids that can be

trapped in the film or migrate in the gas phase and they proposed an oxidative mechanism to account for these modifications as shown in figure 10 below.

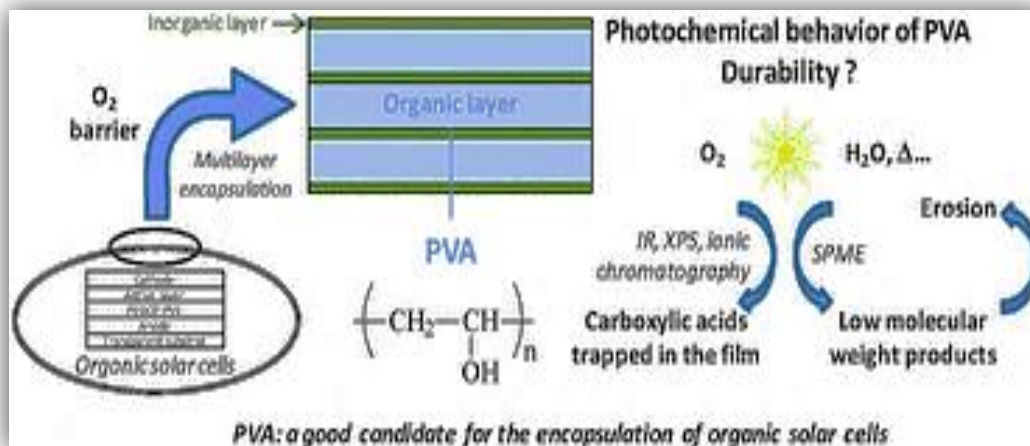


Figure 10: PVA excellent for multilayer [Gaume, Wong-wah-chung, Rivaton, Thérias, & Gardette, 2011]

However, the most appealing property of PVA is “high stability upon irradiation in the absence of oxygen, even after long exposure in conditions of accelerated aging”, says Gardette. Indeed, PVA is an excellent candidate for the multilayer encapsulation system of Organic Solar Cells (OSCs) due to its high durability, “as long as the PVA layer is protected from air by an inorganic layer as a first outside layer in the inorganic/organic multi-stack”.

CHAPTER 3: METHODOLOGY

Due to toxicity and suspected carcinogenic activity of many cadmium-containing compounds [Ibanez, Solorza, & Gomez-del-Campo, 1991], all experiments were performed under carefully controlled conditions. All reagents were selected as analytical grade or of better quality.

3.1 Instrumentation

In this study, a wide variety of characterization techniques were used to evaluate the materials quality of the semiconductor nanostructures. The techniques broadly deal with the issues such as morphology. The presences of crystalline phases were determined by Ultraviolet-visible spectroscopy (UV-VIS), Atomic Force Microscopy (AFM), X-Ray Diffraction (XRD), Scanning electron microscope (SEM).

3.1.1 UV-Vis Spectroscopy

The PG Instruments T80 UV/VIS is a high-performance double beam UV-Visible automatic scanning spectrophotometer with a fixed 2 nm bandwidth. The instrument covers a wavelength range of 190-1100 nm and comes with a built-in 8-position motorized cell holder as standard. T80 UV/VIS has excellent baseline stability and high resolution. With a large 'fold away' LCD display allowing complete display of spectra, and a large easy to use positive touch keypad, the T80 UV/VIS can be operated in "stand alone" mode without a PC. The main unit of the spectrophotometer can perform photometric measurement, quantitative measurement, spectrum scan, DNA/Protein analysis and can print data.

When interfaced to a PC the included UVWin 5 software offers many additional functions such as kinetics measurement, access to the database, 3D spectrum analysis, GLP laboratory protocol, data export to Word or Excel, multi-user management, etc. The T80 UV/VIS is a universally accepted and well-documented technique, offers high performance, ease of use and reliability. It can be used extensively for qualitative and quantitative analysis in applications including the analysis of foods, drugs, pesticide residues, agricultural products. It is widely used in the medical care,

public health, environmental protection, life science and many other organic and biochemical applications.

3.1.2 Scanning Electron Microscopy (SEM) and Energy Dispersive X-Ray Spectroscopy (EDS)

The morphologies of the nanostructures were studied by Scanning Electron Microscopy (SEM) Fei Nova SEM 200. The SEM images were recorded using Zeiss EVO-40, operated at 20 kV with a Bruker AXS XFlash EDS detector 4010 attached to the same microscope and Nova NanoSEM 430, operated at 20 kV. The samples on the silicon wafers were attached to the aluminum sample holders by using carbon adhesive tabs.

With Nova NanoSEM you can expand your research capabilities by handling a wider range of sample types. Characterize a wide range of samples with unique low vacuum capabilities and ultra-high resolution low voltage imaging; low voltage [1 kV] resolution is 1.4 nm in high vacuum mode, while for non-conductive materials, the Nova NanoSEM is unique in offering the highest resolution (1.8 nm) at low voltages (3 kV). The instrument has both a high current beam (essential for rapid EDS/EBSD/CL/analytical research) and high resolution at a high and low voltage which is essential for image quality across a wide range of sample type. Strong performance in low vacuum mode gives you more analytical power - when you need top quality analytical data on samples like glass, ceramics or other non-conductive materials.

3.1.3 Atomic Force Microscopy (AFM)

The Dimension 3100 Scanning Probe Microscope (SPM) NanoScope® IV, version 5.2 Digital Instruments Atomic Force Microscopy (AFM) was used in this study. Scanning probe microscopy (SPM) consists of a family of microscopy forms where a sharp probe is scanned across a surface and some probe/sample interactions are monitored. The SPM has become popular because of the volume of nanometer-scale information it provides. Unlike conventional microscopes that provide direct images of an object, scanning probe microscopes provide data in the form of topographic relief images. Atomic force microscopy (AFM) is one of the forms of SPM. AFM is used to image and

explore nanoscale features and structures of surfaces, both in the air and in liquid. The topography of surfaces can be obtained normally by two different modes, contact mode and tapping mode.

However, tapping mode is normally used for soft, adhesive or fragile samples since imposed force on samples by tapping mode is much weaker than that by contact mode. If the sample is conductive, scanning tunneling microscopy (STM) is recommended to get images with higher resolution. Imaging surfaces in the liquid can be used to study liquid to solid interfacial phenomena, for example, the adsorption of colloid particles, polymer, and DNA and protein molecules.

3.1.4 X-Ray Diffraction (XRD)

Bruker's AXS XRD D8-Discover instrument without rotation at a 2θ angle between 5° to 80° degree was used. X-ray diffraction (XRD) is an important non-destructive tool for materials characterization. The D8 DISCOVER for thin films combines reflectometry and high-resolution X-ray diffraction on a vertical diffractometer. Using the new motorized reflectometry stage and the V- shaped monochromator benefit of the advantages of Theta/Theta diffraction setup

This also is state-of-the-art machine including Vantec-500 area detector, centric 1/4-circle Eulerian cradle, domed hot stage, hi-flux in-plane hardware, laser/video sample alignment system, Göbel mirror, fine tilt stage, and dual-beam path analyzer module. The system can be configured for grazing-incidence in-plane XRD, grazing incidence XRD, X-ray reflectivity, high-temperature XRD, high-resolution XRD (rocking curves, reciprocal space maps), texture (pole figures), residual stress, and capillary diffraction. Bruker D8 Discover diffractometer is configured in parallel beam geometry with Cu K α radiation (wavelength of about 1.54 Å).

The stoichiometric ratios of pure, multilayer and intercalated semiconductor materials were determined by energy-dispersive X-ray spectroscopy (EDS). The optical properties of the nanostructures were evaluated by UV-vis spectroscopy.

3.2 Chemical reagents

The reagents used are as follows:

Cadmium acetate, $\{\text{Cd}(\text{AcO})_2\}$, thiourea, $\{\text{H}_2\text{NCSNH}_2\}$, ammonium hydroxide 25% (NH_4OH), polyvinyl alcohol (PVA), zinc acetate, $\{\text{Zn}(\text{AcO})_2\}$, triethanolamine (TEA), sodium hydroxide (NaOH) 1M, acetone.

3.3 Experimental procedure

3.3.1 CdO thin film deposition

The chemical bath for the preparation of CdO was set up from about 40-50 ml of cadmium acetate (0.3 M), 40-50 ml of aqueous ammonia (0.05 M). The film deposition was carried out at a desirable temperature (60°C) for about to 60 minutes. Clean glass substrates (was submerged) supported vertically by the wall of the glass beaker containing the chemical bath and the bath was stirred constantly to avoid a powdery deposit on the film surface. The as-deposited films was washed with distilled water and dried before further studies were carried out.

3.3.2 PVA/CdS thin film deposition

A thin layer of CdS is formed on a chemically deposited CdO thin film and vice versa. A cadmium sulfide thin film was deposited on polyvinyl alcohol (PVA) matrix on glass substrates containing the CdO (TCO) using the CBD method. In the reaction bath, about 40-50 ml of 0.05 M ammonia solution was added to a 150 ml beaker containing 3-10 ml of 0.3 M $\{\text{Cd}(\text{CH}_3\text{COO})_2 \cdot 2\text{H}_2\text{O}\}$. The resulting mixture was added to 40-50 ml of 0.6 M thiourea and solution of 3-7% PVA to make up the bath solution. The solution bath was stirred continuously for 5-10 minutes and a previously used glass substrate, which contained the CdO, rinsed in de-ionized water and dried in air, was vertically immersed into the reaction bath. The substrates coated with CdO/PVA/CdS thin films was withdrawn and rinsed with de-ionized water and dried in air. The second steps was prepared separate first and then characterized, if it was found to be less, then the deposition of another TCO of which in this case is ZnO was deposited onto the glass substrate containing the deposited CdO/PVA/CdS.

3.3.3 ZnO thin film deposition

ZnO films were prepared using aqueous solutions of 40 ml of 0.5 M zinc acetate $\{Zn(CH_3COO)_2 \cdot 2H_2O\}$, 30 ml 0.5 M triethanolamine (TEA) and 0.05 M ammonium hydroxide (NH_4OH). Prior to the deposition, the glass reactor containing the deposition solution was left to adjust the temperature of $60^\circ C$ for about 5 minutes to stabilize the temperature of the solution. When the temperature was reached the glass substrate was immersed in the solution. At the end of the deposition time (30 to 60 minutes at temperatures of $60^\circ C$), the slides were taken out, rinsed with distilled water and allowed to dry with warm air.

3.3.4 PVA/ZnS thin film deposition

A thin layer of PVA/ZnS is formed on a chemically deposited ZnO thin film and vice versa. The preparation process for the PVA/ZnS on a previously deposited ZnO was prepared in a similar way to that of PVA/CdS. Each ZnS thin film was prepared on a slide glass substrate. The substrate was blown dry using nitrogen gas. A solution containing 0.5 M zinc acetate, 0.05 M ammonium hydroxide, 0.6 M thiourea, and 0.5 M triethanolamine was mixed in a 200 ml glass reactor beaker. The clean substrate was then immersed in the reaction solution for different depositing times of 60 minutes at $60^\circ C$ in an alkaline medium. After deposition, the sample was rinsed with water and dried using nitrogen.

RESULTS AND DISCUSSIONS

CHAPTER 4

SINGLE LAYER DEPOSITION OF METAL SULFIDE AND OXIDE THIN FILM

4.1 Deposition of metal sulfide/oxide single layer

The chemical bath deposition was used to drive the deposition of the cadmium and zinc sulfide and oxide thin films under a variety of conditions. Conditions optimized include temperature and concentration. The optical properties of thin films are determined from their percent transmittance measurements within the range of 200–1100 nm. The morphologies were determined using AFM, SEM, and powder XRD techniques.

4.1.1 Transmittance of single layer thin film

When light is incident on a material, a fraction of the light beam that is not reflected or absorbed is transmitted through the material. Transmittance data was obtained from the absorption spectra.

Fig: 11 (a-d) Transmittance vs absorbance graph of CdS, CdO, ZnO, and ZnS thin films determined after obtaining the absorbance and transmittance spectrum. UV-Vis transmittance spectra formed at bath or reaction of pH 11 with different reaction temperatures of (60°C, 70°C, and 90°C) are given in the figure below. The transmittance of CdS thin films was red shifted as a result decreased with an increase in deposition temperature. The average transmittance of these films is calculated to 85 %, 80 % and 81 % respectively in the visible range which is good for optoelectronic devices, especially for solar cell window layers, and have sharp fall at the band edge, which is an indication of good crystallinity of CdS in the films at lower temperatures.

These result related to the decrease of deposition temperature so the voids in CdS thin layer fill up with new CdS grains and that normally tends to more thickness and less transmittance. It is not clear as to why the transmittance at temperatures of 70°C is

slightly lower than that of 90°C, however, there was no much difference in the percent transmittance.

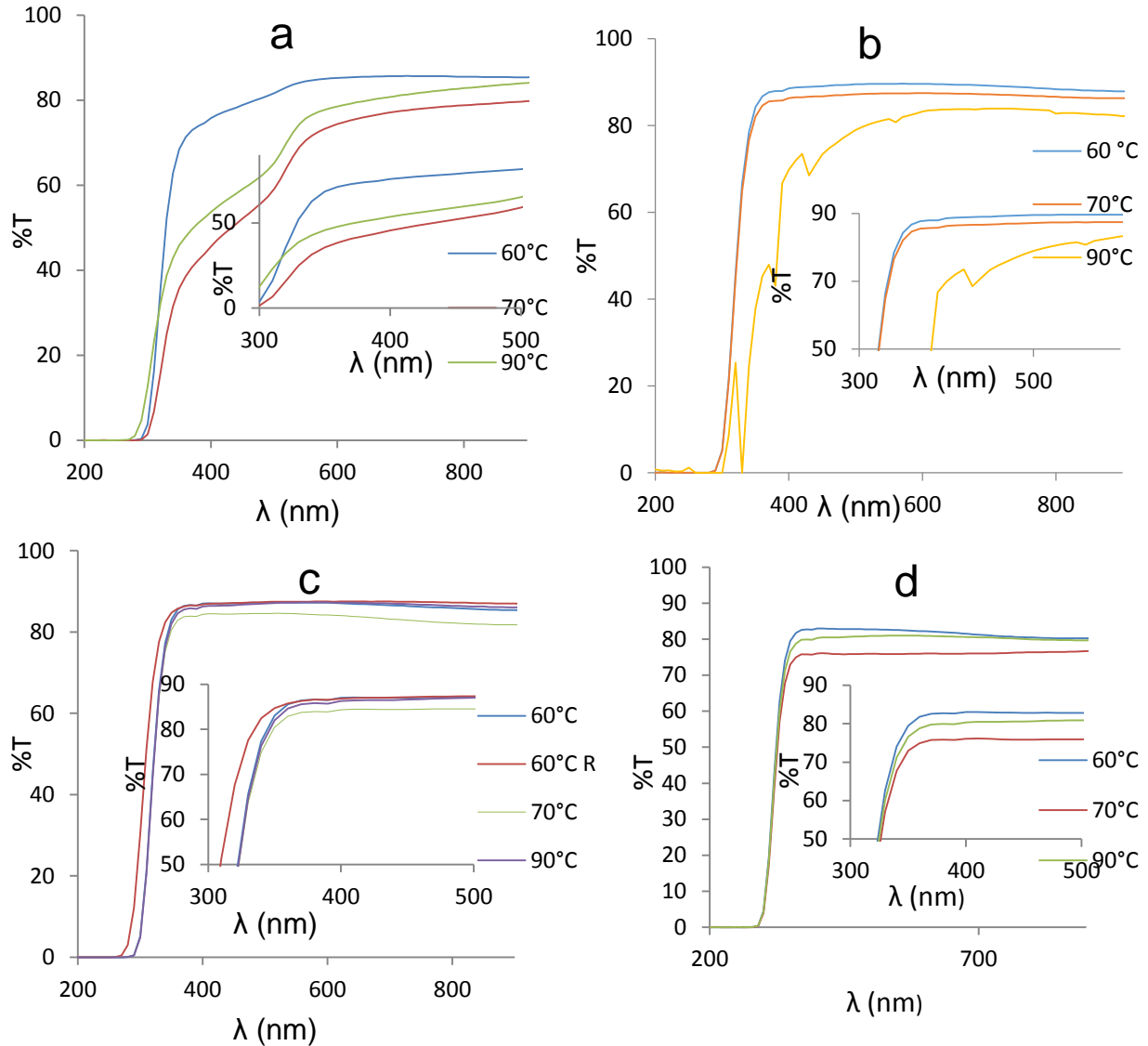


Figure 11: Plots of transmittance versus wavelength showing transmittance dependence of pH 11 at temperature variation, (a) CdS, (b) CdO, (c) ZnO, (d) ZnS

In general, there is a high %T of CdS layer produced in this work that depended on the low thickness of thin film 99.67 nm from AFM. In addition to the decreasing of transmittance can be linked with the agglomeration and increasing in the grain size, and indicating its high surface roughness from SEM and AFM. The CdS films showed optical

transmittance ~85 % in the visible range. The results revealed that the optical deposition of CdS is better at a lower temperature of 60°C at an alkaline solution.

Figure 11 (b) similarly to CdS deposition, %T of CdO decreases with the increase in deposition temperature. The average transmittance of these films was calculated to be 90 %, 87 %, and 81 % respectively, meaning that the %T red shifted with an increase in temperature. This result related to the decrease of deposition temperature so the voids in CdO thin layer fill up with new CdO grains and that tends to more thickness and less transmittance. In addition to the decreasing of transmittance can be linked with the agglomeration and increasing in the grain size, and indicating its high surface roughness with a film thickness of 100.4 nm that was measured with AFM.

CdO is a transparent conducting oxides (TCOs) materials that possess both high electrical conductivity and high optical transparency >80 % in the visible light region of the electromagnetic spectrum [Hames & San, 2004]. The deposited results of CdO films showed optical transmittance between ~80–91 % in the visible range. These results are much better than previous reports that show optical transmittance at 90 % in the visible region. The sharp rise in %T is an identification of good crystallinity of films. Optical transmittance spectra of the thin films are observed to be shifted towards the shorter wavelengths with a variation of temperature. At the high temperature of 90°C, the transmittance is lower than the other varied temperatures, this could be due to the reason that the solution evaporates as the water escapes due to its boiling point and that in CBD good deposition was observed at lower temperatures. It was recommended to use temperatures below 90°C moving forward with the research for deposition of CdO thin film.

Figure 11 (c) the %T of ZnO thin films decreases with the increase in deposition temperature. The average transmittance of these films is calculated to be 90 %, 81 %, and 87 % respectively. It was observed that the deposition of ZnO red shifted with an increase in temperature. This result related to the decrease of deposition temperature so the voids in ZnO thin layer fill up with new ZnO grains and that tends to more thickness and less transmittance. In general, there is a high percent of transmittance for

layers produced in this work that depended on the low thickness of thin film. In addition to the decreasing of transmittance can be linked with the agglomeration and increasing in the grain size, and indicating its high surface roughness with a film thickness of 114 nm. Similarly to CdS and CdO thin film deposition it was observed that at temperatures of 70°C the %T was lower than deposition of 60°C and 90°C, however, this behavior was unclear.

The deposition of ZnO at different temperatures between 60-90°C is reported below. Higher %T was observed at lower temperatures conditions was reported to be T ~90 % at 60°C. The sharp rise in transmittance is an identification of good crystallinity of films. The deposited films at temperatures between 60°C to 90°C are highly transparent in the visible region with an average %T of ~88 %. It was observed that the films obtained at temperatures of 60°C and 90°C show slightly high %T invisible region as compared to the films obtained at 70°C. The decrease in a deposition at 70°C is not clear for ZnO thin film deposition. Deposition of ZnO shows that it is not dependent on alkalinity or acidity hence good crystallinity was observed according to the %T.

Fig: 11 (d) the %T of ZnS thin film decreases with the increase in deposition temperature. The average transmittance of these films is calculated to be 83 %, 76 %, and 80 % red shift respectively. This result related to the decrease of deposition temperature so the voids in ZnS thin layer fill up with new ZnS grains and that tends to more thickness and less transmittance. In general, there is a high percent of transmittance for layers produced in this work that depended on the low thickness of thin film. In addition to the decreasing of transmittance can be linked with the agglomeration and increasing in the grain size, and indicating its high surface roughness. Similarly to CdS, ZnO thin film deposition it was observed that at temperatures of 70°C the transmittance is lower than deposition of 60°C and 90°C. A strong redshift between 70°C and 90°C in the optical spectra due to the reduction in band gap observed and this is implied to the rise of the thickness of localized conditions in the energy gap.

The deposition of CdS, CdO, ZnO and ZnS was performed under the constant concentration of the salts, oxide and sulfide source and the following temperature variation was followed, 60, 70 and 90°C. The initial change was kept at 10 degree Celsius and thereafter doubled. As it was observed that the %T was lower at higher temperatures of 70°C and 90°C. Lower temperature gave higher %T and lower absorption, which results in longer deposition time and better results than working at higher temperatures. According to the deposition of CdS, CdO, ZnO and ZnS the %T was found to be red shifted with an increase in temperature. At lower temperature of 60°C, the %T was blue-shifted. The film thickness was 107.7 nm of the as-deposited ZnS. Film %T decreases with increasing thickness of the film because of an increase in grain size as a result of increasing the film thickness a consequence %T decreases.

The following analysis at figure was the transmittance versus the wavelength depending on pH. Fig: 12 (a) illustrate deposition of CdS at different pH values is reported below also supports that %T is higher at alkaline conditions which are about T ~89-94 % between pH 7-11. All the deposited films are highly transparent in the visible region with an average %T of ~90.8 %. It is observed that the films obtained at lower pH values show slightly high %T invisible region as compared to the films obtained at about pH 2. The films show high transmittance in the visible and near infrared region. It is clear from the transmittance spectrum that the transmittance of the films increases with the wavelength. The sharp rise in transmittance is an identification of good crystallinity of films. Deposition of CdS shows that it is not dependent on alkalinity or acidity hence good crystallinity was observed according to the %T.

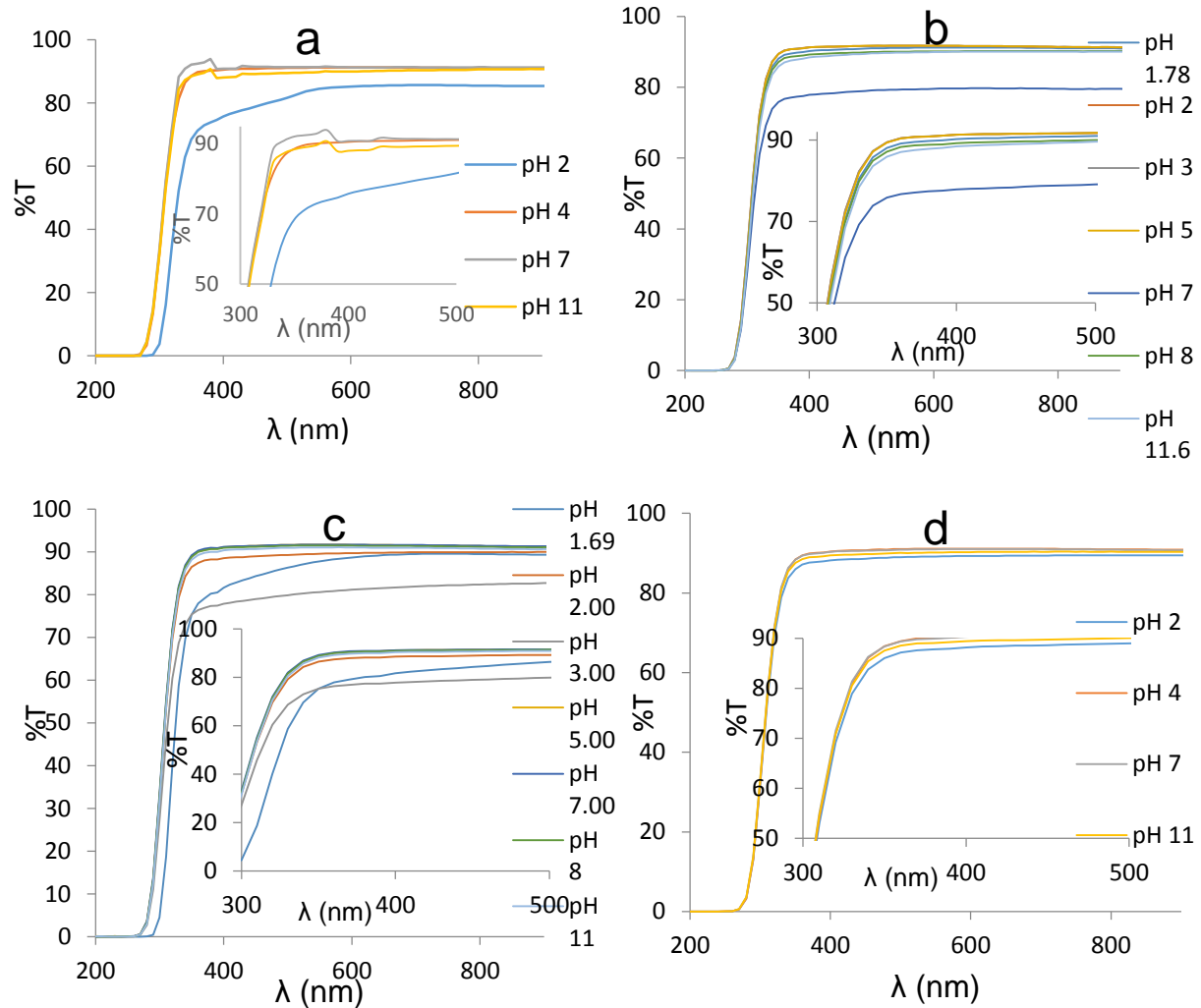


Figure 12: Plots of transmittance versus wavelength showing transmittance dependence of pH variation at 60°C, (a) CdS, (b) CdO, (c) ZnO, and (d) ZnS

Fig: 12 (b) the second optical results show CdO thin film deposition at 60°C varying pH revealed that the CdO deposits a better transparency between pH 5-11 which yields a transparency of ~91 % better than the reported value of 80 % [Hames & San, 2004]. Transmittance spectra of CdO at pH variation films was observed that the films present high %T of (86–91 %) in the visible range which has sharp fall at the band edge, which is an indication of good crystallinity of CdO in the films. The sharp rise in transmittance is an identification of good crystallinity of films. Deposition of CdO shows that it is dependent on alkalinity or acidity hence lower crystallinity was observed according to

the %T at neutral pH. Optical transmittance spectra of the thin films are observed to be shifted towards the shorter wavelengths with a variation of pH.

Fig: 12 (c) shows the deposition of ZnO at different pH indicates that all the films are highly transparent in the visible region with an average %T of ~90 % at pH 1.69-11. The results at pH 3 reported a lower %T of 78 % in the visible region than all the other pH values. In general, there is a high percent of transmittance for layers produced in this work that depended on the low thickness of thin film. In addition to the decreasing of transmittance can be linked with the agglomeration and increasing in the grain size, and indicating its high surface roughness. The sharp rise in percent transmittance is an identification of good crystallinity of films. Deposition of ZnO shows that it is not dependent on alkalinity or acidity hence good crystallinity was observed according to the %T.

Fig: 12 (d) illustrate all the films are highly transparent in the visible region with an average %T of 90 % at pH 2, 4, 7 & 11. The films show high transmittance in the visible and near infrared region. The sharp rise in transmittance is an identification of good crystallinity of films. It was observed that at lower pH the %T was slightly lower than 90 % as compared to pH 4-9. Deposition of ZnS shows that it is not dependent on alkalinity or acidity hence good crystallinity was observed according to the %T. It is clear from the transmittance spectrum that the %T of the as-deposited films increases with the wavelength.

It was worth noting that an increase in a temperature decreases the %T. Due to the results are given that the %T and absorption not being affected by the acidity or alkalinity, pH 11 was the condition that was kept constant through the whole research. It was also observed that deposition at lower temperature yielded lower absorption and higher transmittance which is good for most applications, the condition of 60°C at pH 11 was studied further in this research.

The optical results for single layers were observed above 400 nm wavelength, the absorbance of the samples are low and lie between 0 and 1.0. The films showed a

marginal decrease in absorbance at an ambient temperature of 60°C and this might be attributed to the improvement in crystallinity in the films with the ambient temperature [Kassim, *et al.*, 2009]. Working at ambient temperature may result in the lead to minimizing structural imperfections in the prepared thin films resulting in fewer states within the band gap available for photon absorption. Hence, lower absorbance readings. The decrease in absorbance with increased temperature may also be diffusion of Cd and Zn into the glass substrate [Zendehnam, Shirazi, Doulatshah, & Sadat, 2010] fundamental absorption edge of the samples shift towards shorter wavelengths with increasing temperatures. As it can be observed the temperatures for 70°C and 90°C are all above absorbance of 0.5. This shift indicates an increase of the optical band which is also evidence of a reduction in the semiconductors as proposed by Mattox [Mattox, 1978]. It is seen that the absorption peak ~330 nm remains at the same position. This resulted in higher %T that was observed at lower temperatures of 60°C, the red shift might be due to loss of material during deposition at a higher temperature. These results are in good agreement with the SEM results as the size of the material increased with an increase in temperature, thus resulting in more absorbance of light on the larger particles and transmitting less light from the object. It was concluded that operations of test work were favorable at lower temperatures.

It was observed that the films obtained at higher annealing pH and low temperature shows slightly high transmittance in visible region as compared to the films obtained at lower annealing pH and temperature which is slightly above 60°C. It was confirmed that the pH of the solution plays a major role in the quality of the chemical bath deposited CdS films. To obtain the precise control over the pH of the solution during the deposition, the bath chamber was successfully modified and used. It was worth noting that the deposition of CdO thin film was not dependent on the acidity or alkalinity of the bath solution as far as depositing adherent material on the substrate.

4.2 Surface materials using Scanning electron microscopy (SEM)

SEM provides detailed high-resolution images of the sample by restoring a focused electron beam across the surface and detecting secondary or backscattered electron

signal. An Energy Dispersive X-Ray Analyser (EDX or EDA) reported as part of the results is also used to provide elemental identification and quantitative compositional information. All samples prior to the analysis they were pre-coated with carbon because they are conducting material and were charging. SEM images showing the surface morphology of the CdO, CdS, ZnO and ZnS thin films obtained by chemical bath deposition (CBD) at temperatures of 60°C, 70°C, and 90°C is illustrated below.

4.2.1 Surface analysis of CdO thin film at various temperatures

Fig: 13 (a) shows the SEM images depositing the surface morphology of CdO thin films obtained by chemical bath deposition (CBD) at different temperatures. At a low temperature of 60°C, it was observed that the surface morphology was very uniform, closely packed and consisted mainly of spherical nanoparticles. As the substrate temperature increases, the film surface modifies with grains having well-defined boundaries shown at 60°C. It can also be seen that the deposited film surface is smooth, homogeneous, and continuous covering the entire substrate. Patches of fused grains are minimized and the film surface appears not tightly packed without any cracks or holes confirming an improvement in the film crystallinity with temperature. The prepared CdO thin films have good quality, uniform morphology and covered the entire substrate surface. The particle sizes at 60 °C appeared to be smaller as compared to 70 °C and 90 °C was observed which are dispersed uniformly on the substrate and hence giving rise to better deposition.

Fig: 13 (b) illustrate the deposition of CdO at 70°C. The distribution was observed to be nonuniform and scattered compared to deposition at 60°C. The observed shape was spherical and bigger than Fig: 13 (a) as charging of the as-deposited materials were observed.

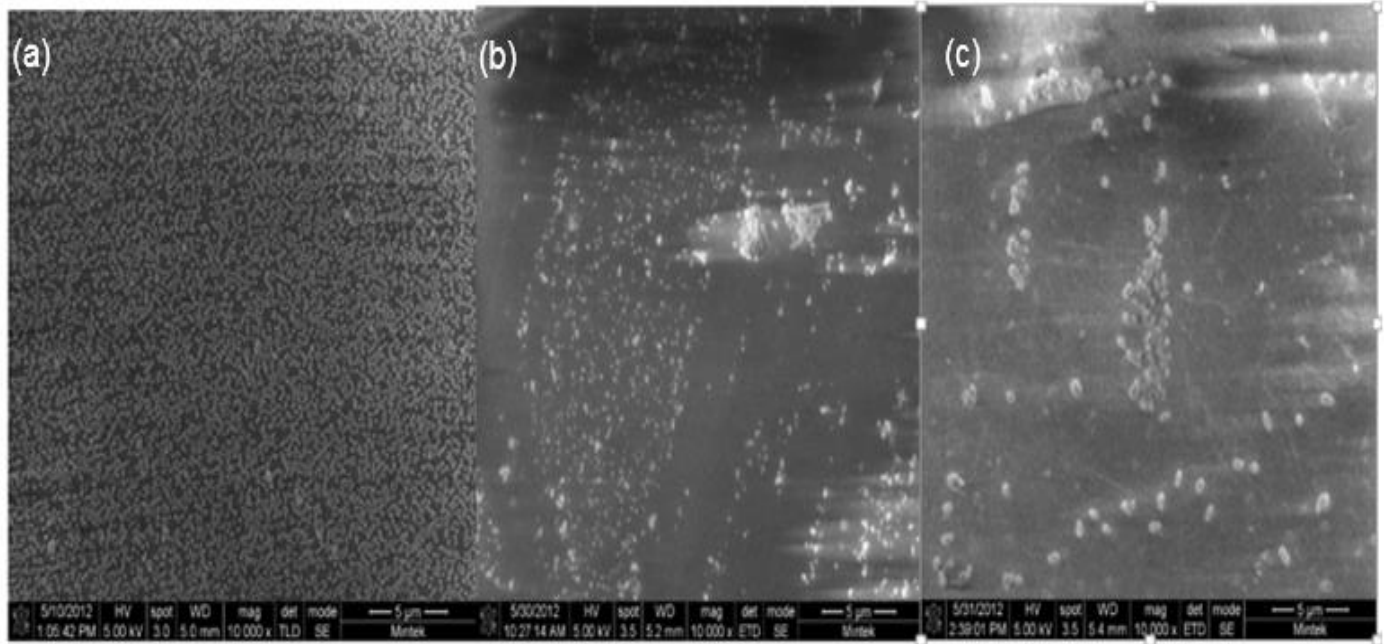


Figure 13: SEM images of CdO thin film at magnifications of 5µm (a) 60°C, (b) 70°C, (c) and 90°C

Fig: 13 (c), it was observed that patches of grains interconnected are evident in the morphology of the film coated at 90°C. It was observed that the surface had scratches with particles that are bigger than that of Fig: 13 (a) and (b). According to this observation, it was evident that the grain sizes increase with an increase in temperature and as the temperature increases the particles size increases with formation of cracks on the substrate.

According to the results it can be concluded that the lower temperature which is 60°C resulted in a better deposition and poor deposition at a higher temperature. Smaller sizes of particles are observed which are dispersed uniformly on the substrate and hence giving rise to better deposition. Lower energy gives rise to a slower rate of deposition resulting from particle growth being influenced by the thermodynamics and consequently kinetically slower rate favored.

The SEM micrographs of the grown films of CdO composites showed fine granular deposition, which was covering the entire glass substrate and with some agglomeration of finer particulates to form bigger clusters depending upon deposition temperature. At

lower temperature (60°C), discontinuous and low-density films were obtained however these finely deposited particles provided nucleation zones for random multidirectional filamentous growth at 70°C. The high distribution of nucleation sites can encourage the formation of aligned structures and their lateral coalescence to form smooth continuous thin films [Vallejos & Blackman, 2011]. Higher synthesis temperatures gave more defined and scattered films. At 90°C the filamentous growth became complex and a finely knit intricate film structure has led to the formation of dense microstructures with high spatial film density. Temperature is governing the morphological orientation of deposited precursors. At low temperature, decomposed aerosol precursors have covered substrate discontinuously in the form of a particle. The increase in deposition temperature has encouraged particles growth in thread/filament shape giving highly continuous and porous thin films.

4.2.2 Surface analysis of CdS thin film at various temperatures

Fig: 14 (a) show the deposition of CdS at 60°C by CBD at pH 11. The spherically shaped particles were closely compact and smooth surface. It was observed that not only were there no adsorbed colloidal particles shown as white boulders on the surface, but there was a remarkable difference in grain sizes and their uniformity as compared to Fig: 14 (b) and (c).

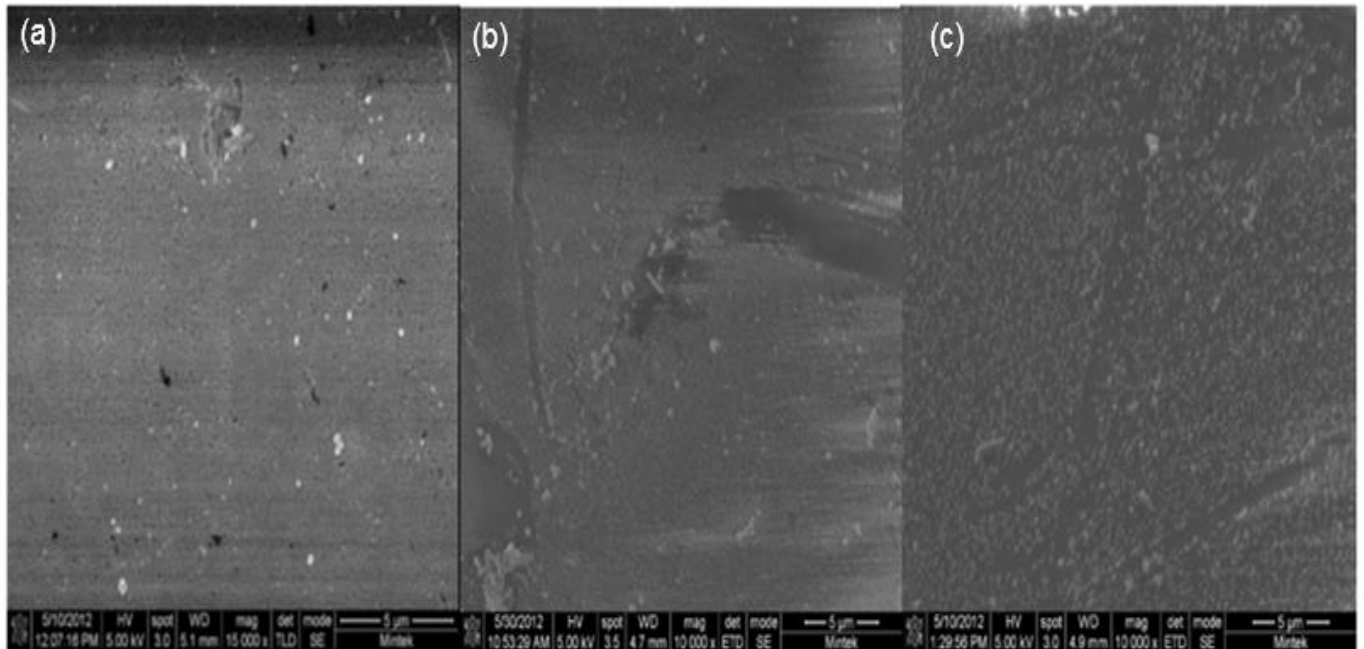


Figure 14: SEM images of CdS thin film at magnifications of 5 μ m (a) 60°C, (b) 70°C, and (c) 90°C

Fig: 14 (b) illustrates the surface morphology of CdS film observed by SEM at 70°C. It was observed that at 70°C patches of the undeposited surface was observed as the deposition was not covering the entire substrate. The particles we observed as being not homogeneous with different particle sizes.

Fig: 14 (c) was the deposition of CdS at 90°C by CBD. The observations made were that at temperatures of 90°C similarly as CdO that the particle size increased with an increase in temperature. Smaller sizes of particles are observed which are dispersed uniformly on the substrate and hence giving rise to better deposition. Lower energy gives rise to a slower rate of deposition resulting from particle growth being influenced by the thermodynamics and consequently, kinetically slower rate favored.

4.2.3 Surface analysis of ZnO thin film at various temperatures

Fig: 15 (a) was the deposition of ZnO at an ambient temperature of 60°C. The remarks made were that at 60°C, the film has good quality, uniform morphology and covered the entire substrate surface with star-shaped flower like imaging. The micrographs show

that the composite films cover the substrate well and are mostly uniform over the entire substrate surface which is important for practical application in devices.

Fig: 15 (b) shows the images of ZnO thin films at 70°C at pH 11. The obtained results were the rather scattered formation and rods were formed as compared to the deposition at 60°C. From the imaging, it was worth noting that the material was rather not closely packed and non-homogeneous.

Fig: 15 (c) shows results of ZnO deposited at temperature of 90°C. According to observations made the sizes of the particles was larger than the deposition at 60°C and 70°C. Rods and star-shaped structure were observed. It was worth noting that the particle size increased in and increase in temperature which also has an effect on how the closely packed the particles are on the substrate.

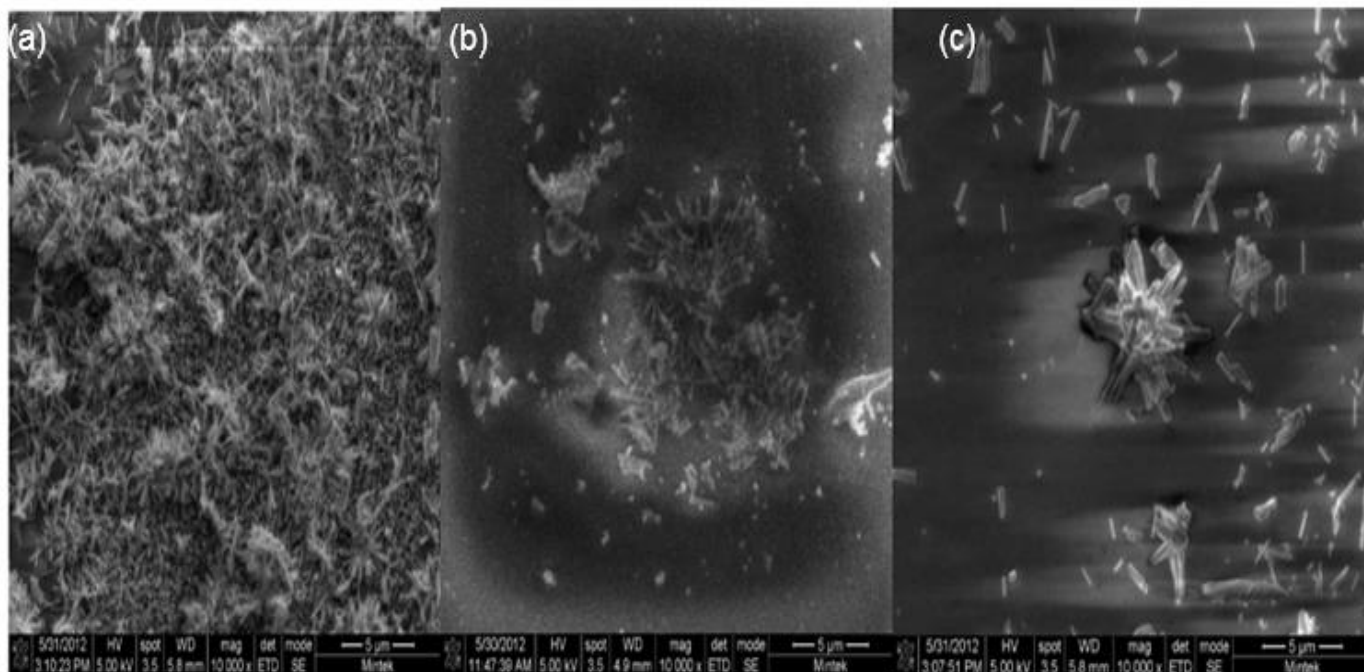


Figure 15: SEM images of ZnO thin film at magnifications of 5µm (a) 60°C, (b) 70°C, and (c) 90°C

From the sets of results it can be concluded that temperature has an effect on the shape and size of the as-deposited material of ZnS.

4.2.4 Surface analysis of ZnS thin film at various temperatures

Fig: 16 (a) demonstrate that smooth formation was observed and the grains appear to be not homogeneous, suggesting that there was no uniform nucleation throughout the surface at temperatures of 60°C. Similarly to the deposition of ZnO deposition the formation of star shapes was also observed.

Fig: 16 (b) explains the deposition of ZnS at 70°C. The clatter of flower like formations was observed, which clearly indicates that the deposition at 70°C was not smooth. It can be observed that the particle size increased as compared to figure 16 (a).

Fig: 16 (c) demonstrates that the particles size are larger than that of Fig: 16 (a) and (b). Observations of rods and star shapes were made which are rather not cluttered. The surface was rather smoother than Fig: 16 (b). The images of Fig: 16 have highly

oriented microstructure composed of pentagram shape. The pores in between the pentagram star shapes certainly influence the optical properties of thin films. This can be correlated with the high value obtained for the number of crystal per unit surface area from XRD analysis. The prepared ZnS thin films have good quality, uniform morphology and covered the entire substrate surface.

From the sets of results it can be concluded that temperature has an effect on the shape and size of the as-deposited material of ZnS. The lower temperature gave a better deposition and poor deposition at higher temperatures of 70°C and 90°C. Smaller sizes of particles are observed which are dispersed uniformly on the substrate and hence giving rise to better deposition. Lower energy gives rise to a slower rate of deposition resulting from particle growth being influenced by the thermodynamics and consequently, kinetically slower rate favored.

The morphology studies showed that lower temperature of 60°C gave a better deposition and poor deposition at a higher temperature. Smaller sizes of particles are observed which are dispersed uniformly on the substrate and hence giving rise to better deposition. Lower energy gives rise to a slower rate of deposition resulting from particle growth being influenced by the thermodynamics and consequently, kinetically slower rate favored. The increase in temperature caused an increase in particle size and hence causing the particles to be scattered. Since the deposition at lower temperatures yielded better morphology, the research was focused on working at a lower ambient temperature of 60°C in an alkaline medium. It was noted that working at low temperatures yielded lower absorption and higher transmittance which is favored since thin films are used as supporting material and has to absorb less energy and transmit more. The energy band gap was also favorable at relatively lower temperatures since it was close to reported values for researchers. The pH did not have much effect on the %T.

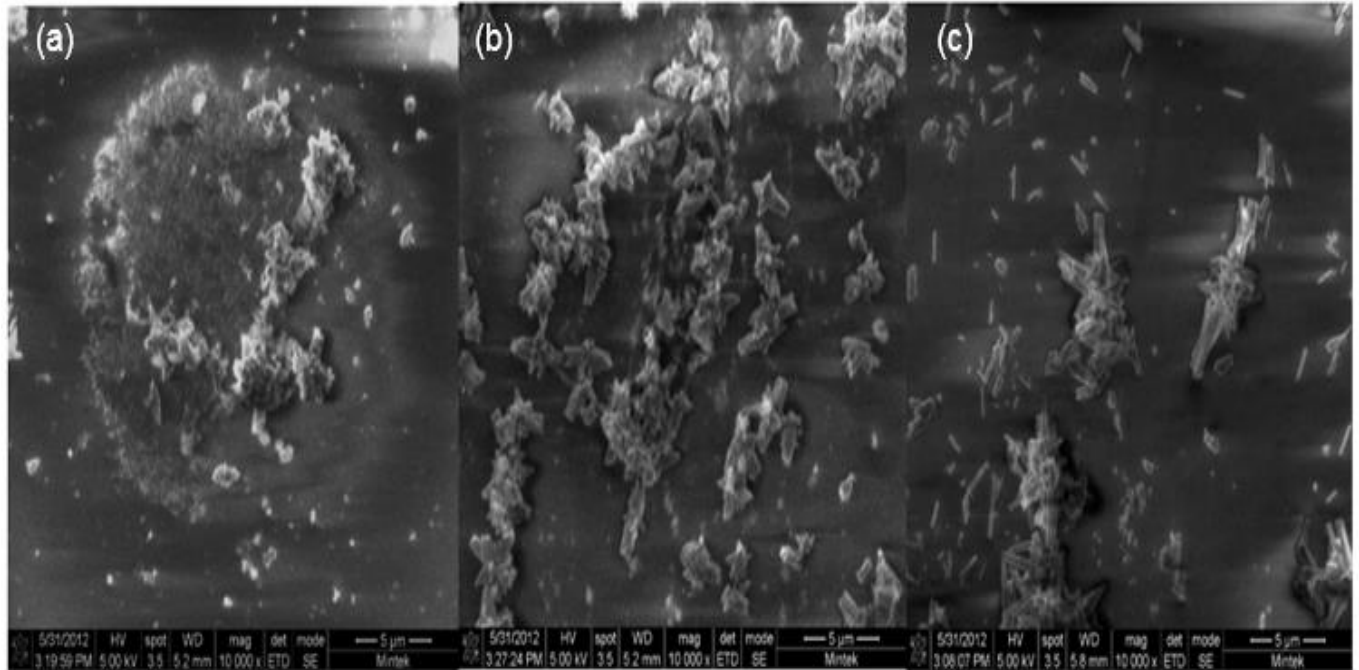


Figure 16: SEM images of ZnS thin film at magnifications of 5µm (a) 60°C, (b) 70°C, and (c) 90°C

SEM imaging illustrates the SEM micrographs of the surfaces of the CdO, CdS, ZnO and ZnS films deposited by CBD at 60°C, 70°C and 90°C taken by [Liu, Vertegel, Bohannan, Sorenson, & Switzer, 2001]. These micrographs show that increasing the deposition temperature results in an increase in grain size and consequently a decrease in voids. When the deposition temperature is 60°C, CdS particles of 50 nm dot the surface of the glass substrate attributing to the controlled nucleation process associated with the low deposition rate.

CdO and CdS films deposited at 60°C have spherical particles of about 100 nm in size. The voids with different sizes ranging from 99 nm to 100 nm for CdO and CdS are still observed, indicating low packing density of the film. The surface of the CdO and CdS films deposited at 70°C is compact and smooth, showing a granular structure with well-defined grain boundaries. It indicates that the increase of the bath temperature is an effective method to diminish voids on the films. But it is noticed that CdO and CdS film deposited at higher temperature 90°C displays a rather larger particle, inhomogeneous surface with overgrowth grains.

ZnO and ZnS deposited at lower temperatures of 60°C have the star-shaped structure of about ~110 nm in size. The different sizes ranged from 107.7 to 114.4 nm of ZnO and ZnS, which also showed low packing density. The deposition at 70°C showed grain size that was bigger and well-defined particles which are smoother than the deposited 60°C. But it is noticed that ZnO and ZnS film deposited at higher temperature 90°C displays a rather larger particle, inhomogeneous surface with overgrowth grains.

4.3 Structural analysis using atomic force microscopy (AFM)

4.3.1 Structural analysis of CdO thin film

Fig: 17 (a) CdO thin film showed that the surface is composed of crystallites with an approximate size of 32.50 nm grouped together into larger agglomerates which are a comparison with SEM imaging, the RMS (Rq) surface roughness was found to be 69.813 nm and Ra of 89.485 nm. Mean crystallite size corresponding to the CdO thin film. Rq is the root mean square average of height deviation taken from the mean image data plane.

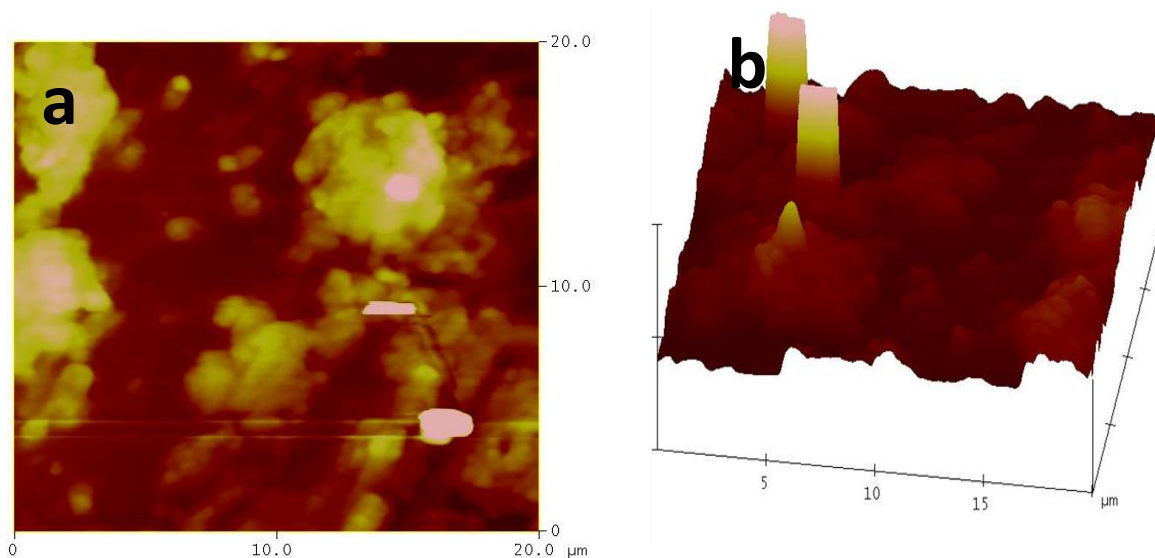


Figure 17: (a) AFM micrographs roughness of CdO thin film at 60°C; (b) AFM 3D micrographs of CdO thin film

Ra is the arithmetic average of the absolute values of the surface height deviations measured from the mean plane. The thickness of the thin film was found to be 100.4 nm which was lower than previously deposited thickness of around 130 and 291 nm [Call, Jabern, Seshan, & Whyte, 1980].

Fig: 17 (b) illustrate that the image are flower like shape. The surface morphology of film shows cauliflower like nano structures grown on glass substrates. It was worth noting that the film morphology is rather non uniform. AFM images show that the film consists of spherical shaped grains. This indicates that the film is well adherent with the substrate.

4.3.2 Structural analysis of CdS thin film

Fig: 18 (a) CdS thin film annealed at 60°C for 60 minutes below shows that the surface is composed of crystallites grouped together into larger agglomerates. The observation was carried out at several locations of the film in order to obtain statistical average value and root means square (RMS) value of surface roughness was found to be 10.022 nm and Ra of 14.530 nm. The thickness of the material was 99.67 nm, which was slightly higher than the CdS films deposited on molybdenum range from about 60–80 nm in thickness [Ates, Yildirim, Kundakci, & Yildirim, 2007].

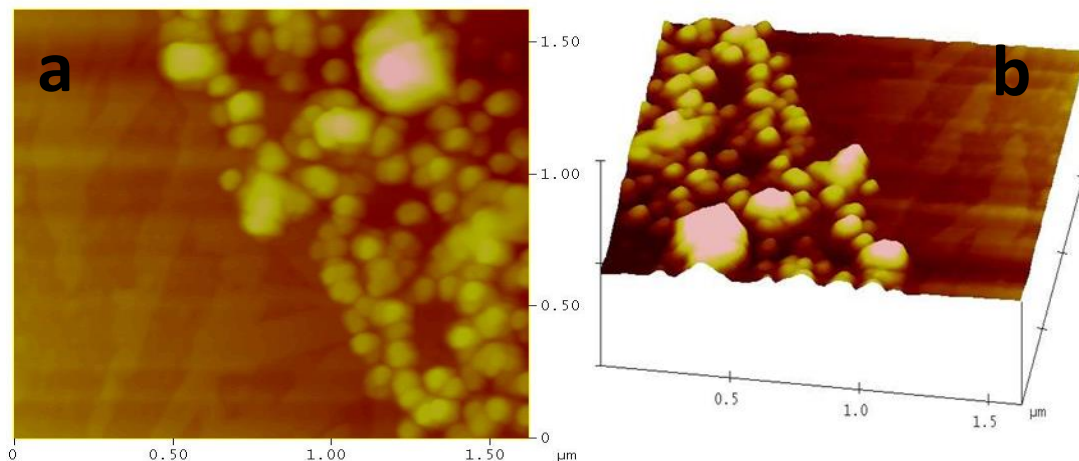


Figure 18: (a) AFM micrographs roughness of CdS thin film at 60°C; (b) AFM 3D micrographs of CdS thin film

Fig: 18 (b) shows that the low peaks observed in the image are due to the broadness of material on the substrate and homogeneity present in these films packed on one side of the substrate. It was worth noting that the film morphology is rather uniform with homogeneous particles. The AFM images exposed high uniformity of the films with round spherical-shaped materials, and also shows the beta phase films. AFM images show that the film consists of closely packed uniform spherical shaped grains without cracks. This indicates that the film is well adherent with the substrate and homogeneous.

4.3.3 Structural analysis of ZnO thin film

Fig: 19 (a) show ZnO thin film showed that the surface is composed of crystallites. The RMS surface roughness was found to be 25.776 nm and Ra of 10.893 nm. The deposited thickness for ZnO thin film was 114.4 nm.

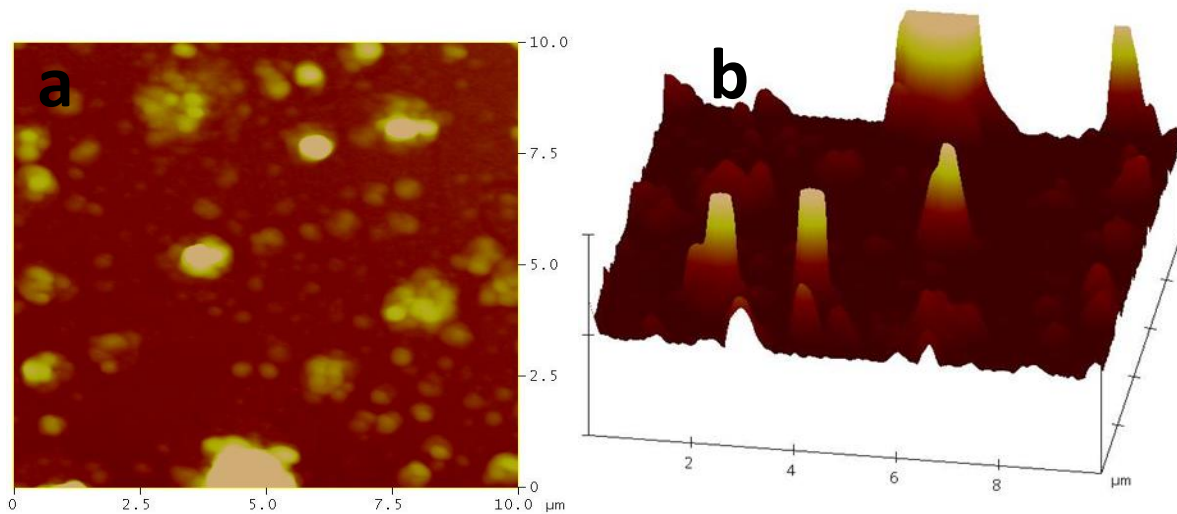


Figure 19: (a) AFM micrographs roughness of ZnO thin film at 60°C; (b) AFM 3D micrographs of ZnO thin film

Fig: 19 (b) illustrates that the AFM images exposed high uniformity of the films with star-shaped materials which show two layers of materials which compose of smaller particles and larger particles. AFM images show that the film consists of closely packed

uniform star-shaped grains without cracks. This indicates that the film is well adherent with the substrate and not homogeneous.

4.3.4 Structural analysis of ZnS thin film

Fig: 20 (a) topography of ZnS thin film showed that the surface is composed of crystallites that were homogeneous and uniform. The RMS surface roughness was found to be 8.989 nm and Ra of 6.207 nm with a thickness of 107.7 nm.

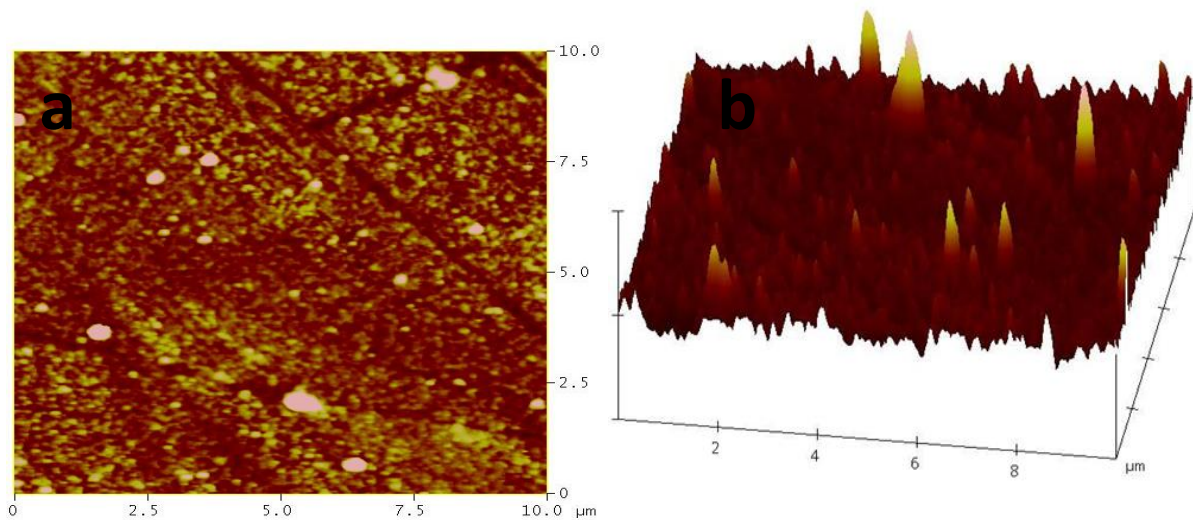


Figure 20: (a) AFM micrographs roughness of ZnS thin film at 60°C; (b) AFM 3D micrographs of ZnS thin film

Fig: 20 (b) It was worth noting that the film morphology was rather uniform and adherent to the substrate. The AFM images exposed high uniformity of the films with star-shaped materials, and also shows the beta phase films. AFM images show that the film consists of closely packed uniform star-shaped grains without cracks. This indicates that the film is well adherent with the substrate and homogeneous with some cracks on the substrate.

The table below illustrates the values of the RMS and Ra of the material deposition of CdO, CdS, ZnO and ZnS thin film.

Table 1: RMS (Rq) and Ra of the material deposition of CdO, CdS, ZnO and ZnS thin film

Material thin film	Bath Temperature (°C)	pH	RMS (Rq) (nm)	Ra (nm)	Thickness (nm)
CdO	60	11	69.813	49.485	100.4
CdS	60	11	14.530	10.022	99.67
ZnO	60	11	25.776	10.893	114.4
ZnS	60	11	8.989	6.207	107.7

Where Rq is the root mean square average of height deviation taken from the mean image data plane and Ra is the arithmetic average. It was worth noting that the thickness of ZnO single layer deposition was 114.4 nm and ZnS layer deposition 107.7 nm. The thickness of the as deposited CdO single layer deposition was found to be 100.4 nm and the deposited CdS was 99.67 nm. The roughness of cadmium series was higher than that of zinc.

4.4 Crystallinity of a compound using X-ray Diffraction (XRD)

4.4.1 Crystal structure of CdO thin film

The films obtained by this technique were white in color, continuous and adhere very well. XRD patterns of the CdO thin films deposited at 60°C showed a nanocrystalline structure and broad peaks along (111) shown below at figure 22. The XRD of CdO thin films showed no peaks for crystalline with a broad peak around 2θ value 26.37°. This evidences the nanocrystalline nature of CdO thin films [Call, Jabern, Seshan, & Whyte, 1980].

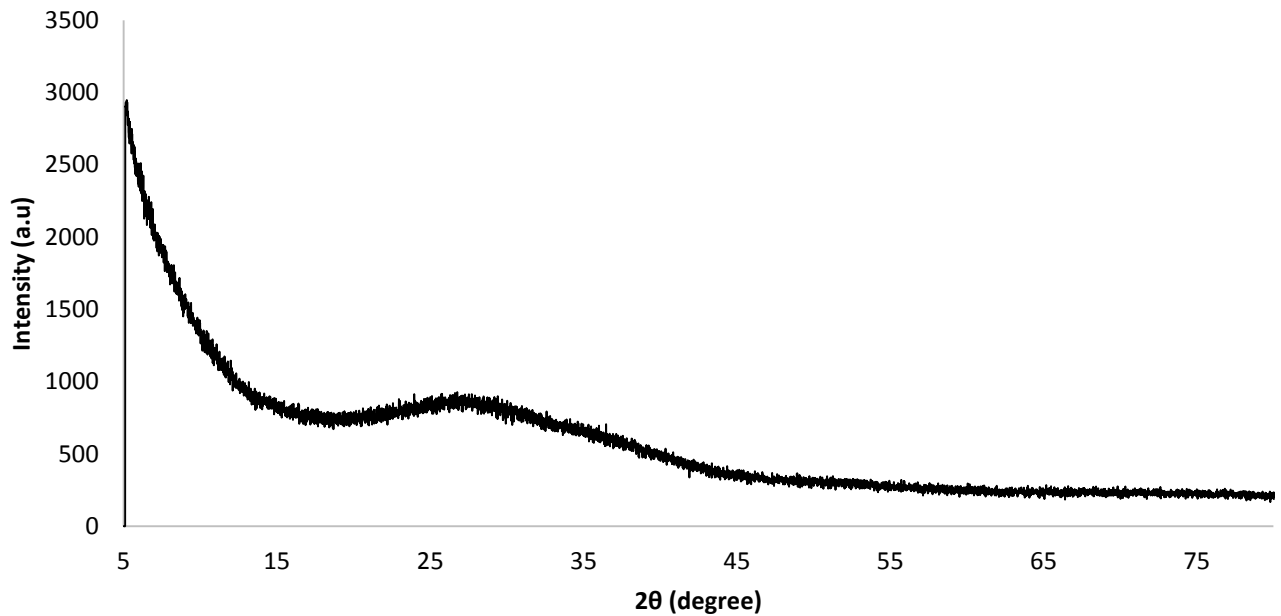


Figure 21: XRD patterns of CdO thin film

The as-deposited film is almost not showing any diffraction peak around preferred orientation of CdO. The small broad peak arises due to the smaller grain size of the film. Some contribution due to strain and instrumental broadening may also affect the peak broadening. One broad peak was observed and film was of mainly nanocrystalline.

4.4.2 Crystal structure of CdS thin film

XRD pattern of as-grown CdS thin film by CBD is illustrated below. Structural studies have shown the formation of CdS film with one broad diffraction peak corresponding to (111) plane as shown below in figure 23. The peak was found to be broad, superimposed on an amorphous background due to the glass substrate. The small broad peak arises due to the smaller grain size of the film. Some contribution due to strain and instrumental broadening may also affect the peak broadening. The reactions from these planes have previously been reported by [Lincot, Froment, & Cachet, 1999] for CBD-CdS thin films grown on Si (111) substrate from a similar bath. [Oladeji & Chow, 1997], also made similar observation reactions from these planes but (200) plane

for the CBD-CdS thin film grown on glass. It has been reported [Zeleya-Angel, *et al.*, 1997] that CdS structure has a stable hexagonal phase and a metastable cubic phase. The quick inference from all these observations is that the mechanisms of CdS thin film growth in a basic aqueous chemical bath favor a cubic structure formation; more so that the growth temperatures, ranging from room temperature to 100°C, are much lower than this transition temperature.

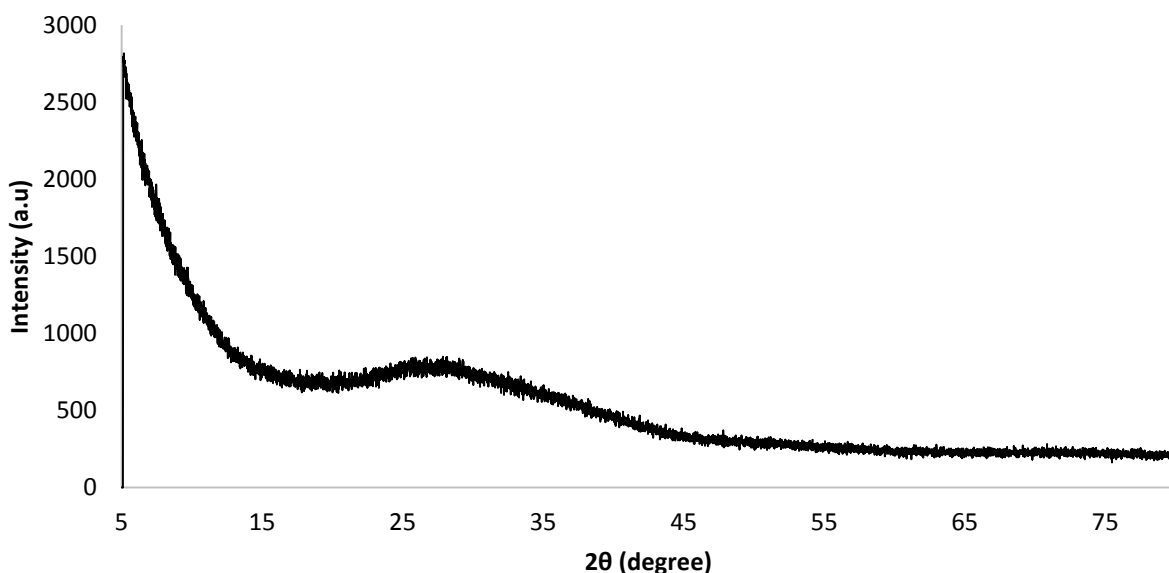


Figure 22: XRD patterns of CdS thin film

However, several other authors [Kaur, Pandya, & Chopra, 1980], [Doña & Herrero, 1997], and [Chu, Olmedo, Yang, Kong, & Liu, 2008] classified the structure of as-grown CBD-CdS thin film from a basic aqueous bath as hexagonal. In the reports [Chu, Olmedo, Yang, Kong, & Liu, 2008] and [Doña & Herrero, 1997] where this claim was backed up by the XRD pattern of the CBD-CdS thin films, a single reaction broad peak located at 25.76° which as a matter of fact could have emanated from the (111) plane of cubic or (002) plane of hexagonal CdS structure, was observed. Based on the readings made by [Zeleya-Angel, *et al.*, 1997] and [Lincot, Froment, & Cachet, 1999], our present result, and other investigations carried out, it was attributed that this latter reaction to

that of (111) plane produce a cubic structure of CdS deposited by CBD. It can be inferred that the films gelling for the existence of more than one summit, as well as the results, showed that the CdS thin films were cubic structure, and we note that one of the peaks are prominent more than its peers, and the reason is due to the Influence of deposition temperature on the growth of these levels, the emergence of multi-gelling composition is normal because the material deposited on the flat bases and amorphous.

4.4.3 Crystal structure of ZnO thin film

XRD pattern of the crystal structure and orientation of ZnO thin film deposited on a glass substrate using CBD, pre-heated at 60°C. From the XRD pattern, one can clearly observe a diffraction peak at $2\theta = 26.11^\circ$ as shown in figure 24. Strong preferential growth is observed along c-axis i.e. (002) plane, suggesting that the prepared ZnO monocrystals have the wurtzite structure [Andeen, Loeffler, Padture, & Lange, 2003].

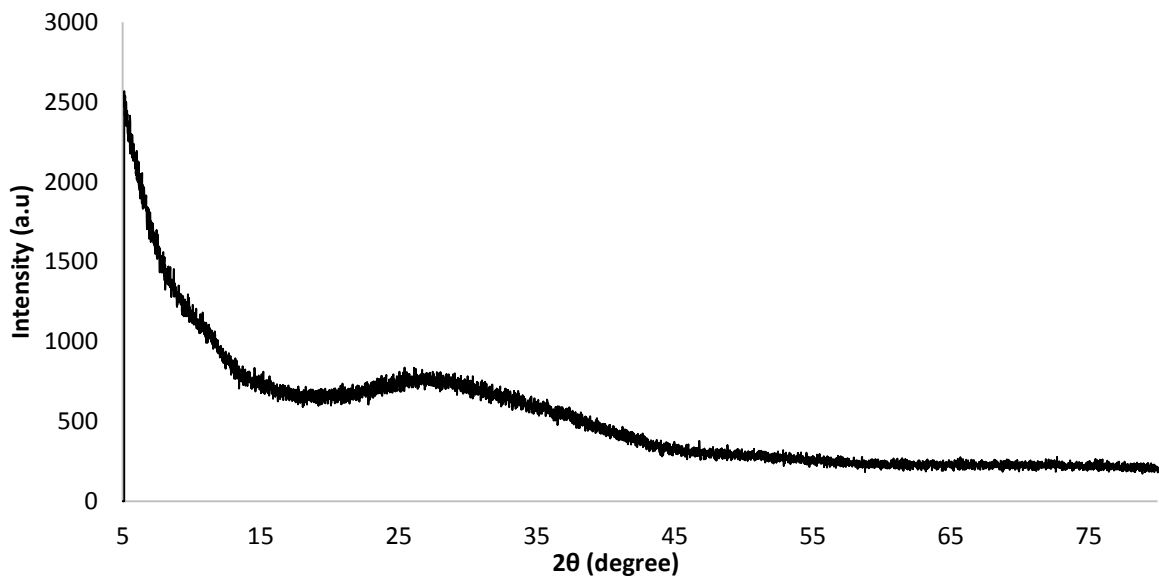


Figure 23: XRD patterns of ZnO thin film

[Suwanboon, 2008], proposed a qualitative idea for the formation mechanism of the preferential oriented thin films could be the minimization of the surface free energy of each crystal plane and usually, films grow so as to minimize the surface energy. Due to

the minimization of surface energy, heterogeneous nucleation readily happens at the interface between film and substrate.

4.4.4 Crystal structure of ZnS thin film

ZnS thin film has been found to grow in cubic (zinc blend) and hexagonal forms depending upon the deposition process. In the present work, the reported hexagonal structure of ZnS is dominated at 2θ relevant with (111) plane as shown in figure 25. XRD pattern showed the typical interplanar spacing corresponding to the cubic phase of ZnS thin film. ZnS exist in sphalerite, cubic (zinc blende) and hexagonal (wurtzite) forms. Several groups reported about the ZnS thin film by CBD method in cubic structure [Sartale, Sankapal, lux-Steiner, & Ennaoui, 2005]. ZnS appears almost in amorphous form.

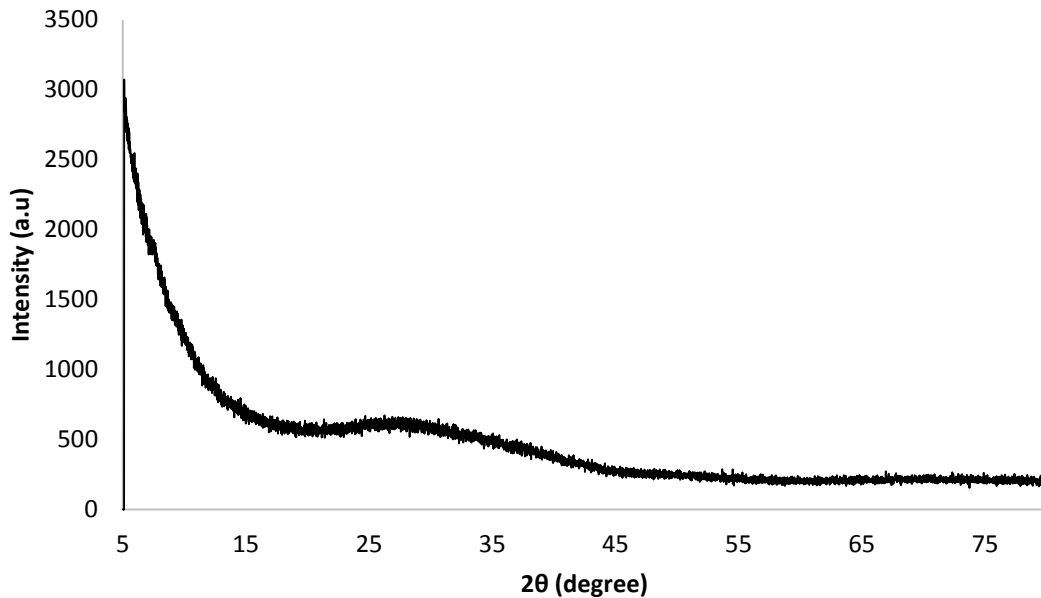


Figure 24: XRD patterns of ZnS thin film

A similar pattern of XRD peaks has been reported by [Lindroos, Kannianen, & Leskela, 1997] for as-deposited CBD-ZnS deposited at a temperature of 60°C. The XRD pattern of ZnS thin films also has been reported by [Johnson, Corletto, Reddy, Forbes, & Miles, 2002], which X-ray diffraction studies of the films produced, did not show any

discernable peaks. In this study, there was only one peak that occurred in XRD pattern on the 2θ scale of 26.22° at (111) also reports were made by [Nasr, Kamoun, & Guasch, 2008].

[Cheng, Chen, & Lee, 2006], and [Johnson, Corletto, Reddy, Forbes, & Miles, 2002], reported the hexagonal structure of ZnS thin film deposited by CBD method. X-ray diffraction pattern of ZnS after single deposition in for this work showed no peaks. The XRD pattern of ZnS thin films also has been reported by [Johnson, Corletto, Reddy, Forbes, & Miles, 2002], which X-ray diffraction studies of the deposited film did not show any discernable peaks. This suggested that the deposited films are very thin (107.7 nm) consisting very few grains. Therefore, multiple depositions were performed on existing ZnS film to increase the thickness to at least 148.38 nm.

A wide (111) peak corresponding to a cubic structure was observed for the multiple deposition films. However, the peak position is shifted from the typical position of 28.5671 (PDF card 65-9585) to 26.22 ; similar results were reported by [Cheng, Chen, & Lee, 2006]. The XRD pattern for the as-deposited film only shows a wide diffraction peak. There is also no obvious diffraction peak for the ZnS film at a different concentration of reagents. This indicates that this ZnS thin were basically amorphous or microcrystalline structure.

MULTILAYERS WITHOUT POLYMER INTERCALATION

4.5 Optical Characterization of Multilayer deposition without polymer intercalation

The optical property of the multilayer film is to study the physical phenomena and optical constant. The multilayer film is possible for two or more wavelength of light to satisfy the conditions for low reflectivity of the film and the film system is considered the achromatized film. However for absorbing film is semi-metallic films the refractive index n has to replace by n^* ($= n-jk$). When a beam of a light passes through the medium it is partly transmitted, reflected and good absorption of the film.

The transmittance was measured by use of T80+ UV-Vis instrument from PG Instruments at the wavelength of 1100-200 nm. The optical study of solid concern not only physical phenomena such as refraction, reflection, transmittance, absorption, polarization, interference, of light but also the interactions of photon energy with matter and the consequent changes in the electron states. The conditions that were kept constant were the temperature and pH of the deposited film which was kept was at 60°C at the pH of 11 for all multilayer deposition shown if figure 26 is discussed in details from 4.5.1 to 4.5.4.

4.5.1 %T of multilayer CdO/CdS thin film

To enhance the optical property of CdO thin film, CdS material was deposited on the interfaces of CdO thin film as a substrate layer. The layer of CdS was deposited on a pre-deposited CdO thin film by forming a CdO/CdS layers. The %T was found to be ~90 % which was increased as compared with the %T of CdO and CdS individual layers at different pH and temperatures. The %T did not increase nor decrease as a result of multilayer deposition on the substrate. The plot shows a sharp rise in transmittance near the band edge attributed to the good crystallinity of the film [Al-Sabayleh, 2008].

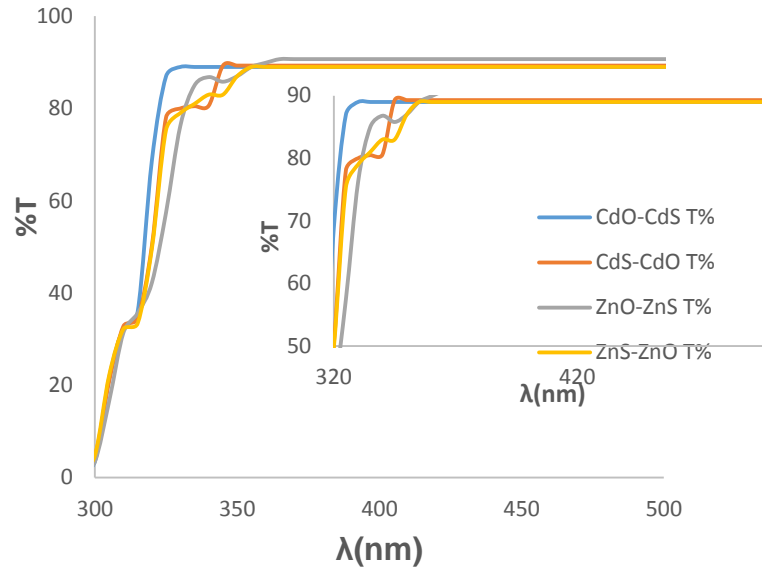


Figure 25: %T of multilayer CdO/CdS, CdS/CdO, ZnO/ZnS, and ZnS/ZnO thin film

Optical transmittance spectra of the thin films are observed to be shifted towards the shorter wavelengths. It was observed that the thickness of material increased whilst no change was observed with the %T. It was worth noting that the increase in %T was in good agreement with the decrease in surface roughness observed from the AFM.

4.5.2 %T of multilayer CdS/CdO thin film

To enhance the optical property of CdO thin films, CdS material was deposited on the interfaces of CdO thin film as a substrate layer. The %T was found to be ~89% which was relatively the same as that of deposited multilayer CdO/CdS thin film. The %T was the same as a result of multilayer deposition on the substrate. The plot shows a sharp rise in transmittance near the band edge attributed to the good crystallinity of the film [Al-Sabayleh, 2008]. It was observed that the increase in %T was in good agreement with the decrease in surface roughness of the deposited material.

4.5.3 %T of multilayer ZnO/ZnS thin film

To enhance the optical property of ZnO thin film, ZnS material was deposited on the interfaces of a pre-deposited ZnO thin film as a substrate layer by CBD technique. The

%T was found to be ~90 % which was the same as the %T of ZnO and ZnS individual layers at various pH and temperatures. The high transmittance of the films together with their large band gap makes them good materials for application as a window layer for solar cells.

4.5.4 %T of multilayer ZnS/ZnO thin film

To enhance the optical property of ZnS thin film, ZnO material was deposited on the interfaces of ZnS thin film as a substrate layer. The %T was found to be ~89 % which was relatively close to the %T of ZnO/ZnS thin film. All the films show highly transparent of above ~89 % in the visible region and some oscillations due to thin film interference effects. The increase in band gap might be attributed to the improvement in crystallinity in the films. It was observed that the increase in %T was in good agreement with the decrease in surface roughness of the deposited material.

The absorbance of the multilayer film was observed above 380 nm wavelength. The films showed a marginal decrease in absorbance at the deposition of CdS/CdO and ZnO/ZnS which was in good agreement with the SEM, AFM and XRD results as the intensity was more and the thickness was less with the particles evenly dispersed on the substrate. The %T was slightly higher on the material of CdS/CdO and ZnO/ZnS this was well supported with the SEM as the particles were smooth. The opposite was the case with deposition of CdO/CdS and ZnS/ZnO as the absorbance was higher which may be a result of the approximation of the deposited particles resulting in the thickness being high. The %T was low this red shift may be due to the roughness of the deposited particles as well as thickness.

4.6 Surface materials using Scanning electron microscopy (SEM)

SEM provides detailed high-resolution images of the sample by restoring a focused electron beam across the surface and detecting secondary or backscattered electron signal. An Energy dispersive X-ray analyzer (EDX or EDA) reported as part of the results is also used to provide elemental identification and quantitative compositional

information. All samples prior to the analysis they were pre-coated with carbon because they are conducting material and were charging.

4.6.1 Surface of multilayer CdO/CdS thin film

The following SEM image shows the surface morphology of the multilayer deposited CdO/CdS composites thin films obtained by CBD technique. No Porosity and roughness were observed from the SEM images. The micrographs show that the composite films cover the substrate well and are mostly uniform over the entire substrate surface which is important for practical application in devices. Spherical shapes which are different with sizes were observed on the images which are well distributed on the surface. The glow on the surface right side was due to the charging of the deposited CdO/CdS on the substrate. It is known that CdS oxidizes to CdO during elevated temperatures, therefore, a need for quantitative analyses was required to determine that CdS was deposited on the pre-deposited CdO material. It was observed that the surface was smoother and tightly packed as compared to the monolayer deposition at the same parameters. These results are well in support with the surface roughness as it was decreased with an increase in layer deposition.

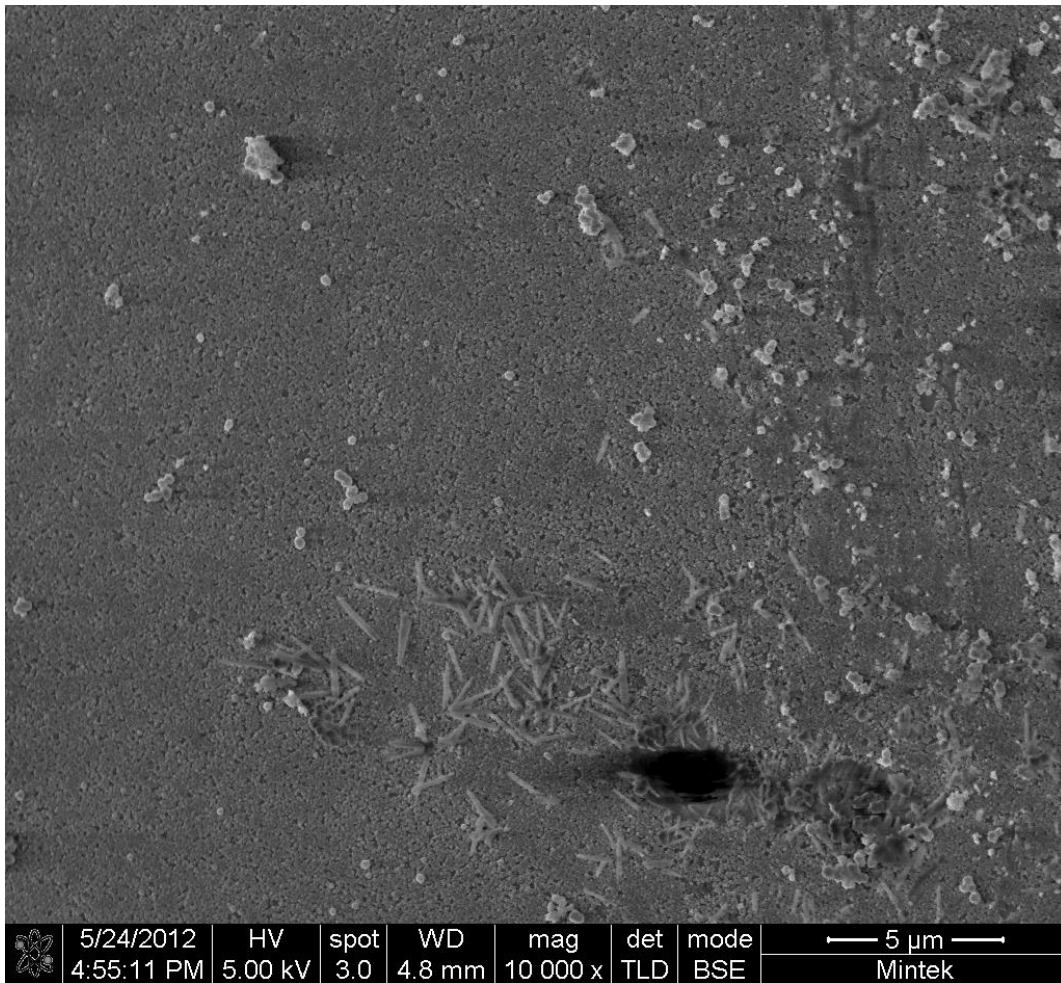


Figure 26: SEM image of multilayer CdO/CdS thin film

Based on observations made in figure 27 the introduction of a second layer of the pre-deposited CdO material had an effect on the surface morphology. It was observed that the homogeneity of the as deposited CdO/CdS had identical spherical shaped structure.

It has been reported by [Bayer, Boyle, Heinrich, O'Brien, Otway, & Robbe, 2000] and [Boyle, Bayer, Heinrich, Robbe, & O'Brien, 2000], that in the case of CBD of CdS, only approximately 2% and less of the initial cadmium concentration is used in film formation, resulting in high levels of cadmium waste. This along with the volatility of ammonia (commonly used in the bath solutions) on a large scale of CBD operations, lead to a significant environmental hazard if not addressed [Kostoglou, Andritsos, &

Karabelas, 2003], [Bayer, Boyle, Heinrich, O'Brien, Otway, & Robbe, 2000], and [Boyle, Bayer, Heinrich, Robbe, & O'Brien, 2000].

4.6.2 Surface of multilayer CdS/CdO thin film

The following SEM image in figure 28 shows the surface morphology of CdS/CdO composite thin films obtained by CBD technique. Roughness and non-uniformity were observed from the SEM images that are clearly adjusted as CdS/CdO composite thin films deposited at of pH 11 and temperature of 60°C . The micrographs show that the composite film is distributed uniformly on the substrate. The composite of MS/MO image showed larger spherical particles than that of CdO/CdS, hence more charging of the material was observed even when the substrate was pre-coated with carbon.

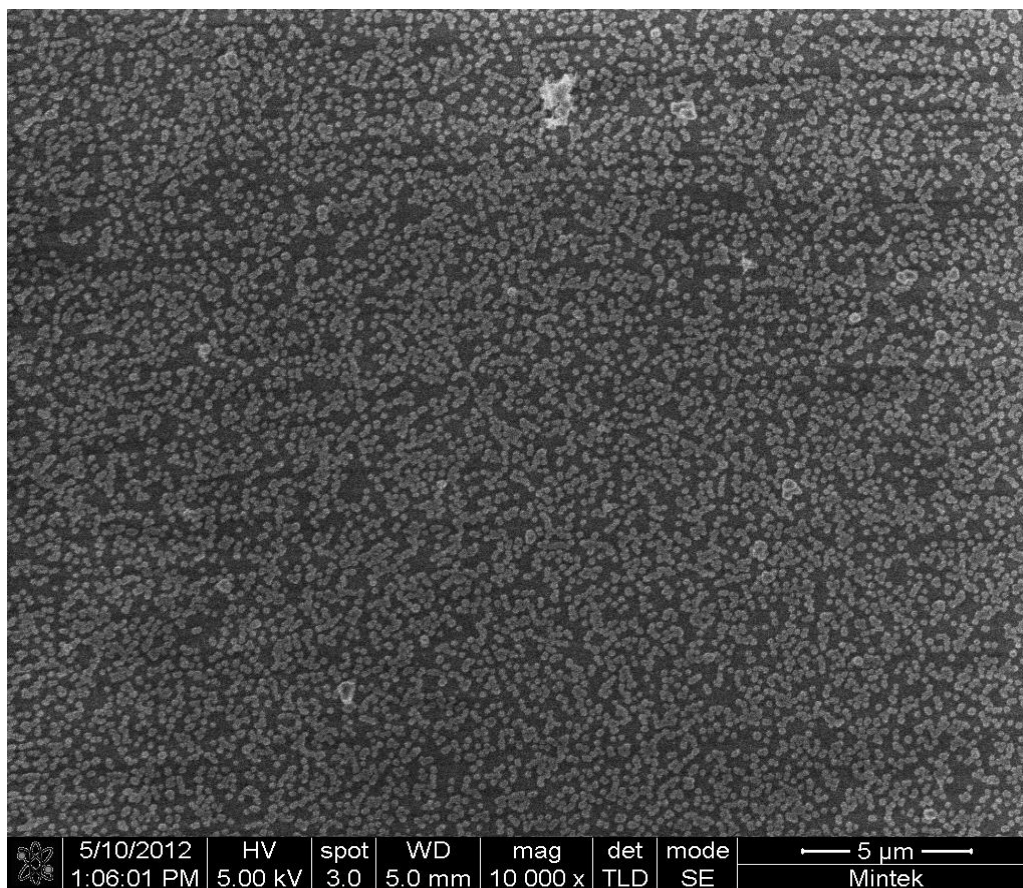


Figure 27: SEM image of multilayer CdS/CdO thin film

Large spherical particles that appear to be increasing in size and homogeneous were observed in the deposition of CdS/CdO. This may also be due to the fact that CdS films get oxidized in the bath to form CdO thin films. It was observed that the deposition of CdS on the pre-deposited CdO had an effect on the morphological studies of the deposited material. The observations made are that the surface was smoother and homogeneous as compared to the monolayer deposition at the same parameters. These results are well in support with the surface roughness as it was decreased with an increase in layer deposition.

4.6.3 Surface of multilayer ZnO/ZnS thin film

The SEM images showing the surface morphology of the ZnO/ZnS composite thin films obtained by CBD technique is shown below. No roughness were observed from the SEM images that are clearly adjusted as the ZnO/ZnS composite thin films were deposited at pH of 11 and temperatures of 60°C. Snowflakes structures were observed for the deposition of ZnO/ZnS which is uniform around the surface. The most intricate snowflake patterns are typically formed during warm and wet conditions. This shape remarkably shows an analogous to that of snowflakes, representing an ideal two-dimensional (2D) growth system as to reported graphene.

No cluster formation was observed and the grains appear to be homogeneous and uniform suggesting that uniform nucleation throughout the surface was observed. The as-deposited thin films show large conglomerate of flake structures. The randomly grown flake-like structures as a result of thermal treatment at 60°C further segregated to micro-nanocrystal structures is shown in figure 29. ZnO/ZnS multilayer yielded interesting and better imaging. This can be correlated with the high value obtained for the number of crystallites per unit surface area from XRD analysis. The observations made are that the surface was smoother as compared to the monolayer deposition at the same parameters. These results are well in support with the surface roughness as it was decreased with an increase in layer deposition.

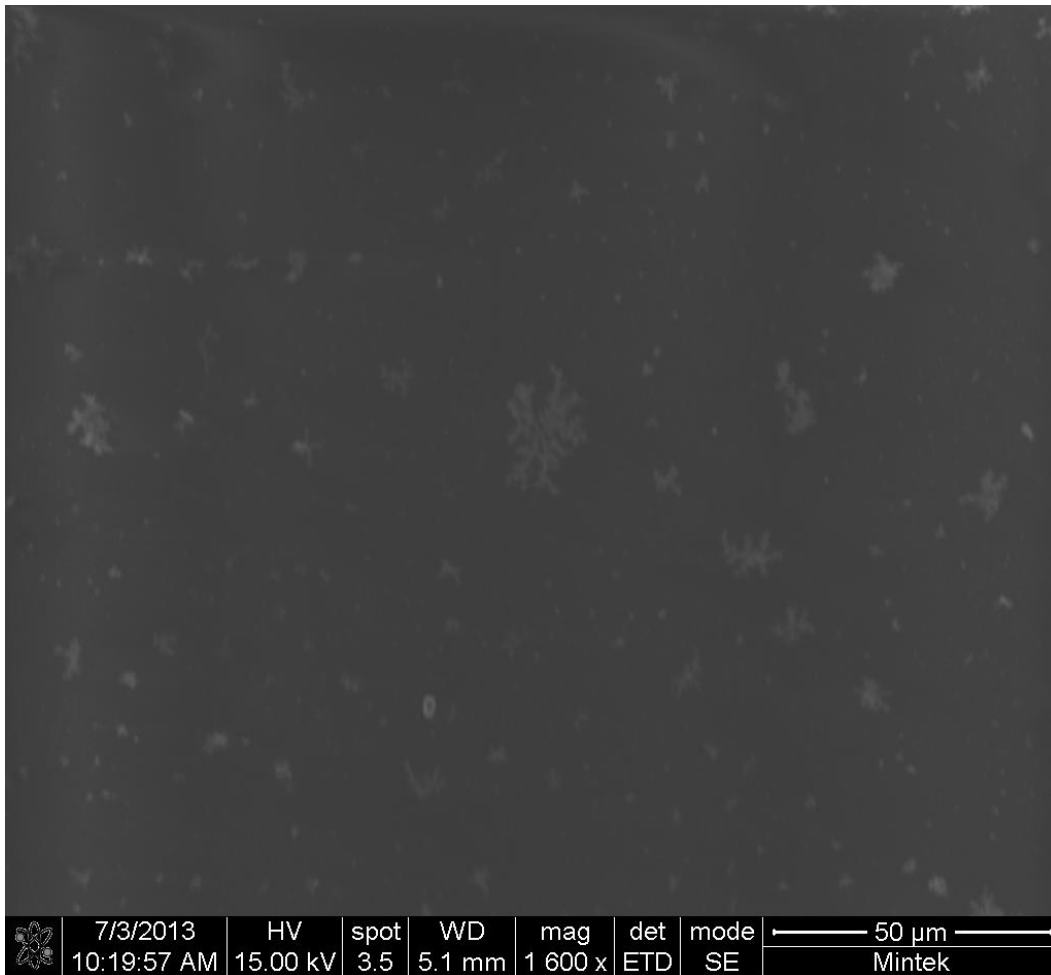


Figure 28: SEM image of multilayer ZnO/ZnS thin film

ZnO has three crystal structures: primitive hexagonal wurtzite, face-centered cubic zinc blende, and face-centered cubic rock-salt structures. In the first two cases, each cation is coordinated with four anions at the corners of the tetrahedron, whereas in the rock salt structure each cation is surrounded by six anions. The reported structure in this work has six anions surrounding the cation as compared to previous the literature [Wu, Bai, Li, Lu, & Shi, 2006]. Based on observations of the as-deposited it was worth noting that the deposition of ZnS on the pre-deposited ZnO had an effect on the morphological studies. As it was observed that snowflake shaped imaging was observed as compared to the deposited ZnO thin film which showed star-shaped structure.

4.6.4 Surface of multilayer ZnS/ZnO thin film

The SEM images showing the surface morphology of the ZnS/ZnO composite thin films obtained by chemical bath deposition (CBD) is shown below in figure 30. The amorphous structure was observed from the SEM images that are clearly adjusted as the ZnS/ZnO multilayer thin film was deposited. The image does not show a clear structure but the structure is a distorted image of that of ZnS/ZnO thin film. At this point, it was clear that the deposition of ZnO on a pre-deposited ZnS thin film has in effect in the structure of the multilayer thin film. The observations made are that the surface was smoother as compared to the monolayer deposition at the same parameters. These results are well in support with the surface roughness as it was decreased with an increase in layer deposition.

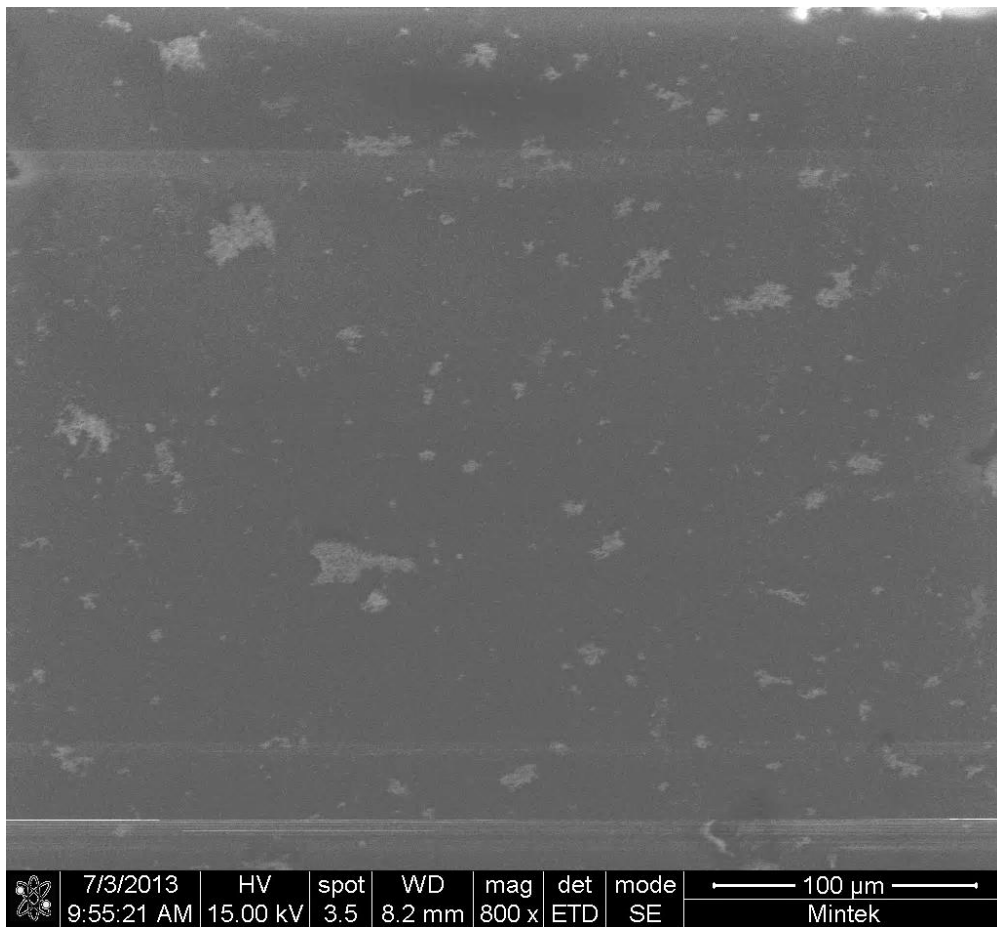


Figure 29: SEM image of multilayer ZnS/ZnO thin film

The SEM image show uniform surface with well-defined grain boundaries. No cluster formation was observed and the grains appear to be homogeneous and uniform suggesting that there was a uniform nucleation throughout the surface. The micrograph depicts that the grains of the as-deposited film is tightly packed. Based on observation of the as-deposited ZnS/ZnO thin film, it was worth noting that the deposition of ZnO on the pre-deposited ZnS had an effect on the surface morphology. This can be correlated with the high value obtained for the number of crystallites per unit surface area from XRD analysis.

4.7 Structural analysis using atomic force microscopy (AFM)

AFM is a technique for obtaining high-resolution images of surfaces on the atomic scale. The AFM images the surface by a force: the cantilever tip scans the sample, and the mechanical raster-scanning system (piezoelectric) measures the deflection of the cantilever from the sample surface. There are two basic modes of operation. The first, when the atomic interactions between the sample and the tip are kept constant by the cantilever. The map of the surface topography is provided by recording the vertical position of the sample relative to the base of the cantilever. AFM microscopy was employed to reveal the surface topography of the thin layers and to measure their roughness. AFM microscopy was employed to reveal the surface topography of the thin layers and to measure their roughness.

4.7.1 Structural analysis of multilayer CdO/CdS thin film

From a topographical of CdO/CdS multilayer, it was possible to deposit smoother thin films at a reduced deposition rate by placing the substrates submerged in solution at lower temperatures. The deposition of multilayer CdO/CdS thin film below represents analysis for the roughness of the multilayer thin film for the enhanced CdO. This image illustrates the high degree of roughness characteristic. Film roughness was studied for the multilayer films and for the layered films of CdO and CdS base. Fig: 31 (a) shows the Ra roughness as determined by AFM, as well as the mean roughness, was found to be 17.699 nm as a function of CdO/CdS cycle ratio. The RMS for multilayer of CdO/CdS was 31.791 nm. The resulting thickness for multilayer deposition of

CdO/CdS thin film was 145.47 nm which was increased from the monolayer thin film. From these results it was observed that an increase in layer increases the thickness of the deposited material, hence the second layer deposited by CBD technique does not wash away the pre-deposited layer on the substrate. Another finding was that the roughness was decreased with an increase in layer deposition resulting in the increase in %T for multilayer deposition resulting in a good crystal structure.

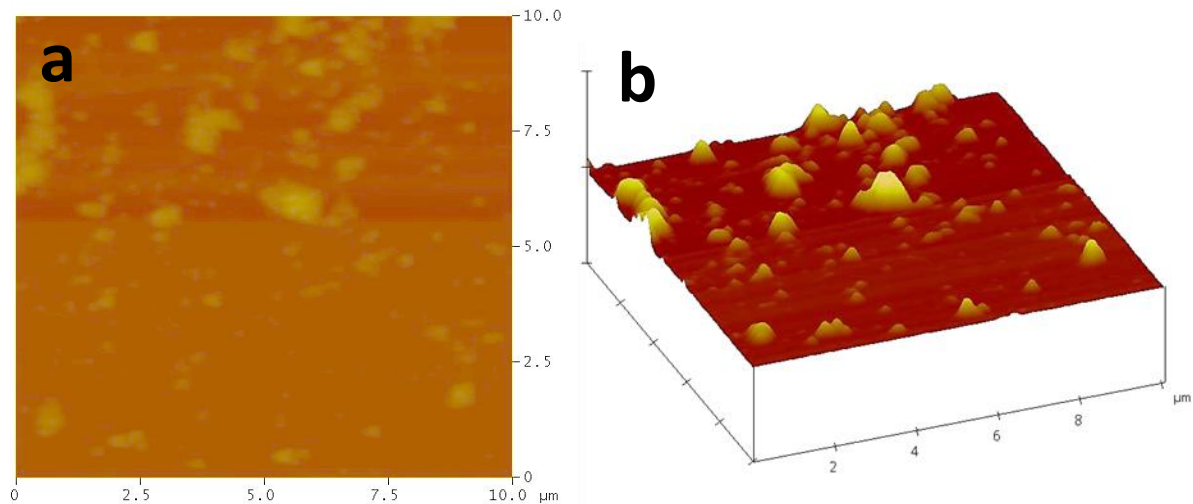


Figure 30: (a) AFM micrographs roughness of multilayer CdO/CdS thin film; (b) AFM 3D micrographs of multilayer CdO/CdS thin film

Fig: 31 (b) illustrates that the large peaks observed in the image are due to the droplets on these films. It was worth noting that the film morphology between the droplets is rather uniform. The reason for the formation of these droplets is not well understood. However, they appear to originate from the target during the chemical deposition process and follow a straight path from the target towards the substrate. The droplet concentration decreases away from the central film region. Clearly, by reducing the density of droplets, a significant improvement in surface morphology can be achieved. With the observed results, it was clear to learn that multilayer deposition has an effect on the structure of the material. The RMS has been increased from 3.53 nm to 31.791

nm and Ra increase from 1.894 nm to 17.699 nm. It was clear that multilayer deposition has an effect on the roughness of the material deposition on the substrate.

4.7.2 Structural analysis of multilayer CdS/CdO thin film

From a topographical of CdS/CdO multilayer, it was possible to deposit smoother thin films at a reduced deposition rate by placing the substrates submerged in solution at lower temperatures. The deposition of multilayer CdS/CdO thin film below represents analysis for the roughness of the multilayer thin film for the enhanced CdS thin film. Fig. 32 shows a comparison between the surfaces films as evaluated with an atomic force microscope (AFM). This image illustrates a degree of roughness characteristic. Film roughness was studied for the multilayer films and for the layered films of CdS and CdO base. The deposition of multilayer CdS/CdO thin film below represents analysis for the roughness of the multilayer thin film for the enhanced CdS. The Ra surface roughness for this film was in the order of 4.840 nm with an RMS of 10.902 nm which is lower than the matrix of CdO/CdS deposition.

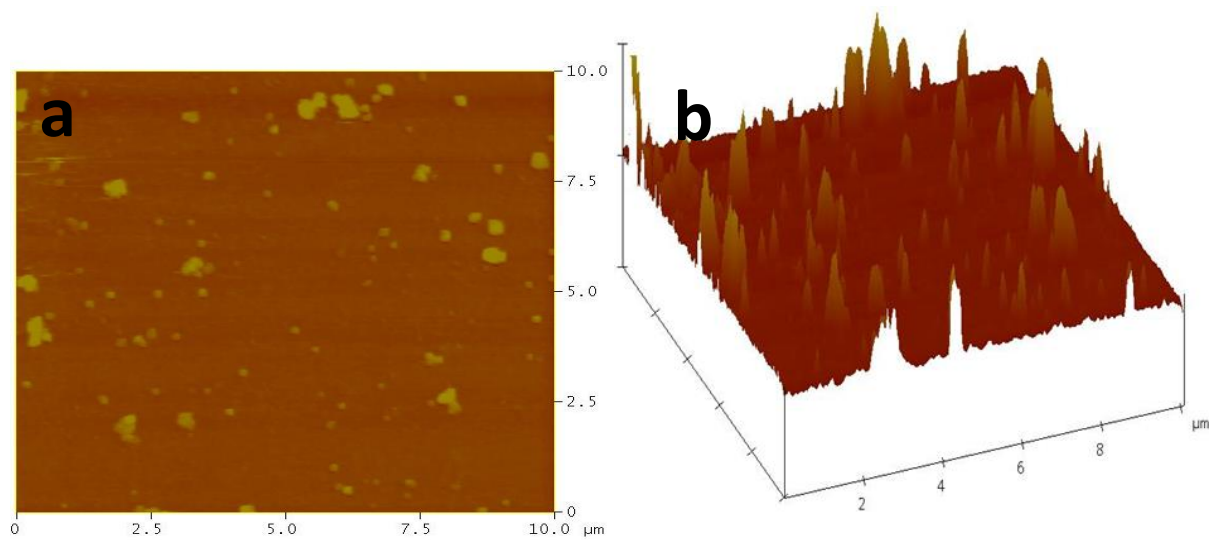


Figure 31: (a) AFM micrographs roughness of multilayer CdS/CdO thin film; (b) AFM 3D micrographs of multilayer CdS/CdO thin film

This can be due to non-uniformity of the grown material on the substrate. Similarly to that of CdO/CdS multilayer thin film the thickness was observed to have increased to

131.0 nm. According to the observed results, an increase in layer increases the thickness of the deposited material.

Fig: 32 (b) It was worth noting that the film morphology between the porosity was rather non uniform and increase in size corresponding to the large chunks of roughness was observed. The roughness is not as homogeneous as the CdO/CdS multilayer thin film, which explains the roughness of the SEM imaging of multilayer of CdS/CdO thin film. It was not clear as to why the roughness of CdS/CdO multilayer thin film was much lower than that of CdO/CdS multilayer thin film. It can be seen that the roughness decreases with the matrix ratio pattern, causing the roughness to vary from 17.699 nm of CdO/CdS to 4.840 nm of CdS/CdO. It significantly means that the matrix ratio plays a significant role in the roughness of the thin film. It was observed that the substrate was a less important factor in film roughness, although it was important in determining the adherence of the films.

With the observed results, it was clear to learn that multilayer deposition has an effect on the structure of the material. The surface roughness decrease with an increase in layer deposition from 14.530 nm to 10.902 nm and Ra decreased from 10.022 nm to 4.840 nm. It was not clear that why the behavior was different from the matrix of CdS/CdO which showed a decrease in roughness. It was observed that the roughness of the material decreased with an increase in layer deposition, which similar findings were observed for the deposition of CdO/CdS multilayer deposition. These result in the increase in %T multilayer deposition from 85 % monolayer to 89 % multilayer. The increase in thickness indicates a good crystal structure as compared to the monolayer thin film. The thickness of the multilayer deposition increased from 99.67 nm to 131.0 nm.

4.7.3 Structural analysis of multilayer ZnO/ZnS thin film

Fig: 33 (a) topography of ZnO/ZnS multilayer, the RMS roughness as determined by AFM, as well as the mean roughness Ra, was found to be 12.850 nm as a function of ZnO/ZnS cycle ratio. The RMS for multilayer of ZnO/ZnS was 18.553 nm. Smoother

observations were made as a result of lower RMS roughness. The thickness was increased to 128.8 nm from 114.4 nm giving a good indication that deposition of the second layer did not wash away the pre-deposited layer. The increase in thickness of multilayer material indicated a good crystallinity as compared to the very thin monolayer.

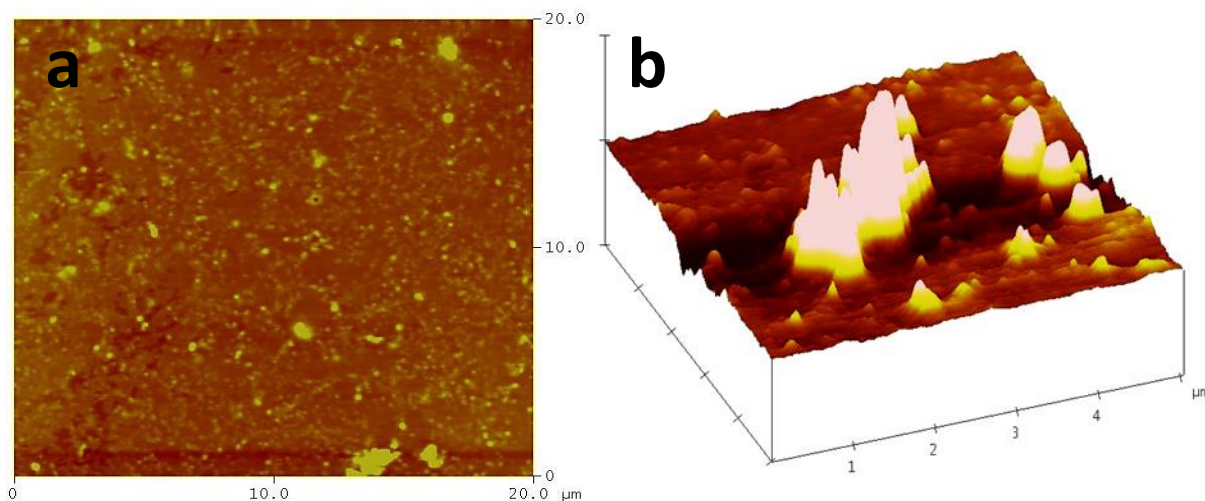


Figure 32: (a) AFM micrographs roughness of multilayer ZnO/ZnS thin film; (b) AFM 3D micrographs of multilayer ZnO/ZnS thin film

Fig: 33 (b) illustrates that the large peaks observed in the image are due to the droplets present on these films. It was worth noting that the film morphology between the droplets is rather uniform. The reason for the formation of these droplets is not well understood. However, they appear to originate from the target during the chemical deposition process and follow a straight path from the target towards the substrate. The droplet concentration decreases away from the central film region. Clearly, by reducing the density of droplets, a significant improvement in surface morphology can be achieved. It was not clear as to why the roughness of ZnS/ZnO multilayer thin film was much lower than that of ZnO/ZnS multilayer thin film. Due to the decrease in roughness, it was expected that the %T would also be affected similarly to the deposition of CdO/CdS, CdS/CdO and ZnS/ZnO multilayer deposition. The %T was the

same as the deposition of monolayer thin film and this might be due to the droplets that were observed for multilayer deposition of ZnO/ZnS thin film.

4.7.4 Structural analysis of multilayer ZnS/ZnO thin film

Fig: 34 (a) shows AFM analysis is ideal for quantitatively measuring the nanometric dimensional surface roughness and for visualizing the surface nanotexture of the deposited multilayer film. From a topographical of ZnS/ZnO multilayer, the RMS roughness as determined by AFM, as well as the mean roughness, was found to be Ra was 7.579 nm as a function of ZnS/ZnO cycle ratio. The RMS for multilayer of ZnS/ZnO was 5.634 nm. By clear indication of the structure, it can be seen that more than one material was deposited onto the substrate. The distribution of the material on the substrate appeared to be homogeneous with spherical shapes. Similar observation to that of ZnO/ZnS multilayer deposition was made as the thickness has increased with an increase in layer deposition. The thickness for ZnS/ZnO was 148.38 nm whilst the roughness was decreased resulting in an increase in %T from 83 % to 90 %.

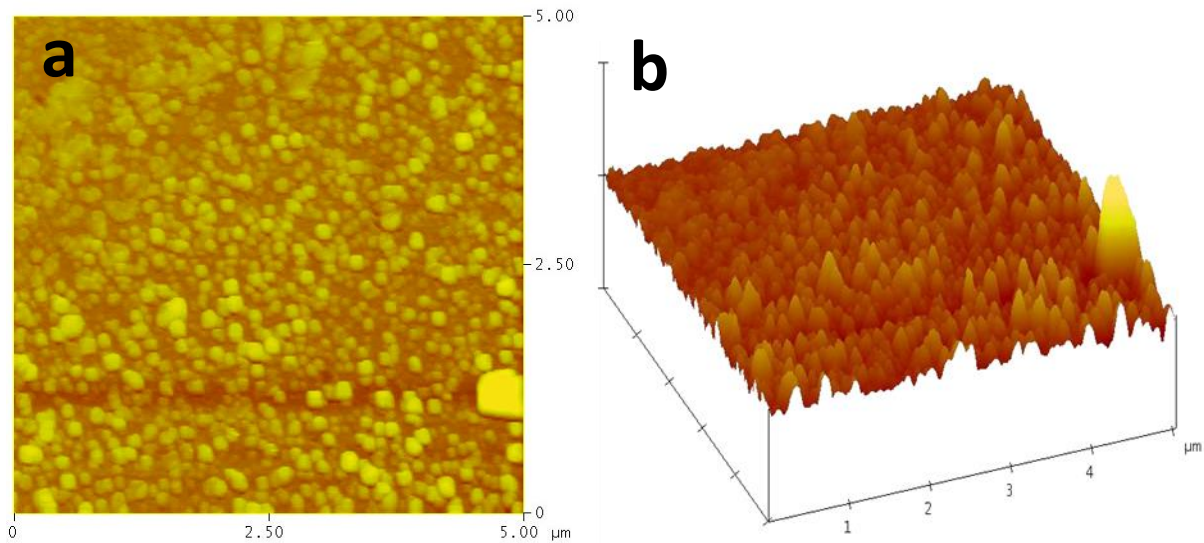


Figure 33: (a) AFM micrographs roughness of multilayer ZnS/ZnO thin film; (b) AFM 3D micrographs of multilayer ZnS/ZnO thin film

Fig: 34 (b) illustrates that the peaks observed in the image are nicely even and homogeneous in the films. It is worth noting that the film morphology between the peaks was rather uniform and clearly shows that more than one material was coated on the substrate. It can be seen that the roughness decrease with the matrix ratio pattern, causing the roughness to vary from Ra 12.850 nm of ZnO/ZnS to 5.634 nm of ZnS/ZnO. It significantly means that the matrix ratio plays a significant role in the roughness of the thin film. The author was of the opinion that the substrate was a less important factor in film roughness, although it was important in determining the adherence of the films. From the observed data, it was not clear as to why the ratio matrix of CdO/CdS and ZnS/ZnO increase the material roughness and that of CdS/CdO and ZnO/ZnS decrease in material roughness. The increase in thickness in the multilayer deposition and the decrease in roughness illustrate a good crystal structure as compared to the monolayer thin film.

It can be seen that the roughness decreases with the matrix ratio pattern, causing the roughness to vary from Ra 12.850 nm of ZnO/ZnS to 5.634 nm of ZnS/ZnO. It significantly means that the matrix ratio plays a significant role in the roughness of the material film. The author was of the opinion that the substrate was a less important factor in film roughness, although it was important in determining the adherence of the films. With the observed results, it was clear to learn that multilayer deposition has an effect on the structure of the material. The RMS has been decreased from 18.553 nm to 7.579 nm and Ra decreased from 12.850 nm to 5.634 nm.

The table below illustrates the values of the RMS and Ra of the material deposition of CdO/CdS, CdS/CdO, ZnO/ZnS and ZnS/ZnO multilayer thin film.

Table 2: RMS (Rq) and Ra of the material deposition of CdO/CdS, CdS/CdO, ZnO/ZnS and ZnS/ZnO multilayer thin film

Material thin film	Bath Temperature (°C)	pH	RMS (Rq) (nm)	Ra (nm)	Thickness (nm)
CdO/CdS	60	11	31.791	17.699	145.47

CdS/CdO	60	11	10.902	4.840	131.0
ZnO/ZnS	60	11	18.553	12.850	128.8
ZnS/ZnO	60	11	7.579	5.634	148.38

Where R_q is the root mean square average of height deviation taken from the mean image data plane and R_a is the arithmetic average.

It was worth noting that the thickness of the as-deposited ZnO single layer deposition decreased with multilayer deposition of ZnO/ZnS this can be because ZnO layer was lost during deposition from 114.4 nm to 128.8 nm. The behavior for thickness was different from that of ZnS layer deposition as it was observed that the thickness of ZnS increased with multilayer deposition of ZnS/ZnO from 107.7 nm to 148.38 nm. The thickness of cadmium series was similar as the thickness was observed to increase for CdS layer deposition and increase for CdO layer deposition with multilayer deposition and intercalated layers were observed to have decreased in thickness. The deposition of CdS layer deposition increased from 99.67 nm to 131.0 nm for multilayer deposition of CdS/CdO deposited layer. The observations were rather similar for CdO layer deposition as it was observed that the thickness increased from 100.4 nm to 145.47 nm. According to the observed results, it was illustrated that an increase in layer increased the thickness of the multilayer thin film and hence decreased the roughness of the surface, resulting in the decrease in %T. It was worth noting that the increase in thickness indicated good crystallinity of the deposited material.

4.8 Crystallinity of a compound using X-ray Diffraction (XRD)

4.8.1 Crystal structure of multilayer CdO/CdS thin film

XRD pattern of the crystal structure and orientation of CdO/CdS thin film deposited on a glass substrate using CBD, pre-heated at 60°C. Fig: 35 shows XRD pattern of the film was deposited by using cadmium acetate as a source of a Cd^{2+} ion with deposition time 60 min and pH=11 on the glass substrate. The 2θ values of diffraction peaks observed are 8.2° and a broad peak at 27.3° respectively. Based on observations made, the introduction of CdS material on the Predeposited CdO thin film has an effect

on the crystal structure. The as deposited CdO/CdS thin film has a monocrystalline structure.

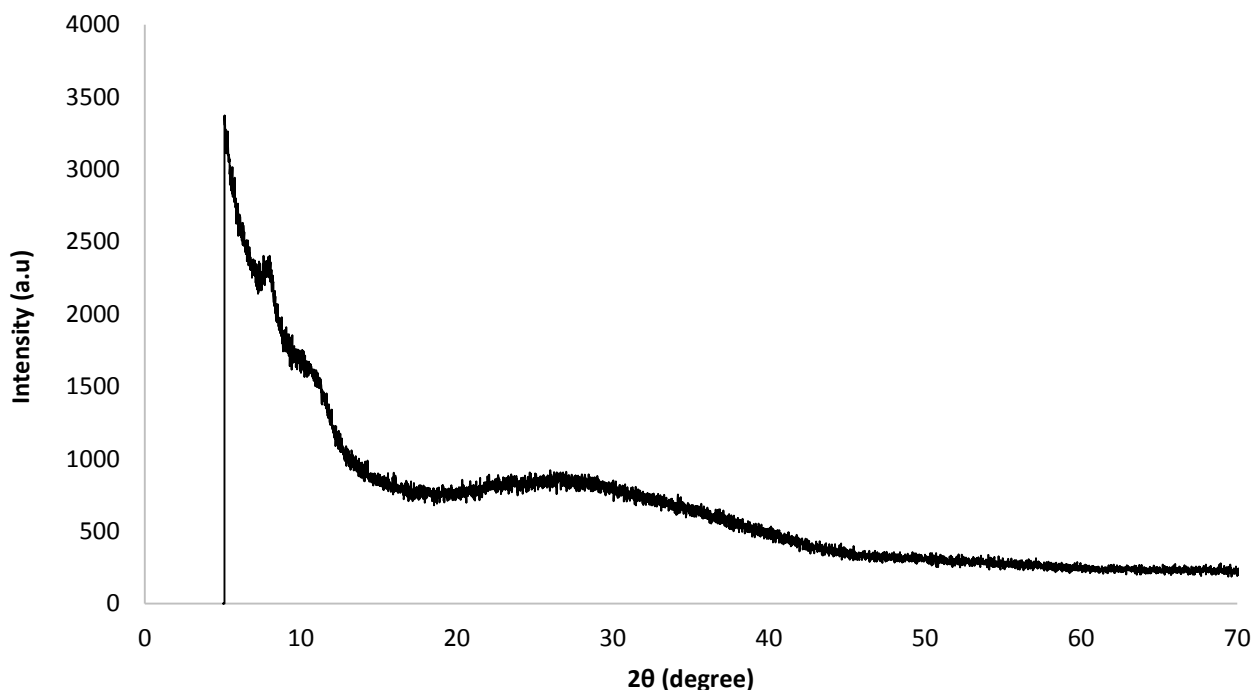


Figure 34: XRD patterns of multilayer CdO/CdS thin film

According to the results of the CdO/CdS thin film, it is shown that multilayer deposition also has an effect on the structure of the material, as it was observed that the intensity increase with an increase in multilayer layer of Cd. The results correspond with the roughness of the deposited material. The structure of CdS thin film was a cubic polycrystalline structure which is different from the structure obtained from the deposition of multilayer CdO/CdS thin film. It was worth noting that multilayer deposition has an effect on the structure of the as-deposited material.

4.8.2 Crystal structure of multilayer CdS/CdO thin film

XRD pattern of the crystal structure and orientation of CdS/CdO thin film deposited on a glass substrate using CBD, pre-heated at 60°C is discussed in details. The 2θ values of diffraction peaks observed are 11.878° and 26.527° respectively as shown in figure

36. Based on observations made, the introduction of CdO material on the predeposited CdS thin film has an effect on the crystal structure as the intensity increases. The as-deposited CdS/CdO thin film has a hexagonal structure with one large broad peak. However, several other authors [Kaur, Pandya, & Chopra, 1980], [Doña & Herrero, 1997, and [Chu, Olmedo, Yang, Kong, & Liu, 2008] classified the structure of as-grown CBD-CdS thin film from a basic aqueous bath as hexagonal.

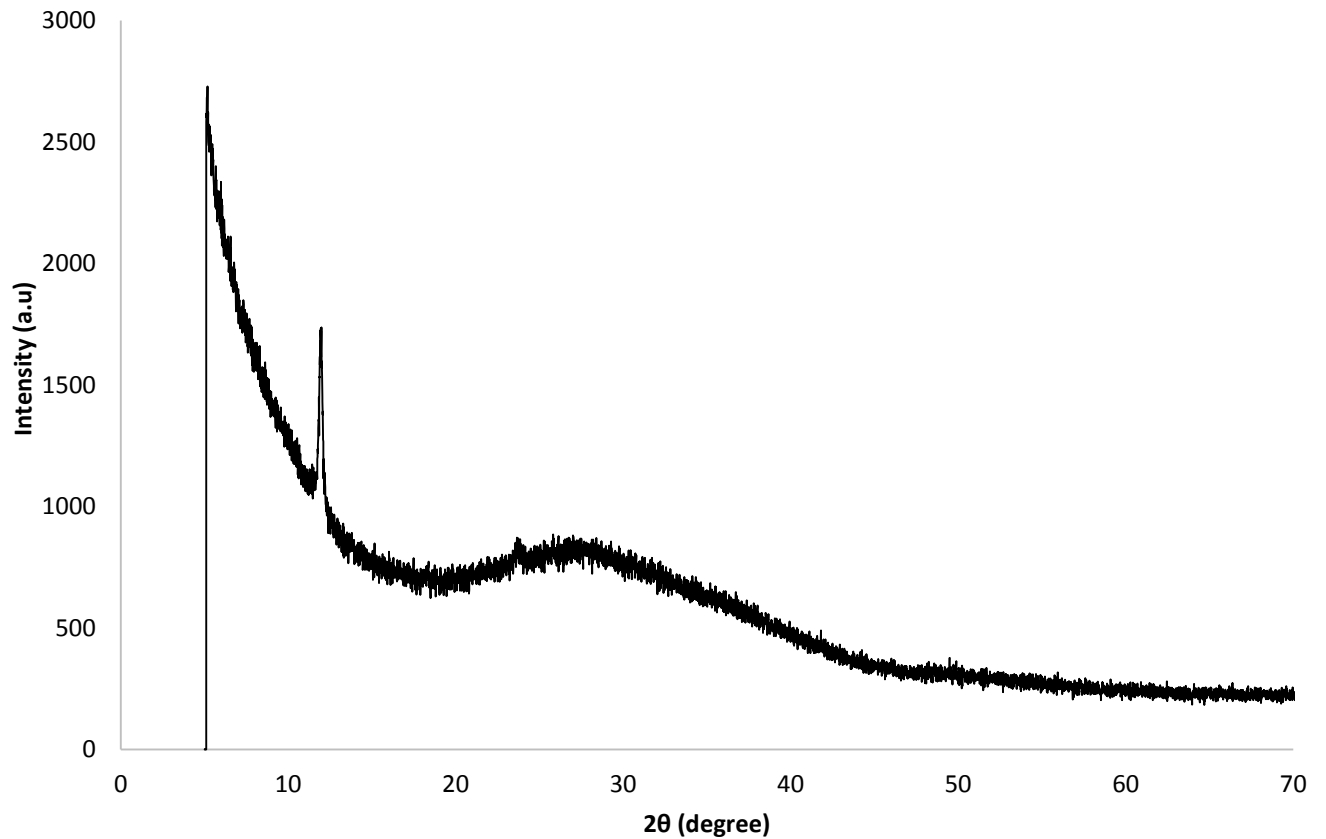


Figure 35: XRD patterns of multilayer CdS/CdO thin film

According to the results of the CdS/CdO thin film, it is shown that multilayer deposition also has an effect on the structure of the material. The results are in corresponds with the roughness of the deposited material. It was worth noting that multilayer deposition has an effect on the structure of the as-deposited material.

4.8.3 Crystal structure of multilayer ZnO/ZnS thin film

XRD pattern of the crystal structure and orientation of ZnO/ZnS thin film deposited on a glass substrate using CBD, pre-heated at 60°C is discussed in details. The 2θ values of diffraction peaks observed are 21.385° and 43.375° respectively as shown in figure 37. Based on observations made, the introduction of ZnS material on the predeposited ZnO thin film has an effect on the crystal structure of the material deposited. Two peaks were observed at showing that an increase in Zn on the material. The presence of diffraction peaks of ZnO/ZnS indicates that the film is polycrystalline with cubic structure. It is revealed that the films have peaks corresponding to (111), (220) and (311).

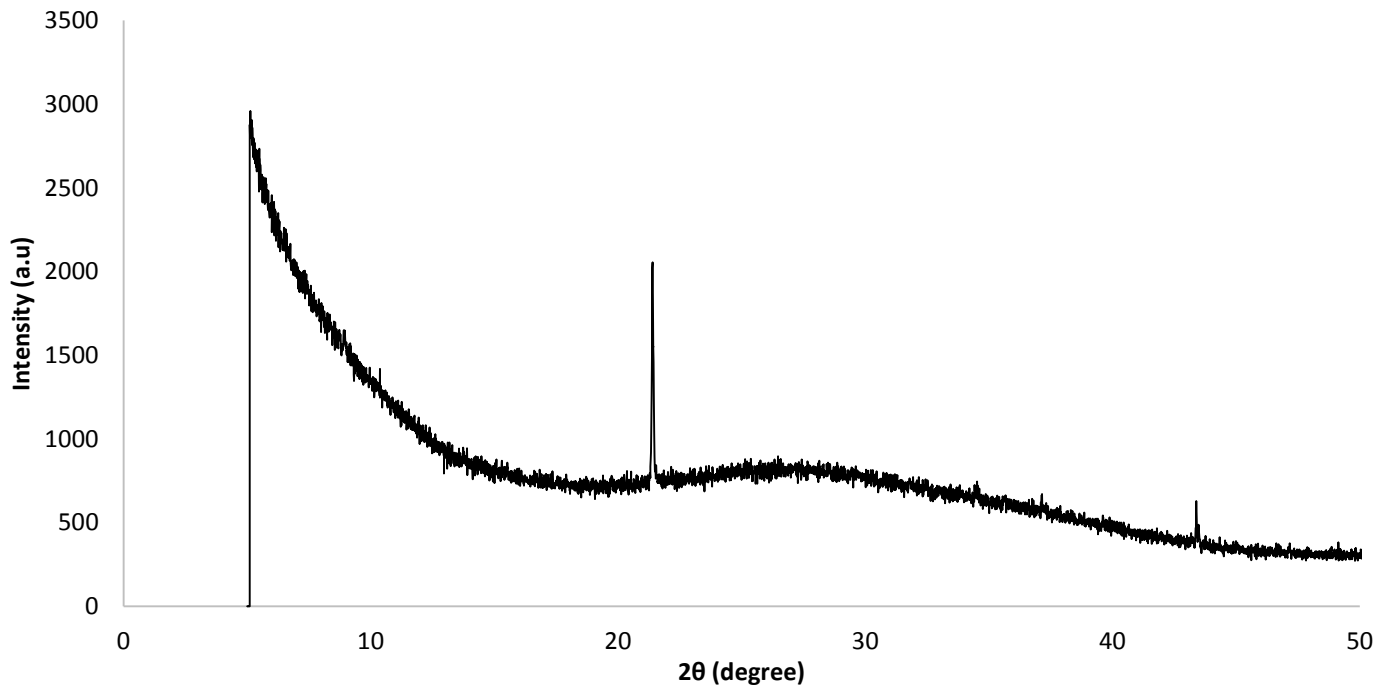


Figure 36: XRD patterns of multilayer ZnO/ZnS thin film

The central broad peak hump was due to the amorphous glass substrate. According to the results of the ZnO/ZnS thin film, it is shown that multilayer deposition also has an effect on the structure of the material. The results are in corresponds with the roughness of the deposited material. The structure for ZnO and ZnS thin film

amorphous which is different from the structure obtained from the deposition of multilayer ZnO/ZnS thin film. The disadvantage of polycrystalline films: First, the grain boundaries result in enhanced migration of dopants, device shunting, and high recombination; Secondly, inhomogeneity results in efficiency losses. It was worth noting that multilayer deposition has an effect on the structure of the as-deposited material.

4.8.4 Crystal structure of multilayer ZnS/ZnO thin film

XRD pattern of the crystal structure and orientation of ZnS/ZnO thin film deposited on a glass substrate using CBD, pre-heated at 60°C is discussed in details. The 2θ values of diffraction peaks observed are 12.488° respectively shown at figure 38. Based on observations made, the introduction of ZnO material on the predeposited ZnS thin film also has an effect on the crystal structure. The presence of diffraction peaks for deposition of ZnS/ZnO multilayer deposition indicates that the film is polycrystalline. It is revealed that the films have peaks corresponding to (002).

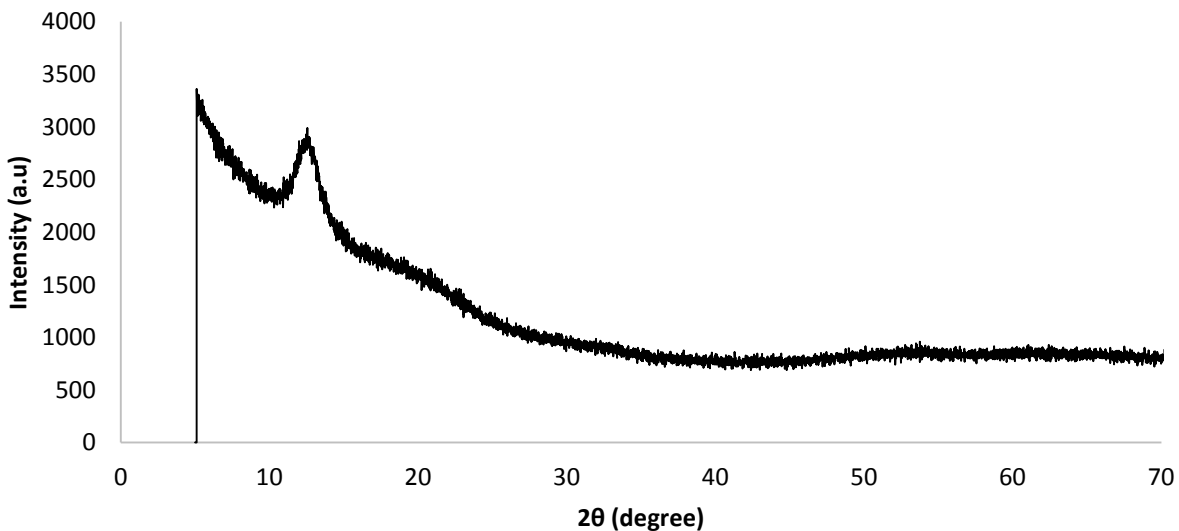


Figure 37: XRD patterns of multilayer ZnS/ZnO thin film

There was only one peak that occurred in XRD pattern at 2θ of 12.488° at (002). Compared with the deposition of multilayer CdO/CdS, CdS/CdO and ZnO/ZnS thin film

it was worth noting that the as deposition layers increases, the diffraction of samples lower due to the thickness of the films coated. It was worth noting that multilayer deposition has an effect on the structure of the as-deposited material.

MULTILAYERS WITH POLYMER INTERCALATION

4.9 Optical Characterization of Multilayer deposition without polymer intercalation

The optical property of the intercalated multilayer film is to study the physical phenomena and optical constant is shown below in figure 39.

4.9.1 %T of intercalated CdO/PVA/CdS thin film

To further enhance the optical property of CdO, PVA, and CdS thin films were formed on the interfaces of CdO thin film as a passivation and a substrate layer. The layer of PVA was deposited on a pre-deposited CdO thin film by forming a CdO/PVA/CdS layers. Fig: 39 shows the %T was found to be ~88 % which was a comparison with the %T of CdO/CdS multilayer thin film layers.

4.9.2 %T of intercalated CdS/PVA/CdO thin film

To further enhance the optical property of the CdS, CdO, and PVA thin films were formed on the interfaces of CdS thin film as a passivation and a substrate layer.

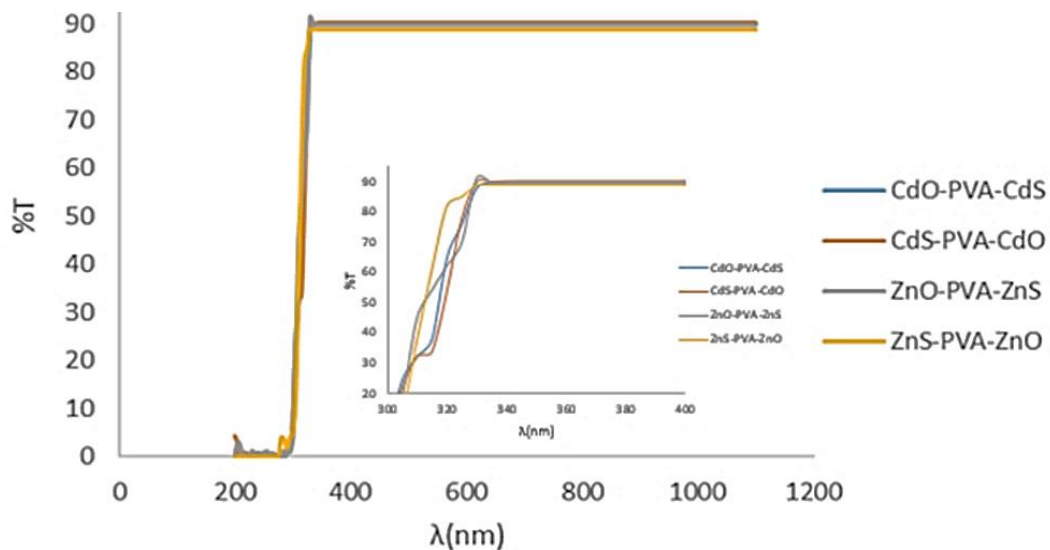


Figure 38: %T of intercalated CdO/PVA/CdS, CdS/PVA/CdO, ZnO/PVA/ZnS, and ZnS/PVA/ZnO thin film

The layer of PVA was deposited on a pre-deposited CdS thin film by forming a CdS/PVA/CdO layers. The %T was found to be ~90.3 % which was a comparison with the %T of CdS/CdO with %T of 89 % multilayer thin film layers.

4.9.3 %T of intercalated ZnO/PVA/ZnS thin film

To further enhance the optical property of ZnO, ZnS, and PVA thin films were formed on the interfaces of ZnO thin film as a passivation and a substrate layer. The layer of PVA was deposited on a pre-deposited ZnO/ZnS thin film by forming a ZnO/PVA/ZnS layers. The %T was found to be ~89.9 % which was a comparison with the %T of ZnO/ZnS with %T of 90 % multilayer thin film layers. Optical transmittance spectra of the thin films are observed to be shifted towards the shorter wavelengths.

4.9.4 %T of intercalated ZnS/PVA/ZnO thin film

To further enhance the optical property of ZnS, ZnO, and PVA thin films were formed on the interfaces of ZnO thin film as a passivation and a substrate layer. The layer of PVA was deposited on a pre-deposited ZnS thin film by forming a ZnS/PVA/ZnO layers. The %T was found to be ~88.9 % which was a comparison with the %T of ZnS/ZnO with %T of 89 % multilayer thin film layers. Deposition of ZnS shows that it is not dependent on alkalinity or acidity hence good crystallinity was observed according to the %T. The intercalation of PVA did not improve the optical properties of the film.

The intercalated absorbance was observed at the wavelength of 380 nm which result that the absorbance of the samples was low and also lie between 0 and 1.0. The films showed a marginal increase in absorbance at the deposition of CdO/PVA/CdS and ZnS/PVA/ZnO as the deposition was observed to have the highest absorption which was similar to results observed from XRD this can be due to the amorphously of the deposited material hence less %T was observed. The lowest absorption behavior was observed for ZnO/PVA/ZnS and CdS/PVA/CdO, as a result, the XRD results had higher intensities and peaks were observed.

4.10 Surface materials using Scanning electron microscopy (SEM)

SEM provides detailed high-resolution images of the sample by restoring a focused electron beam across the surface and detecting secondary or backscattered electron signal. An Energy Dispersive X-Ray Analyser (EDX or EDA) reported as part of the results is also used to provide elemental identification and quantitative compositional information. All samples prior to the analysis they were pre-coated with carbon because they are conducting material and were charging.

4.10.1 Surface of intercalated CdO/PVA/CdS thin film

The following SEM image in figure 40 shows the surface morphology of the multilayer CdO/PVA/CdS composites thin films obtained by CBD technique. No roughness were observed from the SEM images that are clearly adjusted as the CdO/PVA/CdS composite thin films were annealed at the room temperature at 60°C. The micrographs show that the composite films cover the substrate well and are mostly uniform over the entire substrate surface which is important for practical application in devices. The as-deposited film has been found to exhibit a uniform, homogeneous and granular morphology covering entire substrate surface. All the grains are almost spherical in shape (nanocrystalline).

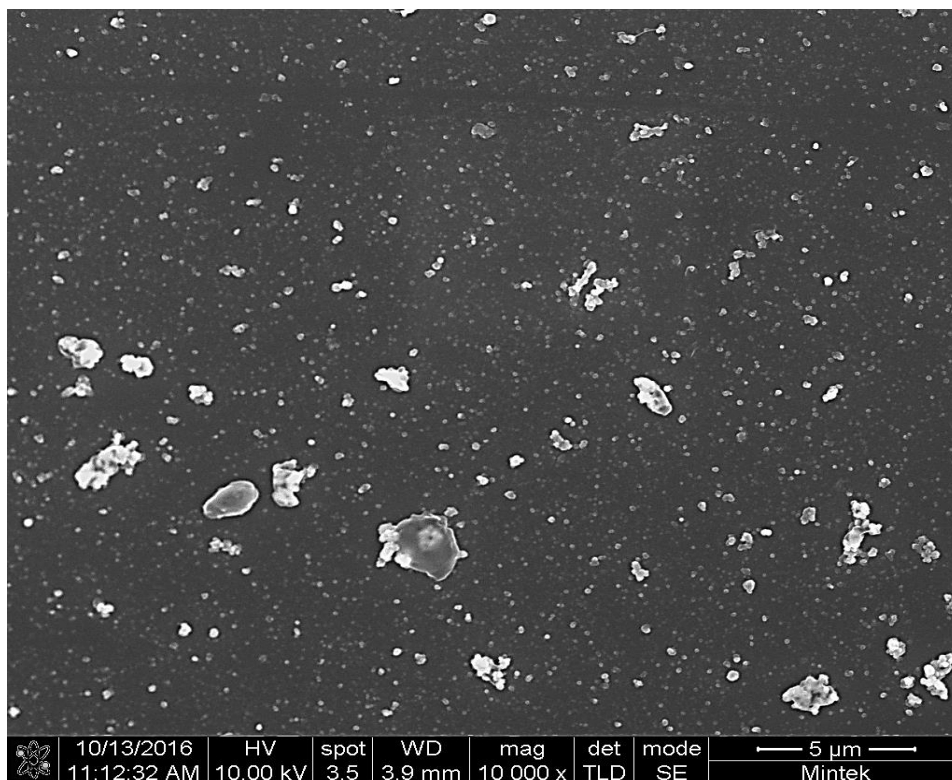


Figure 39: SEM image of intercalated CdO/PVA/CdS thin film

The spherically shaped particles were observed through the SEM analysis. The element in the film appears to be uniform with decreased porosity. The film exists as nanostructure grain without any crack and pinhole on the surface. Morphology indicates that the substrate is almost completely covered spherical grain surface. Based on results of SEM imaging it was seen that the intercalation with PVA has an effect on the morphology of the material. The spherically shaped surface was observed which was likely improved inhomogeneity and surface coverage. The micrograph depicts that the grains of the as-deposited film are tightly packed. This can be correlated with the high value obtained for the number of crystallites per unit surface area from XRD analysis.

4.10.2 Surface of intercalated CdS/PVA/CdO thin film

The following SEM image in figure 41 shows the surface morphology of the multilayer CdS/PVA/CdO composites thin films obtained by CBD technique. No Porosity and roughness were observed from the SEM images that are clearly adjusted as the

CdS/PVA/CdO composite thin films were annealed at the room temperature at 60°C. The micrographs show that the composite films cover the substrate well and are mostly uniform over the entire substrate surface which is important for practical application in devices.

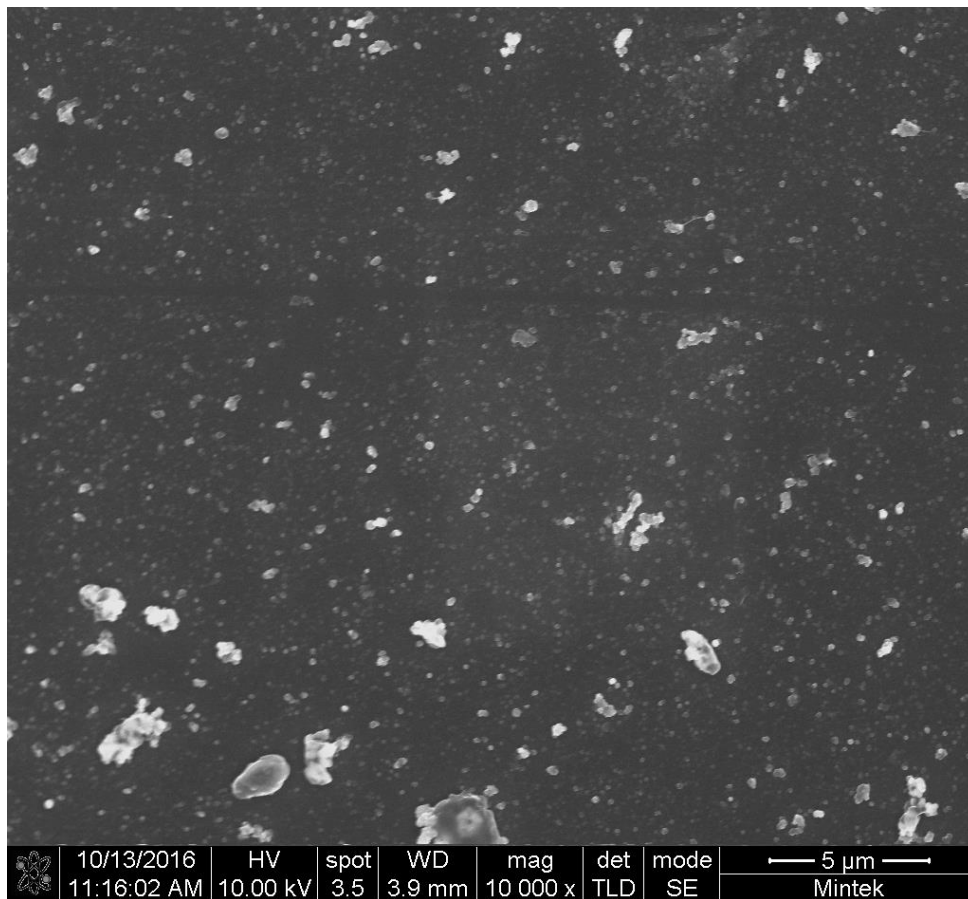


Figure 40: SEM image of intercalated CdS/PVA/CdO thin film

The as-deposited film has been found to exhibit a uniform, homogeneous and granular morphology covering entire substrate surface which clearly shows more than one type of layer deposited on the substrate. All the grains are almost spherical in shape (nanocrystalline). Based on this work it was worth noting that intercalation of PVA had an effect on the surface morphology. The intercalation of CdS/PVA/CdO had improved on the morphology homogeneity with a spherical-shaped structure that was well distributed on the surface substrate. The micrograph depicts that the grains of the as-

deposited film is tightly packed. This can be correlated with the high value obtained for the number of crystallites per unit surface area from XRD analysis.

4.10.3 Surface of intercalated ZnO/PVA/ZnS thin film

The following SEM image in figure 42 shows the surface morphology of the multilayer ZnO/PVA/ZnS composites thin films obtained by CBD technique. No Porosity and roughness were observed from the SEM images that are clearly adjusted as the ZnO/PVA/ZnS composite thin films were annealed at the room temperature at 60°C. The micrographs show that the composite films cover the substrate well and are mostly uniform over the entire substrate surface which is important for practical application in devices.

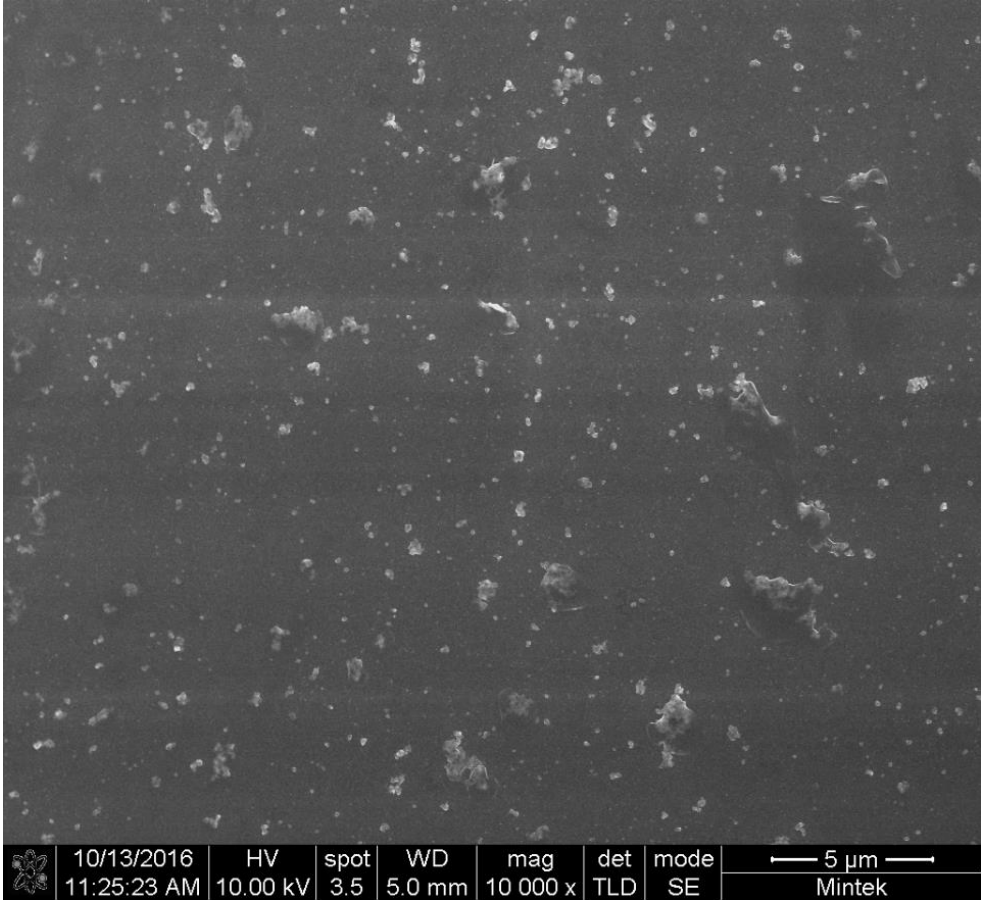


Figure 41: SEM image of intercalated ZnO/ZnS/PVA thin film

The surface of films grown by ZnO/PVA/ZnS displays a smoother and more homogeneous surface. In fact, the matrix ratio of ZnO/PVA/ZnS multilayer deposition films showed to be smooth and uniform. Based on observations made the PVA intercalation had an effect on the surface morphology. As with the deposition ZnO/ZnS thin film star-shaped snowflake shaped observation. However, the introduction of PVA has spherical observation made.

4.10.4 Surface of intercalated ZnS/PVA/ZnO thin film

The following SEM image in figure 43 shows the surface morphology of the multilayer ZnS/PVA/ZnO composites thin films obtained by CBD technique. Porosity and roughness were observed from the SEM images that are clearly adjusted as the ZnS/PVA/ZnO composite thin films were annealed at the room temperature at 60°C. The micrographs show that the composite films cover the substrate well and are mostly uniform over the entire substrate surface which is important for practical application in devices.

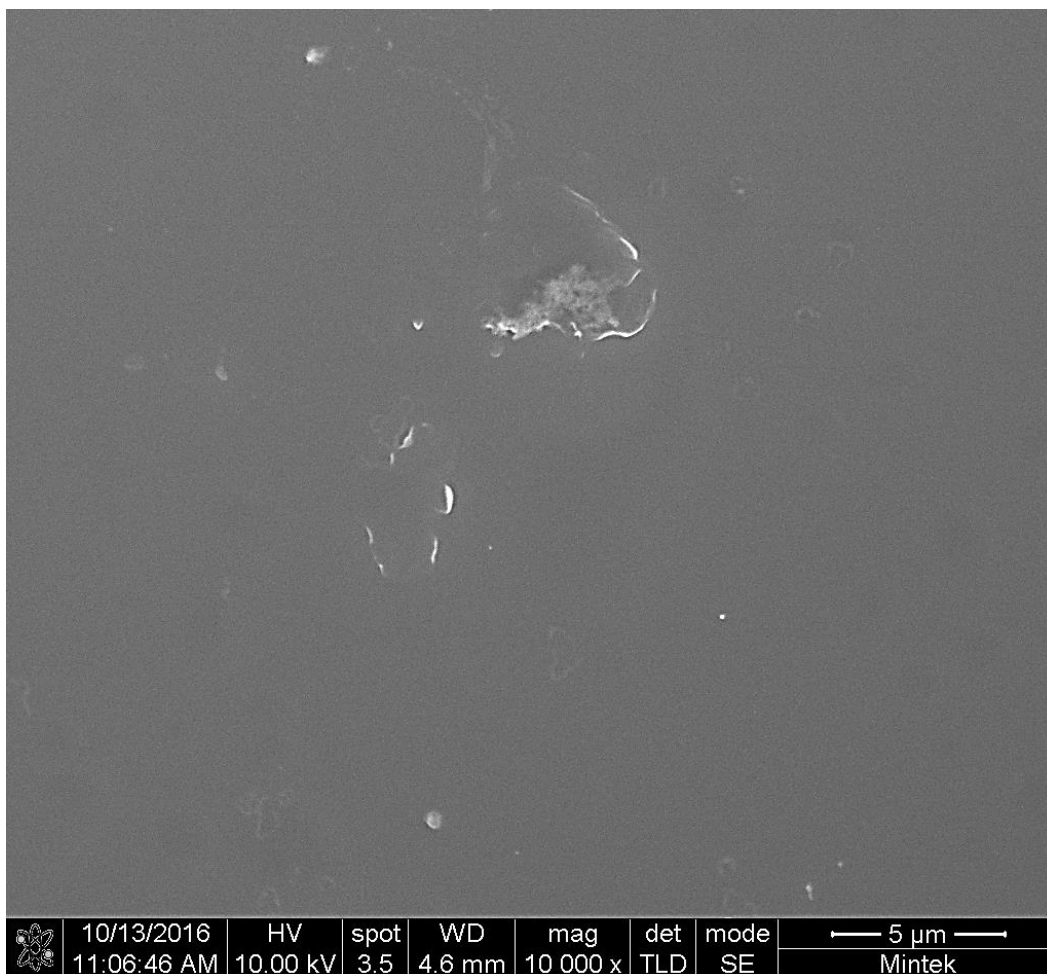


Figure 42: SEM image of intercalated ZnO/PVA/ZnS thin film

These micrographs reveal that the ZnS/PVA/ZnO thin films. It was observed that the high compactness of these films which are continuous and homogeneous and rather agglomerate. Dispersed spherical structures are observed and thin films formed were highly agglomerated. Intercalation of PVA has an effect on the surface morphology.

4.11 Structural analysis using atomic force microscopy (AFM)

AFM is a technique for obtaining high-resolution images of surfaces on the atomic scale. The AFM images the surface by a force: the cantilever tip scans the sample, and the mechanical raster-scanning system (piezoelectric) measures the deflection of the cantilever from the sample surface. There are two basic modes of operation. The first, when the atomic interactions between the sample and the tip are kept constant by the

cantilever. The map of the surface topography is provided by recording the vertical position of the sample relative to the base of the cantilever. The second part is when the tip-specimen distance was kept constant whilst the system records the changes in the vibrational amplitude and resonant frequency of the cantilever. AFM microscopy was employed to reveal the surface topography of the thin layers and to measure their roughness.

4.11.1 Structural analysis of intercalated CdO/PVA/CdS thin film

AFM analysis is ideal for quantitatively measuring the nanometric dimensional surface roughness and for visualizing the surface nanotexture of the deposited multilayer film. Fig: 44 (a) The topographical of CdO/PVA/CdS multilayer the RMS roughness as determined by AFM, as well as the mean roughness of the intercalated material, was found to be Ra was 2.489 nm as a function of CdO/PVA/CdS cycle ratio. The RMS for multilayer of CdO/PVA/CdS was 6.878 nm. By clear indication of the structure, it can be seen that more than a single material was deposited onto the substrate. The distribution of the material on the substrate appeared to be homogeneous with spherical shapes.

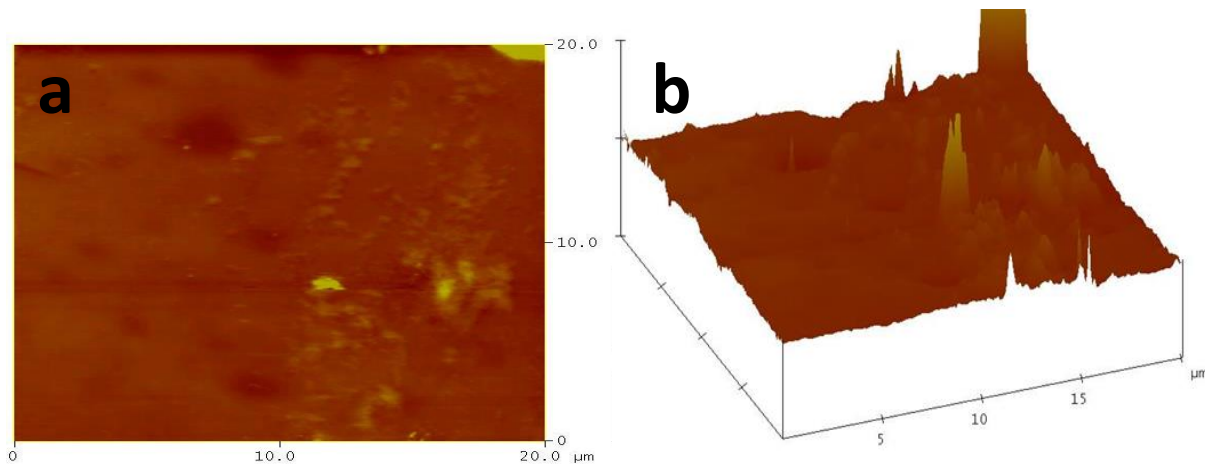


Figure 43: (a) AFM micrographs roughness of intercalated CdO/PVA/CdS thin film; (b) AFM 3D micrographs of intercalated CdO/PVA/CdS thin film

It was observed from the surface image that the particles are uniformly distributed on the surface of the film. The thickness of the deposited multilayer intercalation was decreased from 145.47 nm to 52.67 nm, these results indicate that some of the material being washed away during deposition.

Fig 44 (b) illustrate that the grains of CdO/PVA/CdS form large clusters looking like cauliflower. Based on observations made it can be seen that intercalation with PVA has an effect on the roughness of the material. The RMS was seen to decrease from 31.791 nm to 6.878 nm and the Ra was decreased from 17.699 nm to 2.489 nm. The thickness of the intercalation only has an effect on surface roughness and even the crystal structure of the deposited material.

4.11.2 Structural analysis of intercalated CdS/PVA/CdO thin film

Fig: 45 (a) The RMS roughness as determined by AFM, as well as the mean roughness of the intercalated material, was found to be Ra was 4.313 nm as a function of CdS/PVA/CdO cycle ratio. From a topographical of CdS/PVA/CdO multilayer, the RMS for multilayer of CdS/PVA/CdO was 10.501 nm. By clear indication of the structure, it can be seen that more than one type of material was deposited onto the substrate. The distribution of the material on the substrate appeared to be homogeneous with spherical shapes. It was observed from the surface image that the particles are uniformly distributed on the surface of the film. The thickness of the deposited intercalation was decreased by from 131.0 nm to 37.15 nm, these results in some of the material being washed away during deposition.

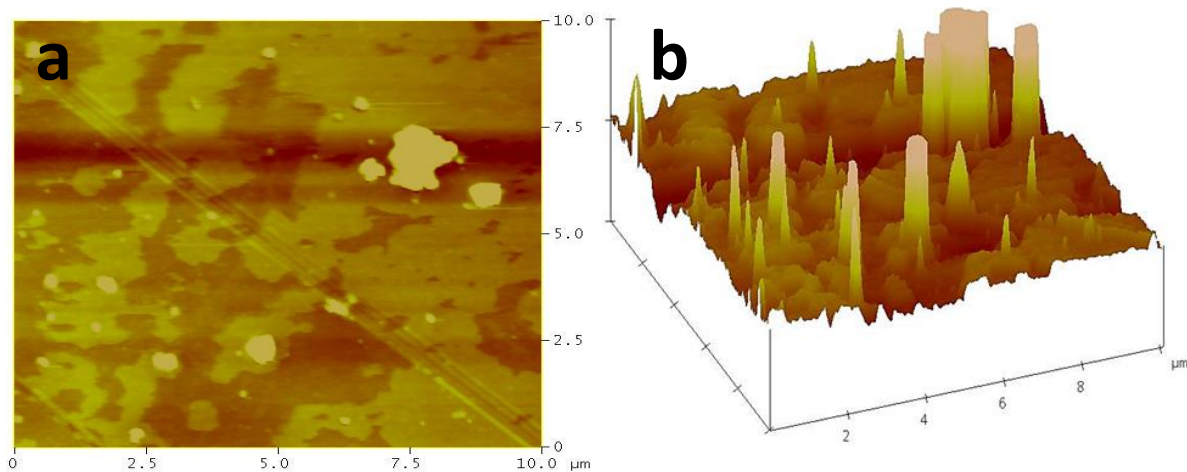


Figure 44: (a) AFM micrographs roughness of intercalated CdS/PVA/CdO thin film; (b) AFM 3D micrographs of intercalated CdS/PVA/CdO thin film

Fig 45 (b) illustrates that the large peaks observed in the image are due to the large chunks of the spherical shaped deposited material. It is worth noting that the film morphology between the porosity was rather un-uniform and increase in size corresponding to the large chunks that were observed to have been charging on SEM imaging. It was worth noting that according to the imaging more than two different materials were deposited. It was observed that similar to the ratio of CdO/PVA/CdS the intercalation of PVA to the material has an effect on the roughness of the film. It was seen that the deposited CdS/PVA/CdO thin film ratio, the RMS slightly decrease from 10.902 nm to 10.501 nm and the Ra decrease from 4.840 nm to 4.313 nm. At this point, it is not clear if the intercalation only has an effect in surface roughness or even the crystal structure of the deposited material.

4.11.3 Structural analysis of intercalated ZnO/PVA/ZnS thin film

Fig: 46 (a) The RMS roughness as determined by AFM, as well as the mean roughness of the intercalated material, was found to be Ra was 2.799 nm as a function of ZnO/PVA/ZnS cycle ratio. From a topographical of ZnO/PVA/ZnS multilayer, the RMS for multilayer of ZnO/PVA/ZnS was 4.882 nm. By clear indication of the structure,

it can be seen that more than one material was deposited onto the substrate. The distribution of the material on the substrate appeared to be homogeneous with spherical shapes. It was observed from the surface image that the particles are uniformly distributed on the surface of the film. The thickness of the intercalated deposition was decreased from 128.8 nm to 102.45 nm.

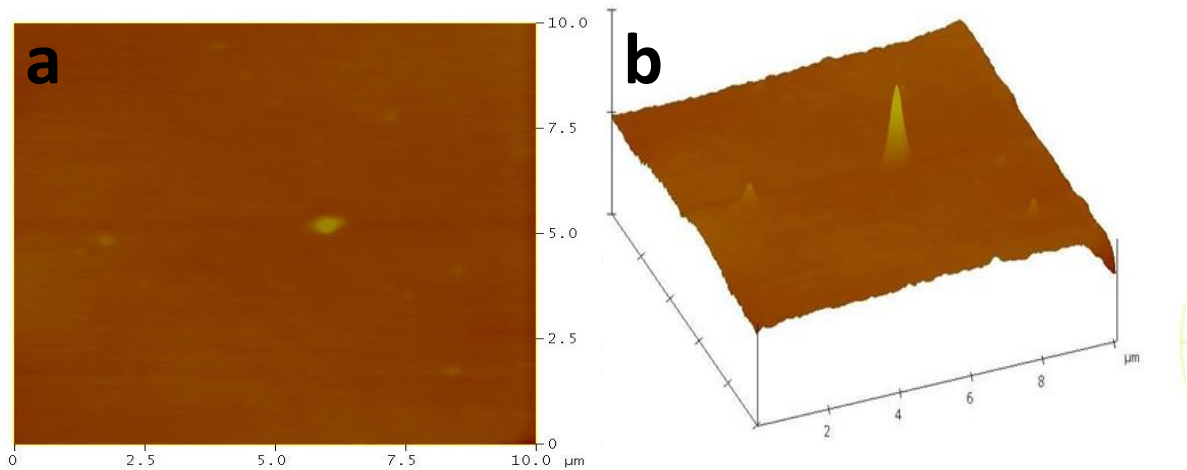


Figure 45: (a) AFM micrographs roughness of intercalated ZnO/PVA/ZnS thin film; (b) AFM 3D micrographs of intercalated ZnO/PVA/ZnS thin film

Fig 46(b) illustrates that the large peak observed in the image are due to the droplets present on these films. It is worth noting that the film morphology between the droplets was rather uniform. From observations made of the structural analysis made, it was worth noting that the intercalation of PVA on the material had an effect on the surface roughness. Based on the roughness analysis the RMS was decreased from 7.579 nm to 4.882 nm and the Ra was also decreased from 12.850 nm to 2.799 nm. According to this results the surface roughness decrease with an increase in layer deposition.

4.11.4 Structural analysis of intercalated ZnS/PVA/ZnO thin film

Fig: 47 (a) The RMS roughness as determined by AFM, as well as the mean roughness of the intercalated material, was found to be Ra was 7.200 nm as a function of ZnS/PVA/ZnO cycle ratio. From a topographical of ZnS/PVA/ZnO multilayer, the RMS for multilayer of was 11.960 nm. By clear indication of the structure, it can be

seen that more than one material was deposited onto the substrate. The distribution of the material on the substrate appeared to be homogeneous with spherical shapes. It was observed from the surface image that the particles are uniformly distributed on the surface of the film. The thickness of the intercalated deposition was decreased from 148.38 nm to 116.6 nm, this indicate a loss of material during deposition.

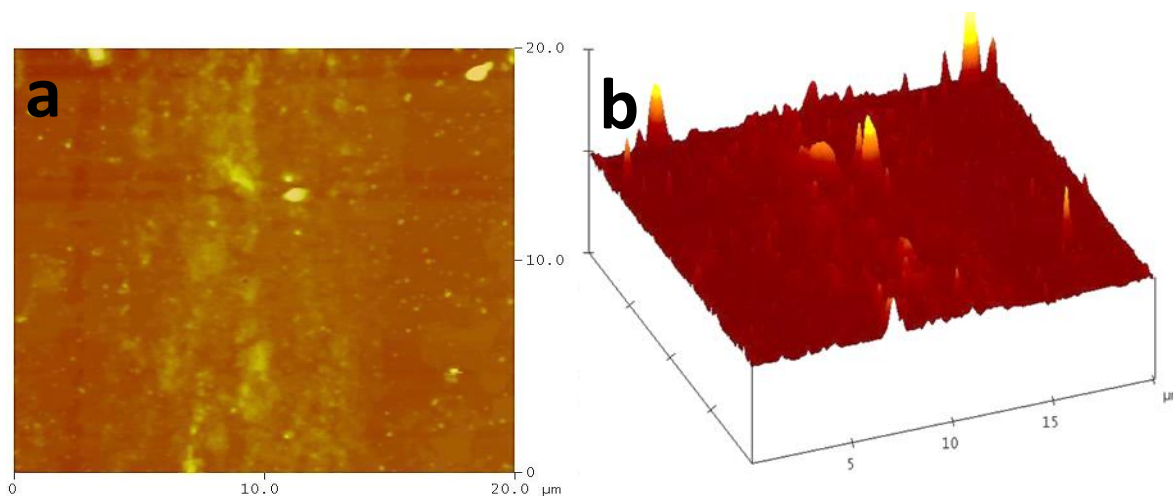


Figure 46: (a) AFM micrographs roughness of intercalated ZnS/PVA/ZnO thin film; (b) AFM 3D micrographs of intercalated ZnS/PVA/ZnO thin film

Fig: 47 (b) It was observed that similar to the ratio of ZnS/PVA/ZnO the intercalation of PVA to the material has an effect on the roughness of the film. It was seen that the deposited ZnS/PVA/ZnO thin film ratio, the R_q slightly decrease from 11.960 nm to 7.579 nm and the R_a decrease from 7.200 nm to 5.634 nm. Due to the observation made it was concluded that an increase in layer deposition decreases the surface roughness.

The roughness from CdO decrease with increase in stack deposition. It was observed that the roughness of the as deposited CdO layer decrease with multilayer deposition of CdO/CdS from $R_q = 69.813$ nm to 31.791 nm whilst the intercalation with PVA was observed to have an effect on surface roughness as the CdO/PVA/CdS decreased the roughness by $R_q = 52.67$ nm. The roughness from CdS thin film to CdS/CdO multilayer was observed to also decreased from $R_q = 14.530$ nm to 10.902 nm. The intercalation

with PVA was observed to have an effect on surface roughness as the CdS/PVA/CdO decreased the roughness by $R_q = 10.501$ nm. The observations were rather not in the same matrix as the roughness of ZnO layer to ZnO/ZnS multilayer thin film decreased the surface roughness from $R_q = 25.776$ nm to 18.553 nm whilst the ZnO/PVA/ZnS decreased by $R_q = 4.882$ nm. There was no clarity as to why the behavior is not similar to that of CdO and CdS ratio matrix. The roughness of the as-deposited ZnS layer was observed to increase the roughness as the deposition of ZnS/ZnO multilayer from $R_q = 8.989$ nm to 7.579 nm whilst the intercalated ZnS/PVA/ZnO increased to $R_q = 11.960$ nm.

The table below illustrates the values of the RMS and Ra of the material deposition of intercalated CdO/PVA/CdS, CdS/PVA/CdO, ZnO/PVA/ZnS and ZnS/PVA/ZnO multilayer thin film.

Table 3: RMS and Ra of the material deposition of intercalated CdO/PVA/CdS, CdS/PVA/CdO, ZnO/PVA/ZnS and ZnS/PVA/ZnO multilayer thin film

Material thin film	Bath Temperature (°C)	pH	RMS (nm)	Ra (nm)	Thickness (nm)
CdO/PVA/CdS	60	11	6.878	2.489	52.67
CdS/PVA/CdO	60	11	10.501	4.313	37.15
ZnO/PVA/ZnS	60	11	4.882	2.799	102.45
ZnS/PVA/ZnO	60	11	11.960	7.200	116.6

Where R_q is the root mean square average of height deviation taken from the mean image data plane and R_a is the arithmetic average.

It was worth noting that the thickness of ZnO single later deposition increase with multilayer deposition of ZnO/ZnS to ZnS/ZnO can be because ZnO layer was lost during deposition from 128.8 nm to 148.38 nm and the intercalated ZnO/PVA/ZnS decreased in thickness of 102.45 nm to 116.6 nm. The behavior for thickness was similar to that of ZnS layer deposition as it was observed that the thickness of ZnS was

increased with multilayer deposition of ZnS/ZnO from 107.7 nm to 148.38 nm and the intercalated layer decreased with layer deposition 116.6 nm of ZnS/PVA/ZnO. The thickness of cadmium series was different as the thickness was observed to decrease for CdS layer deposition and increase for CdO layer deposition with multilayer deposition and intercalated layers were observed to have decreased in thickness. The deposition of CdS layer deposition also increased from 99.67 nm to 131.0 nm for multilayer deposition of CdS/CdO whilst the intercalated layer of CdS/PVA/CdO was decreased to 37.15 nm. The observations were rather similar for CdO layer deposition it was observed that the thickness increased from 100.4 nm to 145.47 nm whilst the intercalated layer of CdO/PVA/CdS decreased to 52.67 nm.

There was a relationship between the thickness and the RMS on the single layers to the multilayer as well as the intercalated materials. It was found that the roughness was higher for deposition of single layers both for Cd and Zn matrix. The roughness decrease as the layers increases, the case was not similarly as the thickness increased for multilayer deposition and was seen to have decreased upon intercalation. It was concluded that the surface roughness decrease with increase in deposition layer.

4.12 Crystallinity of a compound using X-ray Diffraction (XRD)

4.12.1 Crystal structure of intercalated CdO/PVA/CdS thin film

XRD pattern of the crystal structure and orientation of CdO/PVA/CdS thin film deposited on a glass substrate using CBD, pre-heated at 60°C is discussed in details. Based on observations made, the introduction of PVA material on the pre-deposited CdO/CdS thin film also has a huge effect on the crystal structure of the material. The presence of not having a diffraction peak indicates that the film as amorphous as shown in figure 48.

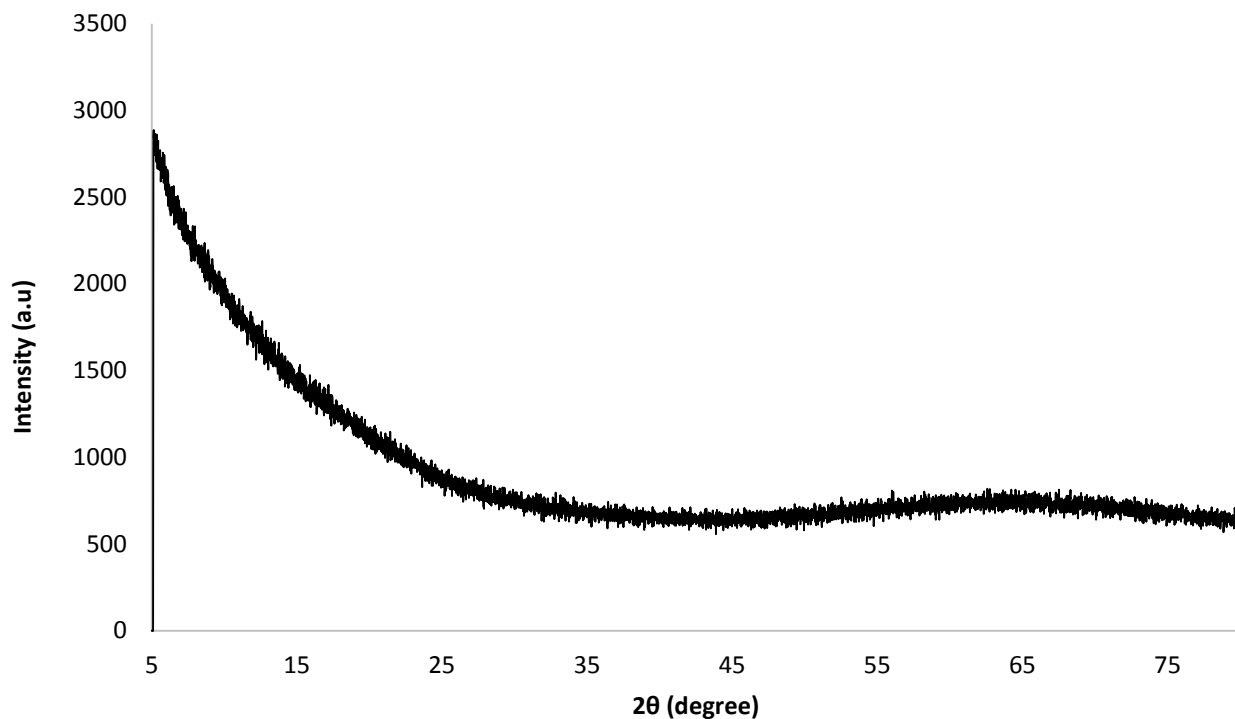


Figure 47: XRD patterns of intercalated CdO/PVA/CdS thin film

From the results, it was observed that the XRD studies in this work of the film produced did not show any discernable peaks. As the deposition layers increases, the diffraction of samples lower due to the thickness of the films coated. CdO/PVA/CdS appears almost in amorphous foam. These results are well in correspondence with the AFM structure and SEM morphology as the roughness of the material decrease with the deposition of the PVA. No prominent peaks were observed and films were of mainly amorphous nature probably due to poor adhesion and smaller thickness. The matrix of the intercalated CdO/PVA/CdS was not enhanced as compared to the CdS/PVA/CdO thin films, resulting in that the intercalation of PVA did not enhance the CdO/PVA/CdS.

4.12.2 Crystal structure of intercalated CdS/PVA/CdO thin film

XRD pattern of the crystal structure and orientation of CdS/PVA/CdO thin film deposited on a glass substrate using CBD, pre-heated at 60°C is discussed in details below. Based on observations made, the introduction of PVA material on the pre-

deposited CdS/CdO thin film also has a huge effect on the crystal structure of the material. The XRD patterns have shown three peaks close to $2\theta = 26.033^\circ$, 37.055° and 41.335° are attributed to the (100), (002) and (101) planes respectively of hexagonal structure shown in figure 49 below.

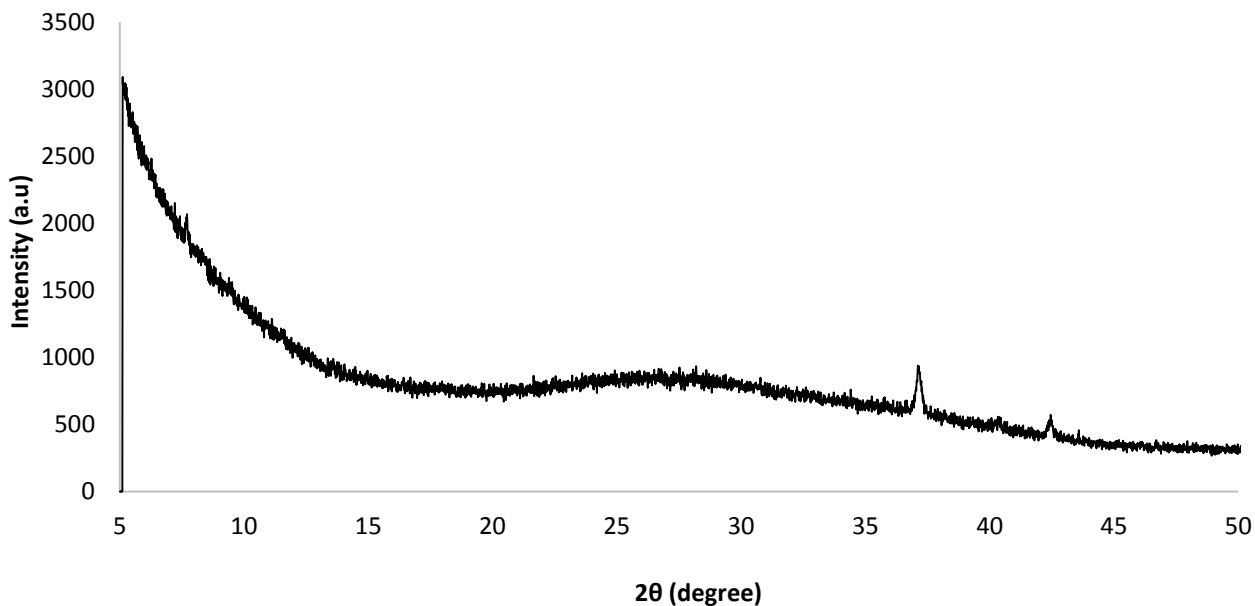


Figure 48: XRD patterns of intercalated CdS/PVA/CdO thin film

The dominant peak that was observed for deposition of CdS/CdO was not present for the intercalated material. This may be due to the present of the PVA on the previously deposited CdS. The XRD patterns showed the formation of polycrystalline structure. These results are well in correspondence with the AFM structure and SEM morphology as the roughness of the material decrease with the deposition of the PVA. The intercalated matrix of CdS/PVA/CdO was enhanced and therefore favored than the CdO/PVA/CdS matrix.

4.12.3 Crystal structure of intercalated ZnO/PVA/ZnS thin film

Based on observations made, the introduction of PVA material on the pre-deposited ZnO/ZnS thin film also has a huge effect on the crystal structure of the material. The XRD patterns have shown two peaks close to $2\theta = 21.322^\circ$ and 27.307° related to (111) (220).

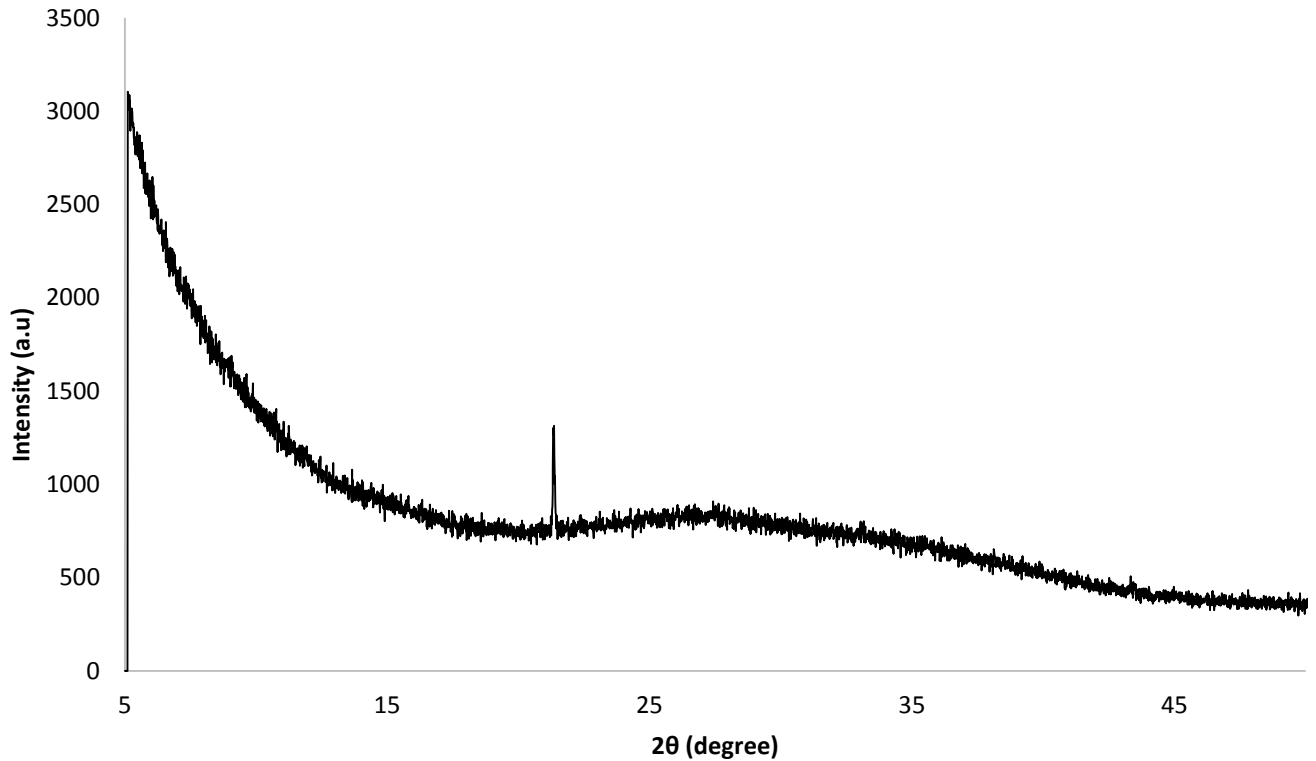


Figure 49: XRD patterns of intercalated ZnO/PVA/ZnS thin film

The XRD patterns showed the formation of a monocrystalline structure. The intercalated matrix of ZnO/PVA/ZnS shown in figure 50 was enhanced and therefore favored than the ZnS/PVA/ZnO matrix.

4.12.4 Crystal structure of intercalated ZnS/PVA/ZnO thin film

XRD pattern of the crystal structure and orientation of ZnS/PVA/ZnO thin film deposited on a glass substrate using CBD, pre-heated at 60°C shown at figure 51 is discussed in details. Based on observations made, the introduction of PVA material on the pre-

deposited ZnS/ZnO thin film also has a huge effect on the crystal structure of the material. The presence of no diffraction peaks indicates that the film is amorphous. In general, the polymer does not contain any peak because it is amorphous.

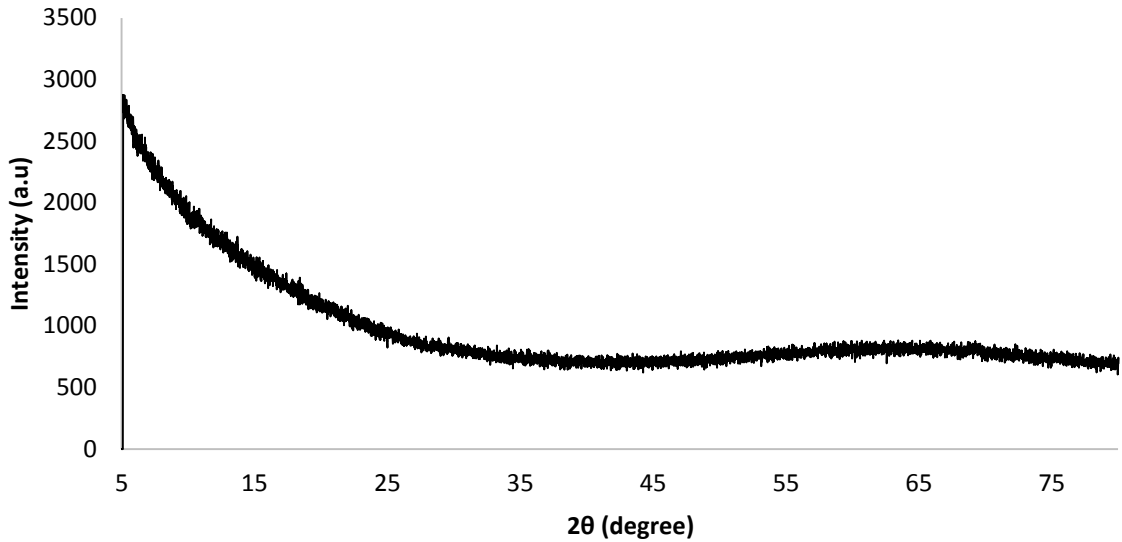


Figure 50: XRD patterns of intercalated ZnS/PVA/ZnO thin film

These results are well in correspondence with the AFM structure and SEM morphology as the roughness of the material decrease with the deposition of the PVA. No prominent peaks were observed and films were of mainly amorphous nature probably due to poor adhesion and smaller thickness. The intercalated matrix was not favored nor preferred for the ZnS/PVA/ZnO matrix.

CHAPTER 5: CONCLUSIONS AND RECOMMENDATIONS

5.1 Conclusions

Multilayer thin films with and without polymer intercalations have been deposited onto a glass substrate by CBD. The effect of the deposition parameter on the structural, optical and electrical properties of the multilayer film was investigated.

For single layer deposition %T was red shifted with an increase in temperature. The particle size was increased as the temperature was increased, resulting in lower %T. The larger the particle size, the more absorption of light onto the particle. At 60°C the particles were closely packed and uniform. A broad peak was observed for single layer deposition which was dominant of nanocrystalline structure for CdO, Cubic for CdS and ZnS, and monocrySTALLINE for ZnO thin film.

The SEM morphology of the MS and MO of CdS and CdO thin film as compared to ZnS and ZnO shows nanoparticles that are spherical in shape and that of ZnS and ZnO thin film show nanorods (nanostructure) that are star shaped.

Multilayer thin film of MO/MS and MS/MO had an effect on the morphology, roughness, thickness, optical properties and structure of the deposited material. The Zn series had star shaped flower like structure and the Cd series had spherical shape. The thickness of Cd and Zn was around ~100 nm for the MO/MS and MS/MO. The %T blue shifted to ~90 %, the increase in %T was attributed to the improvement in crystallinity in the film. Oscillation in the spectra was due to multilayer interference. The roughness and thickness was increased. The structure was improved from nanocrystalline to monocrySTALLINE for CdO to CdO/CdS, cubic to hexagonal for CdS to CdS/CdO, monocrySTALLINE to cubic polycrySTALLINE for ZnO to ZnO/ZnS, and cubic to polycrySTALLINE for ZnS/ZnO the multilayer deposition of MO/MS and MS/MO.

The morphology of multilayer deposition of CdO/CdS thin film has better deposition as good on the substrate showed homogeneity and uniformity on the substrate. The CdS/CdO thin film was non uniform, because the micrographs show that the composite

films cover the whole substrate well and are mostly un-uniform over the entire substrate surface which is important for practical application in devices. The deposition of ZnO/ZnS showed snowflakes shapes which are hexagonal which were in support with XRD and the deposition of ZnS/ZnO which was confirmed by low intensity observed by XRD showed amorphous shaped structure. It is evident that the surface multilayer deposition was smoother as compared to the monolayer deposition which was in good agreement with the decrease in surface roughness and an increase in %T.

Intercalation of PVA had no effect on the optical properties of MO/MS and MS/MO thin films. The %T was red shifted at relatively %T ~88%. Intercalation had an effect on the shape, roughness, thickness, and structure of the MO/MS and MS/MO thin film. Spherical patterns were observed for both Zn and Cd series. The surface roughness and thickness was decreased. The structure for CdO/PVA/CdS and ZnS/PVA/ZnO had no prominent peak which was amorphous in nature and CdS/PVA/CdO was hexagonal and that of ZnO/PVA/ZnS was monocrystalline.

The intercalated material of ZnS/PVA/ZnO observed that the high compactness of these films which were continuous, homogeneous and rather agglomerate. Dispersed spherical structures are observed and thin films formed were highly agglomerated. The deposited particle of ZnO/PVA/ZnS thin film was very smooth and uniform spherical shape particles dispersed on the substrate. Intercalated Cd series were uniform, spherically shaped with a decrease in porosity.

Clearly, using a simple technique like CBD, it was a success to grow MO/MS layers of CdO/CdS and ZnO/ZnS multilayer was observed with %T values as high as 90 %. Nevertheless, more work toward optimizing both deposition and annealing of CBD-MO/PVA/MS thin films is required, in order to obtain a viable CBD-TCO layer. This work merely reports a preliminary step toward using only CBD technique to fabricate a MO/MS layer of multilayer deposition by intercalation with a PVA polymer by increasing the morphology on the surface of the substrate. Careful studies of concentration, pH, agitation and temperature treatments was studied thorough investigations of CBD-

MO/PVA/MS film by studying their crystallinity, stoichiometry, and composition as a function of annealing temperature are still needed to achieve this goal.

In summary, ZnO/ZnS multilayer nanoflakes with flowerlike morphology have been controllably synthesized by the CBD method using NH_4OH and TEA as capping molecules as a result multilayer deposition has an effect on the structure of the MO/MS. The SEM images reveal the improvement in flower size of ZnO/ZnS as an effect of heat treatment. The CBD method is constructive for the preparation of large area nanoflake ZnO/ZnS multilayer thin films at the expense of a few initial ingredients. CdO/CdS multilayer spherical shapes morphology has been controllably synthesized by the CBD method using NH_4OH as capping molecules. The as-deposited material was rough at the deposition of single layer deposition whilst the thickness was around ~ 100 nm. It was observed that the particle size increased with an increase in temperature resulting in a decrease in %T of the increase in grain size.

The structure of the single layer deposition was observed to have a large broad peak and the morphology was not tightly packed. The thickness of the deposited material increased as the second inorganic layer was deposited and the surface roughness decreased. It was evident that the multilayer deposition had an effect on the thickness and structure of the material and hence the structure was intensified and more sharp peaks were observed. The multilayer surface was more tightly packed as compared to monolayer deposition at the same temperatures as a result of smoother surface roughness. The intercalated metal oxide/metal sulfide deposition decreased the thickness as well as the surface roughness. The findings were that the deposited material surface roughness decreased with a decrease in layer deposition whilst the thickness increased for multilayer deposition and thus decreased for intercalation deposition, this can be as a result of loss of material while inserting the organic layer in between the inorganic layers.

The choice of the substrate was a less important factor in film roughness, although it was important in determining the adherence of the films. At temperatures of 70°C and above led to films of poor quality as compared to deposition at temperatures of 60°C .

The significant factors affecting the development, adhesion, and quality of the deposited film were the solution pH and temperature. A noteworthy observation was that film deposited onto commercial glass substrate disintegrated on rinsing with water. A further note was that surface nucleation rate depend on both the supersaturation of the solution and the substrate material. In contrast, surface particle growth rate was influenced by supersaturation alone. The substrate material also determined the contact angle between the particle and substrate and hence the shape of the surface particle.

5.2 Recommendations

- Electron diffraction measurements to ascertain whether the samples are amorphous or polycrystalline.
- Hall Effect measurements should be carried out to determine the conductivity type.
- Use of tin oxide coated glass substrate, due to the film deposited onto commercial glass substrate disintegrated on rinsing with water.
- Use of a different technique such a spin coating or spray pyrolysis for intercalation of a polymer.

REFERENCES

- Adamopoulos, G. B., Gillin, W., Georgakopoulos, S., Shkunov, M., & Baklar, M. (2011). Structural & Electrical Characterization of ZnO Films Grown by Spray Pyrolysis and Their Application in Thin-Film Transistors. *Advanced functional materials*, 525-531.
- Afify, H., Terra, F., & Momtaz, R. (1996). Substrate temperature effects on the tin oxide films prepared by spray pyrolysis. *Material Science*, 149-153.
- Ågoston, P., Albe, K., Nieminen, R. M., & Puska, M. (2009). Intrinsic n-type behaviour on transparent conducting oxide: A comparative hybrid functional study of In₂O₃, SnO and ZnO. *Physical review letters*, 245-501.
- Ahn, K. S., Shet, S., Deutsch, T., Jiang, C. S., Yan, Y., Al-Jassim, M., et al. (2008). Enhancement of photoelectrochemical response by aligned. *Power Sources*, 387.
- Ajimsha, R. S., Jayaraj, M. K., & Kukreja, L. M. (2008). Electrical Characteristics of n-ZnO/p-Si Heterojunction Diodes Grown by Pulsed Laser Deposition at Different Oxygen Pressures. *Electronic Materials*, 770-775.
- Al-Sabayleh, M. (2008). The effect of substrate temperature on the optical properties of spray deposited ZnS thin films prepared from non aqueous media. *Science Engineering*, 17-20.
- Andeen, D., Loeffler, L., Pature, N., & Lange, F. F. (2003). Crystal chemistry of epitaxial ZnO on (1 1 1) MgAl₂O₄ produced by hydrothermal synthesis. *Crystal Growth*, 103-109.
- Armarego, W., & Chai, C. (2009). Purification of laboratory chemicals. (6th, Ed.) *Elsevier*, 520-523 .
- Arterton, B., Brightwell, J. W., Mason, S., Ray, B., & Viney, I. V. (1992). Impact of phase concentrations on structure and electroluminescence of ZnS:Cu. *Crystal Growth*, 1008.
- Ates, A., Yildirim, M., Kundakci, M., & Yildirim, M. (2007). Investigation of optical and structural properties of CdS thin films. *Chinese Journal of Physics*, 135-141.
- Bädeker, K. (1907). The first thin film TCO. *Annalen der Physik* , 749.
- Bao, J., Zimmerler, M. A., Capasso, F., Wang, X., & Ren, Z. F. (2006). Broadband ZnO single-nanowire light-emitting diode. *Nano Letters*, 1719-1722.
- Bayer, A., Boyle, D., Heinrich, M., O'Brien, P., Otway, D., & Robbe, O. (2000). Developing environmentally benign routes for semiconductor synthesis: improved approaches to the solution deposition of CdS for solar cell applications. *Green Chemistry*, 79-85.

- Bayram, C., Teherani, F., Rogers, D. J., & Razeghi, M. (2008). A hybrid green light-emitting diode comprised of n-ZnO/ (InGaN/GaN) multi-quantum-wells/p-GaN. *Applied Physics*, 81-111.
- Bellotti, E., Brennen, K. F., Wang, R., & Ruden, P. P. (1988). Monte Carlo study of electron initiated impact ionization in bulk zincblende and wurtzite phase ZnS. *Applied Physics*, 47-65.
- Beyer, W., Hupkes, J., & Stiebig, H. (2007). Transparent conducting oxide films for thin film silicon photovoltaics. *Thin solid films*, 147-154.
- Bhachu, D., Waugh, M., Zeissler, K., Branford, W., & Parkin, I. (2011). Textured fluorine doped tin oxide films formed by chemical vapour deposition . *European* , 11613-11621.
- Blum, H., Stutzman, L., & Dodds, W. (1952). Gas absorption of carbon dioxide from air by sodium and potassium hydroxides. *Industrial and Engineering Chemistry*, 44(12), 2969-2974.
- Boyle, D., Bayer, A., Heinrich, M., Robbe, O., & O'Brien, P. (2000). Novel approach to the chemical bath deposition of chalcogenide semiconductors. *Thin Solid Film*, 150-154.
- Britt, J. (1993). Thin-film CdS/CdTe solar cell with 15.8% efficiency. *Applied Physics*, 2851-2852.
- Call, R., Jabern, K., Seshan, K., & Whyte, J. (1980). Structural and electronic properties of three aqueous deposited films: CdS, CdO, ZnO for semiconductor and photovoltaic applications. *Solar Energy Matter*, 373-380.
- Catlow, C., Sokol, A., & Walsh, A. (2011). Microscopic origins of electron and hole stability in ZnO. *Chemical communication*, 3386.
- Chen, B., Wang, X., Zhang, Q., Xi, X., Cai, J., & Qi, H. (2010). Synthesis and characterization of the interpenetrated MOF-5. *Material chemistry*, 3758.
- Cheng, H., Chen, C., & Lee, C. (2006). Thin-film transistors with active layers of zinc oxide (ZnO) fabricated by low-temperature chemical bath method. *Thin Solid Film*, 142-145.
- Chopra, K. (1969). *Thin film phenomena*. New york: McGraw hill, 20-25.
- Chopra, K. K. (1982). Chemical solution deposition of inorganic films. *Physics of Thin Film*, 167-235.
- Chopra, K., Kainthla, R., Pandya, D., & Thakoor, A. (1982). *Physics of Thin Film*. London: Academic press.
- Chu, S., Olmedo, M., Yang, Z., Kong, J., & Liu, J. (2008). Electrically pumped ultraviolet ZnO diode lasers on Si. *Applied Physics*, 181106.
- Contreras, M., Nakada, T., Hongo, M., Pudova, O., & Sites, J. (2003). *Photovoltaic energy conversion*. Rhodes island: Brown alumni magazine, 153-155.

- Coutts, T., Young, D., & Li, X. (2011). Characterization of transparent conducting oxides. *MRS bulletin*, 58-65.
- Desai, J., Pathan, H. M., & Joo, O. (2005). Nanocrystalline haematite thin film by chemical solution spray. *Semiconductor Science and Technology*, 705-709.
- Doña, J., & Herrero, J. (1997). Chemical Bath Deposition of CdS Thin Films: An Approach to the Chemical Mechanism through Study of the Film Microstructure". *Electrochemical Society*, 4081-4091.
- Dongre, J., Nongriya, V., & Ramrakhiani, M. (2009). Structural, optical and photoelectrochemical characterization of CdS nanowire synthesized by chemical bath deposition and wet chemical etching. *Applied Science*, 6115-6120.
- Edelson, V. (2007). *Concentration crisis*. Chicago: Brown alumni magazine, 150-153.
- Edwards, P., Porch, A., Jones, M., Morgan, D., & Perks, R. (2004). Basic materials physics of transparent conducting oxides. *Dalton transactions*, 2995.
- Einsele, F., Rostan, P. J., Schubert, M. B., & Rau, U. (2007). Recombination and resistive losses at ZnO/a-Si:H/c-Si interfaces in heterojunction. *Applied Physics*, 094507.
- El-Shaer, A., Bakin, A., Schlenker, E., Mofor, A. C., Wagner, G., Reshanov, S. A., et al. (2007). Fabrication and characterization of n-ZnO on p-SiC heterojunction diodes on 4H:SiC substrates. *Superlattices Microstructure*, 387-391.
- Gaume, J., Wong-wah-chung, P., Rivaton, A., Thérias, S., & Gardette, J. (2011). Photochemical behavior of PVA as an oxygen barrier polymer for solar cell encapsulation. *RSC Advances*, 1471-1481.
- Gilbert, B., Frazer, B. H., Zhang, H., Huang, F., Banfield, J. F., Haskel, D., et al. (2002). Effect of pH on the properties of ZnS thin films grown by chemical bath deposition. *Thin Solid Film*, 4-8.
- Ginley, D., & Bright, C. (2011). Transparent conducting oxides. *MRS bulletin*, 15-18.
- Goldner, R., & Haskal, H. (1975). Indium tin oxide-coated silicon as a selective absorber. *Applied optics*, 2328-2330.
- Gratzel, M. (2005). Solar Energy Conversion by Dye-Sensitized Photovoltaic Cells. *Inorganic chemistry*, 6841-6851.
- Green, M. A., & Wenham, S. R. (1994). Modelling, simulation and optimization of n-p-n-p silicon multilayer solar cells. *Open Journal of Microphysics*, 2907-2909.
- Green, M., Emery, K., King, D., & Igari, S. (2000). Solar cell efficiency tables progress in photovoltaic. *Research and applications*, 187-196.

- Greenwood, N., & Earnshaw, A. (1984). *Chemistry of the elements* (2nd ed.). Leeds: Oxford: Pergamon, 645-747.
- Gutiérrez-Lazos, C., Rosendo, E., Juárez, H., García-Salgado, G., Díaz, T., Rubín-Falfán, M., et al. (2008). Hexagonal phase of CdS thin films obtained by oscillating chemical bath. *Electrochemical Society*, 158-162.
- Hames, Y., & San, S. (2004). CdO/Cu₂O solar cells by chemical deposition. *Solar Energy*, 291-294.
- Hammer, K. (1943). Principles of Optics: Electromagnetic Theory of Propagation, Interference. *Applied Physics*, 169.
- Hara, K., & Arakawa, H. (2003). Dye-sensitized Solar Cells. *John Wiley and Sons*, 663-700.
- Harako, S., Yokoyama, S., Ide, K., Zhao, X., & Komoro, S. (2008). Visible and infrared electroluminescence from an Er-doped n-ZnO/p-Si light emitting diode. *Physical Status Solid*(1), 19-22.
- Hasse, M., Qui, J., DePuydt, J., & Cheng, H. (1991). Blue and green diode lasers in ZnSe-based quantum wells. *Applied Physics*, 1272.
- Herrero, J., Gutierrez, M., Dona, J., Martinez, M., Chaparro, A., & Bayon, R. (2000). Photovoltaic windows by chemical bath deposition. *Thin Solid Film*, 28-33.
- Hodes, G., & Dekker, M. (2003). Chemical solution deposition of semiconductor films. *Thin Solid Film*, 89.
- Hsueh, K. P., Huang, S. C., Li, C. T., Hsin, Y. M., Sheu, J. K., Lai, W. C., et al. (2007). Tilted Epitaxial ZnO Nanospikes on Si(001) by Chemical Bath Deposition. *Applied Physics*, 132111.
- Hu, J., & Gordon, R. (1992). Textured aluminum-doped zinc oxide thin films from atmospheric pressure chemical vapor deposition. *Applied physics*, 880.
- Huang, M. H., Mao, S., Feick, H., Yan, H., Wu, Y., Kind, H., et al. (2001). Room-temperature ultraviolet nanowire nanolasers. *Science*, 1897-1899.
- Hutson, A. (1957). Hall effect studies of doped zinc oxide single crystals. *Physical review*, 222-230.
- Ibanez, J., Solorza, O., & Gomez-del-Campo, E. (1991). Growth of CdS film for various applications. *Chemistry Education*, 872-874.
- Ibbotson, F. (2007). *The Chemical Analysis of Steel-Works' Materials*. Andorra: Read Books, 28-35.
- Ilenikhena, P. (2008). Comparative studies of improved chemical bath deposited copper sulfide and zinc sulfate thin films at 320 K and possible application. *African Physical Review*, 59.
- Islam, M., Ghosh, T., Chopra, K., & Acharya, H. (1996). XPS and X-ray diffraction studies of the aluminium doped zinc oxide transparent conducting films. *Thin solid films*, 20-25.

- Izaki, M., Mizuno, K. T., Shinagawa, T., Inaba, M., & Tasaka, A. J. (2006). Photochemical construction of photovoltaic device composed of p-copper(I) oxide and n-zinc oxide. *Electrochemical Society*, C668–C672.
- Jeong, S. S., Mittiga, A., Salza, E., Masci, A., & Passerini, S. (2008). Electrodeposited ZnO/Cu₂O heterojunction solar cells. *Electrochimica Acta*, 2226-2231.
- Johnson, D., Corletto, M., Reddy, K., Forbes, I., & Miles, R. (2002). Study on physical properties of ZnS thin films prepared by chemical bath deposition. *Thin Solid Film*, 403-404.
- Kaminska, E., Piotrowska, A., Golaszewska, K., Kruszka, R., Kuchuk, A., Szade, J., et al. (2004). ZnO–GaN tunnel junction for transparent ohmic contacts to p-GaN. *Alloys and Compound*, 129-132.
- Kassim, A., Nagalingam, S., Tee, T., Sharif, A., Abdulah, D., Elos, M., et al. (2009). Effect of deposition period and pH on chemical deposition CuS thin films. *Philippians Journal of Science*, 161-168.
- Katsumi, K. (1995). Semiconductor physical electronics. *Japan Applied Physics*, 4383.
- Kaur, I., Pandya, D., & Chopra, K. (1980). Growth kinetics and polymorphism of chemically deposited CdS films. *Electrochemical Society*, 943-948.
- Kawar, S. (2011). Chalcogenide Thin Films Having Nanometer Grain Size for Photovoltaic Applications. *Chemical Science*, 31-35.
- Kawazoe, H., Yasukawa, M., Hyodo, H., Kurita, M., Yanagi, H., & Hosono, H. (1997). P-type electrical conduction in transparent thin films of CuAlO₂. *Nature*, 939-942.
- Khomane, A. (2011). Crystallographic, morphological, optical and electrical properties of CBD deposited cadmium sulphide thin films. *Applied Science Research*, 273-279.
- Kickelbick, G. (2003). Concepts for the incorporation of inorganic building blocks into organic polymers on a nanoscale. *Progress in Polymer Science*, 83-114.
- Kim, T. W., Kwack, K. D., Kim, H. K., Yoon, Y. S., Bahang, J. H., & Park, H. L. (2003). Optical parameter in ZnO nanocrystalline textured films grow on p-Inp (1 0 0) substrates. *Solid State Community*, 635-638.
- Klocek, P. (1991). *Handbook of Infrared Optical Materials*. Texas: CRC Press, 122-124 .
- Konenkamp, R., Word, R. C., & Godinez, M. (2005). Ultraviolet electroluminescence from ZnO/Polymer heterojunction light-emitting diodes. *Nano Letters*, 2005–2008.
- Kostoglou, M., Andritsos, N., & Karabelas, A. (2003). Incipient CdS thin film formation. *Colloid and Interface Science*, 177-189.

- Leong, E. S., Yu, S. F., & Lau, S. P. (2006). Directional edge-emitting UV random laser diodes. *Applied Physics*, 221109-1—221109-3.
- Lepig, P. (1924). Absorption of carbon dioxide and ammonia from gas bubbles. *Industrial and Engineering Chemistry*, 16(12), 1231-1233.
- Liang, H., & Gordon, R. (2007). Atmospheric pressure chemical vapor deposition of transparent conducting films of fluorine doped zinc oxide and their application to amorphous silicon solar cells. *Material science*, 6388-6399.
- Lincol, D., Forment, M., Cachet, H., Alkite, R., & Kolb, D. (1998). *Advanced electrochem science and engineering*. New york: Wiley,69-73.
- Lincot, D., Froment, M., & Cachet, H. (1999). Chemical deposition of chalcogenide thin films from solutions. *Advances in Electrochemical Science and Engineering*, 165-235.
- Lindroos, S., Kannianen, T., & Leskela, M. (1997). ZnS Thin Films. *Research Science*, 105.
- Liu, F., Lai, Y., Liu, J., Wang, B., Kaung, S., Zhang, Z., et al. (2010). Characterization of chemical bath deposited CdS thin films at different deposition temperature. *Alloys and Compounds, I-II*(493), 305-308.
- Liu, R., Vertegel, A. A., Bohannon, E. W., Sorenson, T. A., & Switzer, J. (2001). Chemical Bath-Deposited ZnO Thin Films: preparation and characterization. *Chemistry Materials*, 508-510.
- Lokhande, C. (1991). A chemical method for preparation of metal sulfide thin films. *Material Chemistry and Physics*, 145-149.
- Martinson, A. B., Elam, J. W., Hupp, J. T., & Pellin, M. J. (2007). ZnO nanotube based dye-sensitized solar cells. *Nano Letters*, 2183-2187.
- Mattox, D. M. (1978). Surface Cleaning in Thin Film Technology. *Thin Solid Film*, 1(53), 81.
- Mayer, B. (1992). Highly conductive and transparent films of tin and fluorine doped indium oxide produced by APCVD. *Thin solid films*, 166-182.
- Minami, T., Miyata, T., Ihara, K., Minamino, Y., & Tsukada, S. (2006). Effect of ZnO film deposition methods on the photovoltaic properties of ZnO-Cu₂O heterojunction devices. *Thin Solid Film*, 47-52.
- Mondal, A., Chanudhuri, T., & Pramanik, P. (1983). Deposition of cadmium chalcogenide thin films by a solution growth technique using triethanolamine as a complexing agent. *Solar Energy Materials*, VII(4), 431-438.
- Mridha, S., Dutta, M., & Basak, D. (2009). photoresponse of n-ZnO/ p-Si heterojunction towards ultraviolet/visible lights: thickness dependent behavior. *Material Science*, 376-379.

- Mryasov, O., & Freeman, A. (2001). Electronic band structure of indium tin oxide and criteria for transparent conducting behaviour. *Physical review B*(23), 233111.
- Müller-Warmuth, W., & Schöllhorn, R. (2012). *Progress in Intercalation research. Physics and chemistry of materials with low-dimensional structures* . Springer Science & Business Media,189-192.
- Nadeem, M., Ahmed, W., & Wasiq, W. (2005). ZnS thin films. *Research Science*, 105.
- Nair, M., & Nair, P. (1989). Chemical bath deposition of CuxS thin films and their prospective large area applications. *Semiconductor Science and Technology*, 441-449.
- Nair, M., Nair, P., & Campos, J. (1988). Effect of bath temperature on the optoelectronic characteristics of chemically deposited CdS thin films. *Thin Solid Film*, 21-34.
- Nair, P., Garcia, V., Gomez-Daza, O., & Nair, M. (2001). High thin film yield achieved at small substrate separation in chemical bath deposition of semiconductor thin films. *Semiconductor Science and Technology*, 855-863.
- Nair, P., Nair, M., Garcia, V., Arenas, O., Pena, Y., Castillo, A., et al. (1998). Semiconductor thin films by chemical bath deposition for solar energy related applications. *Solar Energy Matter*, 313-324.
- Nakada, T., & Mizutani, M. (2002). 18% efficiency Cd-free Cu(In,Ga)Se₂ thin film solar cells fabricated using chemical bath deposition (CBD)-ZnS buffer layers. *Applied Physics*, 165.
- Nanda, K., Sarangi, S., & Sabu, S. (1998). CdS Nanocrystalline films: Composition, surface, crystalline size, structural and optical absorption studies. *Nanostructured Materials*, 1401-1410.
- Nasr, T., Kamoun, N., & Guasch, C. (2008). Physical properties of ZnS thin films prepared by chemical bath deposition. *Applied Surface Science*, 5039-5043.
- Ndukwe, I. (1996). Solar energy materials and solar cells. *Applied Physics*, 123.
- Nonomura, K., Komatsu, D., Yoshida, T., Minoura, H., & Schlettwein, D. (2007). Dependence of the photoelectrochemical performance of sensitised ZnO on the crystalline orientation in electrodeposited ZnO thin films. *Physics and Chemistry*, 1843-1849.
- O'Regan, B., & Grätzel, M. (1991). A low-cost, high-efficiency solar cell based on dye-sensitized colloidal TiO₂ films. *Nature*, 737-740.
- O'Brien, P., & McAleese, J. (1998). Developing and understanding of the processes controlling the chemical bath deposition of ZnS and CdS. *Material Chemistry*, 2309-2314.
- Ohring, M. (1992). *The material science of thin films*. San diego: Academic press,803.
- Oladeji, I., & Chow, L. (1997). Optimization of chemical bath deposition of cadmium sulfide thin films. *Electrochemical Society*, 2342-2346.

- Oladeji, I., Chow, L., Liu, J., Chu, W., Bustamante, A., Fredricksen, C., et al. (2000). Comparative study of CdS thin films deposited by single continuous and multiple dip chemical processes. *Thin Solid Film*, 154-159.
- Ortega, M., Sanatana, G., & Acevedo, A. (1999). Optoelectronic properties of CdO-Ci heterojunctions. *Electrochemical Society*, 294-295.
- Ortega, R., & Borges, D. (1992). *E.C Photovoltaic solar* (11th ed.). Switzerland: Hawood Academic, 520-528.
- Ouachtari, F., Ramili, A., El Bachir, E., Bouaoud, A., Erguig, H., & Elies, P. (2011). Influence of bath temperature, deposition time and S/Cd ratio on the structure, surface morphology, chemical composition and optical properties of CdS thin films elaborated by chemical bath deposition. *Modern physics*, 1073-1082.
- Ozgur, U., Alivov, Y. I., Liu, C., Teke, A., Reshchikov, M. A., Dogan, S., et al. (2005). A comprehensive review of ZnO materials and devices. *Applied Physics*, 103.
- Padam, G., Rao, S., & Maholtra, G. (1988). Studies on solution-grown thin films of $Zn_xCd_{1-x}S$. *Applied Physics*, 770-774.
- Perednis, D. (2003). *Thin film deposition by spray pyrolysis and the application in solid oxide fuel cells*. Zurich: Eidgenossische technische hochschule, 365-368.
- Readigos, A., Garcia, V., Gomez-Daza, O., Campos, J., Nair, M., & Nair, P. (2000). Substrate spacing and thin film yield in chemical bath deposition of semiconductor thin films. *Semiconductor Science and Technology*, 1022-1029.
- Remes, Z., Vanecek, M., Yates, H., Evans, P., & Sheel, D. (2009). Optical properties of SnO₂ thin films deposited by atmospheric pressure CVD. *Thin solid films*, 6287-6289.
- Reynolds, J. (1884). Chemical bath deposition of PbS. *Chemical Society*, 720-721.
- Ruiz, H., Vesteghem, H., Giampaolo, A., Di, & Lira, J. (1997). Zirconia coating coatings by spray pyrolysis. *Surface and Coatings Technology*, 77-81.
- Sang, B., Shafarman, W., & Birkmire, R. (2002). Investigation of chemical bath deposited ZnS buffer layers for Cu(InGa)Se₂ thin film solar cells. *29th IEEE photovoltaic specialists conference*, (p. 520). New Orleans, 520.
- Sartale, S., Sankapal, B., lux-Steiner, M., & Ennaoui, A. (2005). Preparation of nanocrystalline ZnS by a new chemical bath deposition route. *Thin Solid Film*, 480-481.
- Savago, O. (1998). Chemically and electrochemically deposited thin films for solar energy materials. *Solar Energy Material and Solar Cells*(52), 361-388.

- Sebastian, P., & Nair, P. (1992). The influence of bath composition on the photocurrent response and morphology of chemically deposited CdS thin films. *Advanced Materials for Optics and Electronics*, 1(5), 211-220.
- Shandalov, M., & Golan, Y. (2003). Microstructure and morphology evolution in chemical deposited PbSe film on GaAs(100). *European Physical Journal*, 24, 13-20.
- Shandalov, M., & Golan, Y. (2005). Microstructure and morphology evolution in chemical solution deposited PbSe film on GaAs(100). *European Physical Applied physics*, 27-30.
- Sharma, R., Patil, S., Bhavsar, S., Patil, A., & Dori, L. (1999). Compositional effect on optical characteristics of solution growth Cd_{1-x}MnxSe thin films. *Indian Journal of Pure & Applied Physics*, 37, 876-880.
- Sheel, D., Yates, H., Evans, P., Dagkaldiran, U., Gordijin, A., & Finger, F. (2009). Atmospheric pressure chemical vapor deposition of F-doped SnO₂ for optimum performance solar cells. *Thin solid films*, 517, 3061-3065.
- Singhal, A. (2012). *The person guide to inorganic chemistry for the IIT JEE*. New Delhi: Dorling Kindersley, 133-134.
- Smith, H. (2002). *High-Performance Pigments*. Germany: Wiley-VCH, 186-188.
- Souad, A., & Al-Bat'hi, M. (2007). *Characterization of electrodeposited Zn (Se, Te) thin films/polymer (PEO- Chitosan blend) Junction for solar cells application*. Malaya: Semiconductor science and technology, 1883-1885.
- Streintz, F. (1902). Transparent TCO. *Annalen der Physik*, 854.
- Strotmann, U., Reuschenbach, P., Schwarz, H., & Pagga, U. (2004). Development and evaluation of an online CO₂ evolution test and a multicomponent biodegradation test system. *Applied and Environmental Microbiology*, 70(8), 4621-4628.
- Suwanboon, S. (2008). The Properties of Nanostructured ZnO Thin Film via Sol-Gel Coating. *Naresuan University Journal*(2), 173-180.
- Tang, Z. K., Wong, G. K., Yu, P., Kawasaki, M., Ohtomo, A., Koinuma, H., et al. (1998). Room-temperature ultraviolet laser emission from self-assembled ZnO microcrystallite thin films. *Applied Physics*, 83, 3270-3272.
- Teteris, J. (2003). Holographic recording in amorphous chalcogenide thin film. *Solid State and Material Science*, 127-134.

- Vallejos, S. U., & Blackman, C. (2011). Aerosol Assisted Chemical Vapour deposition control parameters for selective deposition of tungsten oxide nanostructures. *Journal of Nanoscience and Nanotechnology*, 8214-8220.
- Venables, J. (2003). *Introduction to surface and thin film processes*. Cambridge: Cambridge University press,372.
- Vipin, K., Sharma, M., Gaur, J., & Sharma, T. (2008). Polycrystalline ZnS thin films by screen printing method and its characterization. *chalcogenide Letters*, VI(11), 289-291.
- Wenas, W. W., & Riyadi, S. (2006). Carrier transport in high-efficiency ZnO/SiO₂/Si solar cells. *Solar Energy Materials and Solar Cells*, 3261–3267.
- West, A. (2003). *Solid state Chemistry and its application*. Singapore: John Willey and sons,180-182.
- Wiberg, E., & Holleman, A. (2001). *Inorganic chemistry* (1st ed.). San Diego: Academic Press,355.
- Wu, X., Bai, H., Li, C., Lu, G., & Shi, G. (2006). Room-temperature fabrication of highly oriented ZnO nanoneedle arrays by anodization of zinc foil. *Chemical Communication*, 1655-1657.
- Yamaguchi, T., Yamamoto, Y., Takaka, T., Demizi, Y., & Yoshida, A. (1996). CdS, ZnS thin film prepared by chemical bath deposition for photovoltaic devices. *Thin Solid Film*, 375-378.
- Yates, H., Evans, P., Sheel, D., Heessels, A., Ammerlaan, J., & Dagkaldiran, U. (2011). Deposition of thin film SnO₂: F onto aluminum foil for use in flexible tandem solar cells. *Thin Solid Films*, 7731-7737.
- Yuhas, B. D., & Yang, P. (2009). Nanowire-based all oxide solar cells. *American Chemical Society*, 3756–3761.
- Zeleya-Angel, O., Castillo-Alvarado, F., Avendano-Lopez, J., Escamilla-Esquivel, A., Contreras-Puente, G., Lozada-Morales, R., et al. (1997). Raman studies in CdS thin films in the evolution from cubic to hexagonal phase. *Solid State Communications*, 161-166.
- Zendehnam, A., Shirazi, M., Doulatshah, S., & Sadat, M. (2010). Effect of temperature and period of post-annealing on the optical properties of ZnO thin films. *American Journal of Physics*, III(4), 305-311.
- Zhang, R., & Kerr, L. (2008). A simple method for systematically controlling ZnO crystal size and growth orientation. *Solid State Chemistry*, 988-994.
- Zhang, R., Cho, S., Lim, G., Hu, X., Stach, E., Handwerker, C., et al. (2016). Metal-metal chalcogenide molecular precursors to binary, ternary and quaternary metal chalcogenide thin film for electronic devices. *Chemistry Communication*, 5007-5010.